Phase Coherence of Two-Component Bose-Einstein Condensates Loaded in State-Dependent Optical Lattices

A Dissertation Presented

by

Hyunoo Shim

to

The Graduate School

in Partial Fulfillment of the Requirements

for the Degree of

Doctor of Philosophy

in

Physics

Stony Brook University

August 2011

Stony Brook University

The Graduate School

Hyunoo Shim

We, the dissertation committee for the above candidate for the Doctor of Philosophy degree, hereby recommend acceptance of this dissertation.

Thomas H. Bergeman – Dissertation Advisor
Adjunct Professor, Department of Physics and Astronomy

Dominik A. Schneble – Chairperson of Defense
Assistant Professor, Department of Physics and Astronomy

Alexandre G. Abanov
Associate Professor, Department of Physics and Astronomy

Hong Y. Ling
Professor, Department of Physics and Astronomy
Rowan University

This dissertation is accepted by the Graduate School.

Lawrence Martin
Dean of the Graduate School

Abstract of the Dissertation

Phase Coherence of Two-Component Bose-Einstein Condensates Loaded in State-Dependent Optical Lattices

by

Hyunoo Shim

Doctor of Philosophy

in

Physics

Stony Brook University

2011

Phase coherence and localization of Bose-Einstein Condensates (BEC) in optical lattices is a notable property that is changing under the superfluid-Mott insulator phase transition. For a single-component BEC, long-range phase coherence across lattice wells is lost as the lattice height is sufficiently increased. Phase coherences of two-component overlapping mixture of BECs, however, are nontrivial because of the interspecies interaction between components, affecting localization of condensates. For such cases, the BECs form two interdependent mean-field lattices made of each

component in addition to optical lattices.

We prepare initial BEC clouds as a collection of small Bogoliubov quasiparticles added to classical mean-fields, and obtain the dynamics under phase space representations, where the density operators are projected onto phase space. Among various phase space representations, we focus on a Truncated Wigner Approximation (TWA) and a positive P representation, and we construct a hybrid model to combine them. Since a high volume of numerical integration is required for sufficient convergence from ensembles, we construct efficient numerical methods to reduce the sample variance.

We demonstrate time evolution of phase coherence of one-com- ponent and two-component BECs in state-dependent optical lattices. For one-component BECs, we show that phase coherence loss depends on lattice heights. In the cycling process of lattice height changes, we investigate nonadiabatic effects depending on initial ramp-up speeds. The hybrid model compared with the TWA exhibits temporal fluctuations in coherence and sudden phase diffusion at the end of ramp-up of a lattice. For two-component BECs, we consider that the two wavefunctions are localized at periodic potential wells whose positions differ by a half-period between the two. Dependence on population imbalance between two components becomes another factor on coherence loss. We show that under gradual loading of an optical lattice effective only to first

component, loss of phase coherence of first atoms is enhanced and that of second atoms is weakened as the fraction of second atoms is increased in the mixture. We also demonstrate effects of localizing mean-field lattices on coherence loss under various lattice heights.

To my parents, Eui-Won Shim and Gum-Hee Choi

Contents

List of Figures

Acknowledgements

First, I would like to deeply thank my advisor, Thomas Bergeman for his passionate guidance and broad support not only in my dissertation studies, but also in my life over the years. I am grateful to all his incessant efforts to help me progress forward beyond my limits, and he has been a great source of keen and insightful ideas, plentiful questions and answers, and great enthusiasm. I am also in enormous debt to Dominik Schneble, who bestowed on me a fortunate introduction to my advisor and helped ease to build my understanding of many topics in BECs. He inspired many of the ideas in this dissertation, and he instilled a sense of humor and excitement in my academic endeavors. I am also thankful to Harold Metcalf, who has been great support to me and created a stimulating atmosphere to AMO people. I was infected by his great contagious sense of humor and joy in aspects of my life, which I hope to keep in the rest of my life. I would like to show my gratitude to Hong Ling, who showed his interest in my posters at the DAMOP meeting every year.

I would like to thank my family. I can safely say that without their encouragement, sacrifice, financial support, unflinching sense of optimism, this would be impossible to exist. I am very grateful to my wife, Yoona Lee, for her unconditional and endless love, patience, warm smile, and being the joy

of my life. In addition, my parents, Eui-Won Shim and Gum-Hee Choi who have been my life-long teachers and also who have shared delight and grief, are more than happiness to me. My mother-in-law, Kisook Lee, has provided firm belief to me, and the sincere and warm-hearted care by my sister, Soo-Jeong Shim, has allowed me discover joy throughout my journey of this study.

My wholehearted gratitude needs to be forwarded to my great friends I met at Stony Brook, some of whose names will be inevitably omitted, for which I apologize. I wish to show my gratitude to friends in Dominik's group, especially Daniel Pertot, Bryce Gadway for their kind help in various aspects in this research. I had the privilege of learning Physics and life from a wonderful set of great-minded and genial friends including Peng Dai, Tao Sun, Yu-tin Huang, Coco Tseng, Xiaoxu Lu, Elli Pomoni, Itai Ryb, Chee Sheng Fong, and Prasad Hegde. I would like to express my sincere gratitude to Keun-Young Kim and Jinmi Yoon, who helped smooth to settle down when I arrived at Stony Brook, and who invited me to many great dinners, and I am thankful to Kyujin Kwak, Kiyoung Lee, Jung Hoon Lee, Sung Tae Cho, Ilmo Sung, Yeunhwan Lim, Jaehyung Choi, Hyejin Ryu, Jay Hyun Jo for many funny talks to let my energies well-balanced.

Chapter 1

Introduction

The superfluid - Mott insulator phase transition [1–4] of Bose Einstein condensates (BEC) in optical lattices [5, 6] has attracted much attention in condensed matter and atomic physics [7, 8] and quantum information and computation [9–13]. A superfluid phase usually obtained for shallow lattices, has zero viscosity, and long-range phase coherence. On the other hand, the Mott insulator phase which is achievable by raising the lattice height has zero compressibility and it has a fixed density within each lattice well with breakdown of long-range phase coherence. The superfluid-to-Mott insulator phase transition in the process of raising the lattice height is a phase transition between a macroscopically populated ground state wavefunction and a strongly correlated many-body state, resulting from competition between strong local repulsion and tunneling [3]. It is a quantum phase transition, since it is a set of intrinsic parameters of BECs including on-site interaction energies and tunneling amplitudes that drive the transition at zero temperature, not extrinsic parameters like temperature.

One interesting observation as mentioned above is that the superfluid phase with no lattice or with a shallow lattice has global phase coherence across the condensate, whereas the Mott insulator phase in a deep lattice has only local phase coherence. The coherence or lack of coherence between atoms in adjacent wells plays a crucial role in the superfluid-Mott insulator phase transition. For example, the work of Orzel et al. [14] with a 1D array of "pancake" condensates displayed high-visibility interference patterns under conditions of phase coherence between adjacent wells, but dramatic reduction of the interference contrast, or visibility, when the wells were deepened and number-squeezing was believed to occur. Later work with 3D optical lattices by Greiner *et al.* [3] exhibited the superfluid to Mott-Insulator phase transition through the interference pattern when the 3D condensates were released.

For single-component BECs in 1D optical lattices, theoretical modeling and analysis of phase decoherence and number-squeezing has been developed mostly from an extended Gross-Pitaevskii equation (GPE) approach [15] or from the Truncated Wigner Approximation (TWA) approach [16]. The TWA which will be mainly used in this work has been subject to careful tests [17] and has emerged as the method of choice for dealing with time evolution of Bose-Einstein condensates in optical lattices, whereas the loss of phase coherence therein creates theoretical difficulties for the time-dependent GPE approach. Higher order corrections have been discussed in Ref. [18] but will not be considered here.

More recently, experiments have addressed the question of phase coherences of systems in which the Bose condensate consists of distinct components, such as different atomic species, different substates or different hyperfine levels. For

example, it has been observed [19] that the presence of ^{41}K atoms reduces the visibility of the interference pattern of marginally-overlapped ^{87}Rb atoms in a 3D optical lattice. Similarly, in condensate of miscible ^{87}Rb atoms in state-dependent 3D optical lattice, the presence of atoms in a second hyperfine level can reduce the superfluid coherence of atoms in a first hyperfine level [20]. Lasers in those works were tuned such that both components undergo phase-matched lattice potentials. These experiments are most closely related to the theoretical discussion of two-component BECs in this study, but there are other recent experimental studies of Bose condensates focusing on diverse aspects of multi-component systems [21–25] and it is easy to imagine further experimental studies probing the rich physics of two-component BECs.

Recently, also, there have been a number of theoretical studies addressing aspects of Bose condensates with two or more components. Perhaps most notable have been discussions of different phase regimes and phase transitions [26–28] and of the extended Bloch band structure [29]. There have also been studies of dynamical effects including those associated with ramping up the optical lattice [30, 31]. In most cases, these and other [32, 33] theoretical studies have used the Bose-Hubbard model (BHM) or time-evolving Bloch decimation (TEBD) approach, both of which become problematic when there are many atoms per well as in the one-component experiments of [14]. It would be interesting to explore the boundaries of the BHM in light of results obtained with the truncated Wigner approach used in the present work.

For BECs in an optical lattice, phase diffusion and phase decoherence are fundamental quantum-mechanical phenomena [34–36]. In this work, we study phase coherences of both one-component and two-component BECs. For one-

component BECs, we investigate how nonlocal phase coherences of BECs are affected by optical lattice heights, and the nonadiabaticity of ramp-up processes. We find that loss of phase coherence is greater as the lattice height is increased and that nonadiabatic ramp-up might create excitations. We also develop and compare theories from two different representations: the TWA which is frequently used in studies of BECs, and a recent hybrid model which combines the TWA and a positive P representation.

For two-component cases, we are especially interested in the behavior of interpenetrating two-component mixtures that are slowly loaded into relatively shallow lattices, such that a single component would remain phase coherent after application of the optical lattice. We focus on the cases of a state-selective lattice in which only one component experiences a lattice potential, or alternatively in which the lattice potentials for each component are shifted by half a period. We find, as in the experimental studies mentioned above [19, 20], that the second component diminishes the phase coherence of the first component, and also experiences decoherence itself relative to the initial fully coherent state.

There are many theoretical and analytical methods for the study of BECs (for a review, [37]): discrete nonlinear Schrödinger equa-tions [38, 39], time-dependent mean-field theory [40], Schwinger-Keldysh close- d time-path formalism [41, 42], quantum kinetic theory [43–46], phase space formulation of coherent states [47, 48], squeezed coherent states in optical lattices [Appendix A], two mode theories [49–54], multimode theories [55].

In this work, we adopt phase space representations to numerically calculate time evolution of wavefunctions of BEC clouds. A phase space for a

physical system is a representation space of all possible states for the system. Each classical state is represented by a point in the phase space. In classical mechanics, a phase space for a mechanical system is commonly expressed as position and momentum coordinates, where a trajectory of points means a history of that particular state. In contrary, no state is represented by a single point in quantum mechanics. A phase space in quantum mechanics differs in that each state is represented by a (quasi-)probability distribution function over the phase space.

A phase space representation transforms a set of observables for a state into a set of corresponding expectation values with a distribution containing the information of the given state. Having prepared a state with a given distribution function in phase space, time evolution of the distribution function and its dynamics are analyzed by a Fokker-Plank equation, which is an analogue of Heisenberg equation, and which determines time evolution of a density operator. Arbitrary physical observables can then be calculated as expectation values with these time-evolved (quasi)probability functions.

Among various possible phase space representations, our numerical calculations rely on the Truncated Wigner Approximation (TWA) which evolved from quantum optics applications [56, 57]. In explaining phase decoherence in 1D optical lattices, the application of the GPE to such a system is limited to shallow lattices and low temperatures unless used in a full 3D approach that includes transverse excited modes [15]. However, the TWA can be used to model dephasing of (single-component) BECs in 1D optical lattices [16, 58].

From the point of view of numerical analysis, however, no single method is sufficient to describe all possibilities of dynamics. For example, the TWA has

been known to be a good approximation only for systems with highly occupied modes [17], since the approximation taken in TWA is dropping third or higher order terms. Thus, for comparison, we employ the positive P representation which, unlike the TWA, is known to represent exact quantum mechanical behaviors, though it is often subject to large deviations from mean trajectories in phase space.

Using the above mentioned representations, we investigate relative phase coherence between lattice wells during a phase transition (for a phase decoherence mechanism, see [34–36, 59]). Experimental studies on phase coherence properties of BECs have relied mainly on time-of-flight images taken after the release of traps and the analysis of visibilities of the interference patterns. The first-order correlations between two adjacent sites calculated in this study are closely related to such visibilities of the interference pattern of condensates released from optical lattices.

The following chapters in this dissertation are organized as below: In Chapter 2, we introduce phase space dynamics, which will be a framework for later application to BECs in optical lattices. We begin by dealing with a concept of characteristic functions and quasiprobability distribution functions as their conjugate functions. The time evolution of such a distribution function is provided by a Fokker-Plank equation. We then translate it into a stochastic differential equation by which one can identify a term corresponding to a classical Gross-Pitaevskii equation and another term corresponding to quantum noise.

In Chapter 3, we apply the phase space method dealt in the previous chapter to a system of two-component BECs, and delve into several branches of

phase space representations. There are a few different ways to define representations, depending on the definitions of integration measures. Among several candidates of phase space representations, we discuss a truncated Wigner representation, a positive P representation and a hybrid model of both representations along with their characteristics. We then prepare an initial state in phase spaces, which includes Bogoliubov quasiparticles (for a review, see [60]).

Chapter 4 shows numerical algorithms implemented in this work, which include a Monte Carlo method and its variations with improved convergence. Since the number of realizations required for a simulation is typically large, efficient algorithms are key ingredients, among which we develop a stratified sampling and an antithetic variate method suited to our BEC calculations. In addition to that, we modify a commonly-used split-operator method to adapt it to coupled-mode systems with noise fields. A dimensionless one-dimensional Gross-Pitaevskii equation is explained too.

The main discussion of phase coherence for various systems is presented in Chapter 5, including cases of one component BECs and two component BECs. The dependence of coherence loss on various experimental parameters, i.e., optical lattice heights, ramp-up times are our first interest for one-component BEC. Then, we compare the TWA method and the hybrid method. For two-component BECs, we first consider how change in the fraction of each component affects phase coherence. An optical lattice that is effective for only one component is ramped up. The other component then sees an effective lattice from the mean-field potential associated with the first component. We consider a range of density ratios of the two components and also a range of lattice heights for the component exposed to the optical lattice, in order to

shed light on the variation of coherence and fragmentation.

We adopt a simple Gaussian variational ansatz for single-particle Wannier functions to explain the qualitative behavior of fragmentation of matter-waves in the above setups. We find that the model shows a good agreement with the trend of fragmentation inferred from the above two TWA calculations. To check further the validity of this model, we investigate a different regime where the second component previously not exposed to a lattice is now fragmented by its own optical lattice, which is displaced a half-period from the original lattice for the first component.

Finally, we conclude all remarks in Chapter 6, with a summary of analysis.

Chapter 2

Phase Space Dynamics

2.1 Phase Space Representations

The Gross-Pitaevskii Equation (GPE) is a classical mean-field equation that describes a wavefunction of Bose-Einstein condensates. Even though Bose-Einstein condensation is a quantum mechanical phenomenon, its treatment by semiclassical mean-field theories has been successful in describing many aspects of the system including phase coherence, vortices, etc. That was partly because quantum fluctuation and thermal fluctuation are small for coherent BECs at $T = 0$ with a large number of bosons. In that case, it resembles a classical state, so it occupies a restricted region in phase space, which is peaked at a point corresponding to a semiclassical mean-field. We can write the wavefunction as

$$\psi(\mathbf{x}) = \sqrt{\rho(\mathbf{x})}e^{i\phi(\mathbf{x})}, \tag{2.1}$$

so it can explain the phase coherence property of Bose Einstein condensates [61].

This approximation to classical fields, however, is not sufficient to describe a system under a phase transition in which effects of quantum fluctuation of the system become strong. Quantum mechanical treatment is required for proper explanation of phase decoherence during a quantum phase transition such as superfluid-Mott insulator transition. While classical particles are represented by a fixed point in phase space, an ensemble of particles in quantum mechanics is represented by a quasiprobability distribution in that space.

As an analogue to the dynamics of a pure-state quantum-mechanical system which is obtained by the Schrödinger equation, the dynamics of a mixed-state quantum-mechanical system (or the time evolution of its density operator) is determined by a master equation for the corresponding probability. In general, an analytic integration of a density operator over time is difficult to attain.

Instead of doing that, it is often useful to represent the density operator as a probability distribution over phase space and then obtain information about its dynamics in terms of evolution of such a probability distribution function. This is called a 'Phase Space Representation' method [62]. There is a discussion of relationship between phase space representations(especially a truncated Wigner approximation) and the Feynman's path integral representation [63].

Since we will consider weakly-interacting BECs in a harmonic potential, we focus on phase space representations for a quantum state in harmonic potentials, in which a creation and annihilation operator, $\hat{a}^\dagger, \hat{a}$ are defined. Before we discuss the phase space representations in detail, we first deal with a coher-

ent state. A coherent state [64, 65] is an eigenstate of an annihilation operator in quantum harmonic oscillators, which is widely used in the quantum optics context. As explained in [35, 66], a BEC can be considered as a coherent state: first of all, a BEC wavefunction has a macroscopic order parameter, $\langle\psi|\hat{a}|\psi\rangle$ that is robust in long time scales, so such a property is satisfied by the coherent state by definition, $\hat{a}|\psi\rangle = a|\psi\rangle$, where a is an order parameter. Second, a wavefunction of superfluid exhibits macroscopic quantum phase coherence [67] which can be explained in the format of coherent states.

A coherent state for the superfluid BEC has been adopted in the study of nonequilibrium dynamics of one-component BECs in [16, 68]. The coherent state description to represent a superfluid phase has been successful also in describing the superfluid fraction of ^4He [69].

One property of a coherent state is that it is the minimum uncertainty state that satisfies the Heisenberg uncertainty bound, $\Delta x \Delta p = \hbar$, thus it is the quantum state closest to a classical mean-field. In general, a minimum uncertainty wavepacket is the wavefunction that mimics a classical system. Quantum fluctuation of a coherent state in phase space is spread around an expectation value corresponding to the classical mean value, but the spread of a coherent state is minimized, compared to other general quantum states which have broader variance.

Now, we continue to discuss phase space representations. There are several different kinds of distribution functions, for example, P, Q, and Wigner distribution function, differing by their definitions of characteristic functions. A characteristic function completely defines a distribution function, and the former is a Fourier transform of the latter and vice versa. The characteris-

tic functions for the single mode P, Q, and Wigner distribution functions for harmonic oscillators are the following [70]:

$$\begin{aligned}
\chi_P(\lambda,\lambda^*) &= \mathrm{Tr}\big[\hat{\rho}\mathrm{e}^{-\lambda^*\hat{\mathrm{a}}}\mathrm{e}^{\lambda\hat{\mathrm{a}}^\dagger}\big], \\
\chi_Q(\lambda,\lambda^*) &= \mathrm{Tr}\big[\hat{\rho}\mathrm{e}^{\lambda\hat{\mathrm{a}}^\dagger}\mathrm{e}^{-\lambda^*\hat{\mathrm{a}}}\big], \\
\chi_W(\lambda,\lambda^*) &= \mathrm{Tr}\big[\hat{\rho}\mathrm{e}^{\lambda\hat{\mathrm{a}}^\dagger-\lambda^*\hat{\mathrm{a}}}\big],
\end{aligned} \tag{2.2}$$

where $\hat{\rho}$ is a density operator, $\hat{a}$ is an annihilation operator, and $\hat{a}^\dagger$ is a creation operator. P, Q, W denotes the P, Q, and Wigner distribution, respectively.

These characteristic functions differ by their ordering of operators. These quantum characteristic functions are moment-generating functions analogous to classical characteristic functions, so that first-order (average), second-order (variance), and higher-order moments are first, second, and corresponding-order derivatives of moment-generating functions with respect to the variable, λ evaluated at the origin. Normally-ordered moments (all creation operators are left, all annihilation operators are right), anti-normally ordered moments, symmetrically-ordered moments are calculated using the P, Q, and Wigner characteristic function respectively as follows:

$$\begin{aligned}
\langle \hat{a}_i^{\dagger m}\hat{a}_j^n\rangle &= (-1)^n \frac{\partial^{m+n}}{\partial(\lambda_i)^m\partial(\lambda_j^*)^n}\chi_P(\lambda,\lambda^*)|_{\lambda=0}, \\
\langle \hat{a}_i^{m}\hat{a}_j^{\dagger n}\rangle &= (-1)^m \frac{\partial^{m+n}}{\partial(\lambda_i^*)^m\partial(\lambda_j)^n}\chi_Q(\lambda,\lambda^*)|_{\lambda=0}, \\
\langle \hat{a}_i^{\dagger m}\hat{a}_j^n\rangle_{\mathrm{sym}} &= (-1)^n \frac{\partial^{m+n}}{\partial(\lambda_i)^m\partial(\lambda_j^*)^n}\chi_W(\lambda,\lambda^*)|_{\lambda=0},
\end{aligned} \tag{2.3}$$

where the subscript, 'sym', means that the product of operators is symmetri-

cally ordered. For example,

$$\begin{aligned}\{\hat{a}^2(\hat{a}^\dagger)^2\}_{sym} &= \frac{1}{6}\Big[(\hat{a}^\dagger)^2\hat{a}^2+\hat{a}^\dagger\hat{a}\hat{a}^\dagger\hat{a}+\hat{a}^\dagger\hat{a}^2\hat{a}^\dagger \\ &\quad +\hat{a}(\hat{a}^\dagger)^2\hat{a}+\hat{a}\hat{a}^\dagger\hat{a}\hat{a}^\dagger+\hat{a}^2(\hat{a}^\dagger)^2\Big]. \end{aligned} \tag{2.4}$$

In many cases, it is difficult to work directly with these moment generating functions for the purpose of calculating ordered moments and their time evolutions, since differentiation is often harder than integration. In such cases, it is preferred to use transformed functions which are easier to calculate. As noted above, the P, Q, and Wigner functions are Fourier transform of the above characteristic functions with respect to conjugate variables α, α^*, which are eigenvalues of coherent states. These probability functions are defined as the following:

$$\begin{aligned} P(\alpha,\alpha^*) &= \frac{1}{\pi^2}\int d^2\lambda e^{-\lambda\alpha^*+\lambda^*\alpha}\chi_P(\lambda,\lambda^*), \\ Q(\alpha,\alpha^*) &= \frac{1}{\pi^2}\int d^2\lambda e^{-\lambda\alpha^*+\lambda^*\alpha}\chi_Q(\lambda,\lambda^*), \\ W(\alpha,\alpha^*) &= \frac{1}{\pi^2}\int d^2\lambda e^{-\lambda\alpha^*+\lambda^*\alpha}\chi_W(\lambda,\lambda^*), \end{aligned} \tag{2.5}$$

where all these quasi-probability functions are transformed with the same integration measures. In terms of these functions, the work of finding ordered moments is shifted from derivatives of characteristic functions to integrals of probability functions, which will make the calculation easier:

$$\langle\hat{a}_i^{\dagger m}\hat{a}_j^n\rangle = \int d^2\alpha P(\alpha,\alpha^*)\alpha_i^{*m}\alpha_j^n,$$

$$\begin{aligned} \langle \hat{a}_i^m \hat{a}_j^{\dagger n} \rangle &= \int d^2\alpha Q(\alpha, \alpha^*) \alpha_i^m \alpha_j^{*n}, \\ \langle \hat{a}_i^{\dagger m} \hat{a}_j^n \rangle_{\text{sym}} &= \int d^2\alpha W(\alpha, \alpha^*) \alpha_i^{*m} \alpha_j^n. \end{aligned} \tag{2.6}$$

Expectation values are obtained by integrating phase space variables with distributions that look like probability functions. The distribution functions, P, Q, and Wigner functions are quasi-probability functions analogous to, but not completely the same as classical probability functions. Here, the term 'quasi-' needs attention, since the functions are not completely semidefinite positive for all α. We will see such an example later. Nevertheless, we will drop the 'quasi-' and use both a 'probability' function and a 'distribution' function interchangeably.

The above transformation from a density operator to a probability function can be reversed using an operator form. For example, a density operator and a distribution function are related in a P representation as the following:

$$\hat{\rho} = \int |\alpha\rangle\langle\alpha| P(\alpha, \alpha^*), \tag{2.7}$$

where $|\alpha\rangle$ is a coherent state.

2.2 Time Evolution of Probability Functions

We first note that a probability function can be derived from a density operator: we take a trace over a density operator to obtain a characteristic function(Eq. 2.2), which can be transformed to a probability function(Eq. 2.5). Note that the trace and the transformation are all linear in a density

operator. Therefore, in any cases, time evolution of probability functions is obtained by finding a Lindblad master equation first (time evolution equation) for density matrices and then applying a series of transformations to the obtained equation of motion.

In general, a master equation is a first-order differential equation that determines the time evolution of a probability of a system to be in a specific state, obtained by applying a transition matrix to a set of all possible states. For a system with a discrete set of states, the master equation becomes,

$$\frac{dP_i}{dt} = \sum_j T_{ij} P_j, \tag{2.8}$$

where P_i is the probability for the system to lie in state i, and T_{ij} is a transition rate from state j to state i.

The Lindblad master equation is a generalized master equation for density matrices. Since the Lindblad equation can describe nonunitary evolution of a density matrix, it is more general than the above-mentioned master equation (Eq. 2.8) and so its role is not restricted to just describe the time evolution of probability distributions, but extended to include interaction between a system and its environment: diagonal elements of a density matrix correspond to populational probabilities of states and its off-diagonal elements contain quantum information about coherence between two states. The Lindblad master equation for a density matrix ρ is

$$\frac{d}{dt}\hat{\rho} = -\frac{i}{\hbar}[H, \hat{\rho}] + \sum_{n,m} h_{n,m}(-\hat{\rho}L_m^\dagger L_n - L_m^\dagger L_n \hat{\rho} + 2L_n \hat{\rho} L_m^\dagger), \tag{2.9}$$

where H is a Hamiltonian, L_m are Lindblad operators that consist of a set of orthonormal basis, matrix elements $h_{n,m}$ determine the dynamics of states similarly as the transition matrix does in classical dynamics. A main distinction from a plain Hamiltonian without L_m is the fact that L_m can now describe dissipative interaction with an environment. For example, a collection of harmonic oscillators damped by a photon emission process is described by the following:

$$\frac{d}{dt}\hat{\rho} = -\frac{i}{\hbar}[H, \hat{\rho}] + \Gamma(-\frac{1}{2}\hat{\rho}a^\dagger a - \frac{1}{2}a^\dagger a\hat{\rho} + a\hat{\rho}a^\dagger), \tag{2.10}$$

where H is a Hamiltonian for simple harmonic oscillators, Γ is a decay rate of the oscillator by photon emission.

The equation of motion for quasi-probability functions is obtained by noting that the above master equation (Eq. 2.9 and Eq. 2.10) acts on the density operators by multiplying a product of creation and annihilation operators. Because of the property of linear transformation from a density operator to a probability function (Eq. 2.2 and Eq. 2.5) and the definition of moments(Eq. 2.6), one can expect that the equation of motion for the quasi-probability function to be similarly in a form, obtained by actions of multiplying the quasi-probability function $P(\alpha, \alpha^*)$ by coherent state amplitudes, α, α^*, which are expectation values of the annihilation and the creation operator ($\alpha = \langle\alpha|\hat{a}|\alpha\rangle$, $\alpha^* = \langle\alpha|\hat{a}^\dagger|\alpha\rangle$).

In fact, in a similar way as there is a correspondence between quantum operators, $\hat{a}, \hat{a}^\dagger$, and coherent state amplitudes, α, α^*, there is a correspondence between algebra of density operator $\hat{\rho}$ and algebra of probability function

$P(\alpha, \alpha^*)$. For the P representation,

$$\begin{aligned}
\hat{a}\hat{\rho} &\leftrightarrow \alpha P(\alpha, \alpha^*), \\
\hat{\rho}\hat{a}^\dagger &\leftrightarrow \alpha^* P(\alpha, \alpha^*), \\
\hat{a}^\dagger\hat{\rho} &\leftrightarrow (\alpha^* - \frac{\partial}{\partial\alpha})P(\alpha, \alpha^*), \\
\hat{\rho}\hat{a} &\leftrightarrow (\alpha^* - \frac{\partial}{\partial\alpha^*})P(\alpha, \alpha^*),
\end{aligned} \tag{2.11}$$

and for the Q representation,

$$\begin{aligned}
\hat{a}\hat{\rho} &\leftrightarrow (\alpha^* + \frac{\partial}{\partial\alpha})Q(\alpha, \alpha^*), \\
\hat{\rho}\hat{a}^\dagger &\leftrightarrow (\alpha^* + \frac{\partial}{\partial\alpha^*})Q(\alpha, \alpha^*), \\
\hat{a}^\dagger\hat{\rho} &\leftrightarrow \alpha^* Q(\alpha, \alpha^*), \\
\hat{\rho}\hat{a} &\leftrightarrow \alpha^* Q(\alpha, \alpha^*),
\end{aligned} \tag{2.12}$$

and finally for the Wigner representation,

$$\begin{aligned}
\hat{a}\hat{\rho} &\leftrightarrow (\alpha^* + \frac{1}{2}\frac{\partial}{\partial\alpha})W(\alpha, \alpha^*), \\
\hat{\rho}\hat{a}^\dagger &\leftrightarrow (\alpha^* + \frac{1}{2}\frac{\partial}{\partial\alpha^*})W(\alpha, \alpha^*), \\
\hat{a}^\dagger\hat{\rho} &\leftrightarrow (\alpha^* - \frac{1}{2}\frac{\partial}{\partial\alpha})W(\alpha, \alpha^*), \\
\hat{\rho}\hat{a} &\leftrightarrow (\alpha^* - \frac{1}{2}\frac{\partial}{\partial\alpha})W(\alpha, \alpha^*).
\end{aligned} \tag{2.13}$$

In order to see how this equivalence can be derived, we first note the

definition of coherent states and Bargmann states:

$$\hat{a}|\alpha\rangle = \alpha|\alpha\rangle, \tag{2.14}$$

$$||\alpha\rangle \equiv \exp\left(\frac{1}{2}|\alpha|^2\right)|\alpha\rangle = \sum_{n=0}^{\infty}\frac{\alpha^n}{\sqrt{n!}}|n\rangle, \tag{2.15}$$

where $|\alpha\rangle$ is a coherent state defined to be an eigenstate of an annihilation operator, and $||\alpha\rangle$ is a Bargmann state. Then,

$$\begin{aligned}\hat{a}^\dagger||\alpha\rangle &= \sum_{n=0}^{\infty}\frac{\alpha^n}{\sqrt{n!}}\sqrt{n+1}|n+1\rangle \\ &= \frac{\partial}{\partial\alpha}||\alpha\rangle.\end{aligned} \tag{2.16}$$

Beginning with the definition of a density operator in the P representation, a density operator can be rewritten in terms of Bargmann states as the following:

$$\begin{aligned}\hat{\rho} &= \int d^2\alpha|\alpha\rangle\langle\alpha|P(\alpha,\alpha^*) \\ &= \int d^2\alpha||\alpha\rangle\langle\alpha||e^{-|\alpha|^2}P(\alpha,\alpha^*),\end{aligned} \tag{2.17}$$

and applying a creation operator on both sides and using Eq. 2.16,

$$\begin{aligned}\hat{a}^\dagger\hat{\rho} &= \int d^2\alpha\frac{\partial}{\partial\alpha}(||\alpha\rangle\langle\alpha||)e^{-|\alpha|^2}P(\alpha,\alpha^*) \\ &= \int d^2\alpha||\alpha\rangle\langle\alpha||e^{-|\alpha|^2}(\alpha^* - \frac{\partial}{\partial\alpha})P(\alpha,\alpha^*).\end{aligned} \tag{2.18}$$

Likewise, we can extend this single mode case to multimodes or functional forms. For example, in the P representation, such operator correspondence

can be written as:

$$\begin{aligned}
\hat{\psi}\hat{\rho} &\leftrightarrow \psi P(\psi,\psi^*) \\
\hat{\rho}\hat{\psi}^\dagger &\leftrightarrow \psi^* P(\psi,\psi^*) \\
\hat{\psi}^\dagger\hat{\rho} &\leftrightarrow (\psi^* - \frac{\partial}{\partial\psi})P(\psi,\psi^*) \\
\hat{\rho}\hat{\psi} &\leftrightarrow (\psi - \frac{\partial}{\partial\psi^*})P(\psi,\psi^*),
\end{aligned} \tag{2.19}$$

where $\hat{\psi}, \hat{\psi}^\dagger$ denote field operators, and ψ, ψ^* the corresponding c-number complex amplitudes.

Using these operator correspondences, we find a Fokker-Planck equation for a P distribution function, which works the same as a master equation for a density operator. For a weakly-interacting BEC as an example [71],

$$\begin{aligned}
\frac{\partial P}{\partial t} = \int_{-\infty}^{\infty} dx \Big[& i\frac{\delta}{\delta\psi(x)}\Big\{H_0\psi(x) + g|\psi(x)|^2\psi(x)\Big\} \\
& -\frac{i}{2}\frac{\delta^2}{\delta\psi^2(x)}g\psi^2(x)\Big]P(t) + c.c.
\end{aligned} \tag{2.20}$$

In general, a Fokker-Planck equation for a probability function f is written in terms of a drift vector, $D_i^{(1)}$, and a diffusion matrix, $[D^{(2)}D^{(2)T}]_{ij}$ as in [71]:

$$\begin{aligned}
\frac{\partial f(x,t)}{\partial t} &= -\sum_i \frac{\partial}{\partial x_i}[D_i^{(1)}(x,t)f(x,t)] \\
&\quad + \frac{1}{2}\sum_i\sum_j \frac{\partial^2}{\partial x_i \partial x_j}[D^{(2)}D^{(2)T}]_{ij}f(x,t).
\end{aligned} \tag{2.21}$$

The corresponding physical state might be naively regarded as following a deterministic trajectory in phase space. However, it turns out that the state

follows a stochastic trajectory, and so care should be taken since it is a probability distribution that evolves in time, not a single point following a trajectory in classical phase space. Furthermore, the diffusion matrix, $D^{(2)}D^{(2)T}$ contains quantum noises, which are completely unpredictable random fluctuations. The presence of this matrix makes the dynamic process stochastic, which will be briefly discussed in the next section.

In fact, the Fokker-Plank equation can be essentially derived beginning with a 'Stochastic Differential Equation(SDE)'. In order to see why the dynamics is characterized by stochastic processes rather than ordinary partial differential equations, we note that the above equation 2.21 can be translated into the following differential equation form:

$$dX_i(x,t) = D_i^{(1)}(x,t)dt + D_i^{(2)}dW(t), \tag{2.22}$$

where $X_i(x,t)$ is a physical state in spacetime (x,t), and $W(t)$ is a stochastic Wiener process, which is also commonly known as a Brownian motion. I will not discuss the details of its derivation, but from this equation, one can notice that $D_i^{(1)}(x,t)$ and $D_i^{(2)}(x,t)$ are the drift and the diffusion term in the above Fokker-Plank equation, respectively. Depending on a choice of diffusion matrices, the characteristics of stochastic processes varies.

2.3 Stochastic Differential Equation

A stochastic differential equation is a differential equation with stochastic process terms, and a stochastic process is a random process that results in

a sequence of random variables in a nondeterministic way. The most well-known example of a stochastic process is Brownian motion (Wiener process) which was introduced to describe a motion of dust particles in the air, or a motion of impurities in a medium. A Brownian motion is defined as a continuous-time stochastic process with normally distributed noises. Each noise at each instant of time is independent to each other and its distribution follows the normal distribution, so that a large move is less probable than a small move. Another example of stochastic processes is a Markov process, which has a memorylessness property. The memorylessness property means that a noise at an instant of time does not depend on the previous history of the process. Many stochastic motions are within the category of quantum Markov processes.

A stochastic differential equation is typically of the form,

$$dX_t = \mu(X_t, t)dt + \sigma(X_t, t)dW_t, \tag{2.23}$$

or equivalently,

$$\frac{dX_t}{dt} = \mu(X_t, t) + D(X_t, t)\xi(t), \tag{2.24}$$

where X_t is a state variable, dW_t is a stochastic process term, $\mu(X_t, t)$ is a drift term, and $D(X_t, t)$ is a diffusion term. The noise, $\xi(t)$ has the property that

$$\xi(t)\xi(t') = \delta(t - t'), \tag{2.25}$$

which means that the noises are uncorrelated in time.

In general, an analytic solution to a stochastic differential equation is hard to obtain. The simplest solvable example of common Wiener processes is a geometric Brownian motion,

$$dX_t = \mu X_t dt + \sigma X_t dW_t, \tag{2.26}$$

where μ and σ are constants. It needs to be noted that each term on the righthand side of the above equation is proportional to the stochastic variable X_t, so that it can be transformed to the following:

$$\frac{dX_t}{X_t} = \mu dt + \sigma dW_t. \tag{2.27}$$

The solution to the above equation is,

$$X(t) = X(0) \exp\left[(\mu - 0.5\sigma^2)t + \sigma\sqrt{t}z\right], \tag{2.28}$$

where $X(0)$ is an initial boundary condition, $\mu - 0.5\sigma^2$ is a deterministic drift rate, $\sigma\sqrt{t}$ is a diffusion or volatility, and z is a normally-distributed random variable independent of time. Note that the volatility (noise) is increasing in time.

The main difference between an ordinary differential equation and the above differential equation is that the latter contains a stochastic random noise term in the above equation. It represents quantum fluctuation present in the dynamics, whose distribution looks different depending on different representations. Another difference is that the term which is linear in time is

not equal to μ, which is expected for an ordinary differential equation with no noise($\sigma = 0$). This fact comes from the Ito's lemma which will be explained in the next section.

2.4 Ito's Lemma

Ito's lemma is a mathematical tool to facilitate calculating a differential of a function containing stochastic processes. The differentiation of a function with respect to time in stochastic calculus is different from in ordinary calculus. The Ito's lemma states that the differential of a function for the drift-diffusion process (Eq. 2.28) is

$$df(X_t, t) = \Big[\frac{\partial f}{\partial t} + \mu\frac{\partial f}{\partial X} + \frac{1}{2}\sigma\frac{\partial^2 f}{\partial X^2}\Big]dt + \sigma\frac{\partial f}{\partial X}dW_t. \tag{2.29}$$

We now see that a function of a stochastic process becomes also another stochastic process, since this equation includes the same stochastic process term(dW_t) but with a different coefficient, $\sigma\partial f/\partial X$. The major difference due to the presence of stochastic process dW_t is that the drift term which is proportional to dt is now also displaced by the random noise. Therefore, the random process not only modifies the dynamics in a microscopic scale (the diffusion term), but also in a macroscopic scale (the drift term).

For example, a differential equation as in the above equation without a stochastic term follows a nondecreasing exponential growth for $\mu > 0$:

$$dX_t = \mu X_t dt + 0 \tag{2.30}$$

$$X(t) \quad = \quad X(0)\exp(\mu t). \tag{2.31}$$

The comparison between this ordinary differential and the stochastic differential shows that the average growth rate is also affected by the variance of fluctuation.

Now that we reviewed the rule of differentiation which is similar to the chain rule of ordinary calculus, we also need a rule of integration for a stochastic process. When we define an ordinary Rieman integral, an integration domain is divided into n subintervals and the area of rectangles is summed over the partitioned intervals. A stochastic integral is defined similarly. A stochastic integral includes two terms, each corresponding to a drift term, and a diffusion term.

$$X_t = X_0 + \int_0^t \mu_s ds + \int_0^t \sigma_s dW_s, \tag{2.32}$$

where the latter diffusion integral term is defined by a Riemann-Stieltjes integral and the above equation is called the Ito stochastic integral. For example, a nontrivial integral of polynomials is of the form:

$$\int_{t_0}^t W(s)^n dW(s) = \frac{1}{n+1}\left[W(t)^{n+1} - W(t_0)^{n+1}\right] - \frac{n}{2}\int_{t_0}^t W(t)^{n-1}dt. \tag{2.33}$$

In addition to that, one of the most important rules in stochastic calculus is the following:

$$(dW_t)^2 = dt \tag{2.34}$$

$$(dW_t)^n = 0 \qquad for \;\; n \neq 2. \tag{2.35}$$

This property allows to identify a Fokker-Plank equation from a SDE as a sum of a drift term which is linear in dt and a noise term which is proportional to $dW_t = \sqrt{dt}$. All higher order terms in the Fokker-Plank equation are not usual stochastic noises, and the second order term is the only stochastic noise.

Chapter 3

Two-Component BECs in Phase Space Representations

3.1 Two-Component GPE

In this chapter, we study applicable models of phase space representations and adapt them to two-component Bose-Einstein condensates. We consider that a mixture of two Bose-Einstein condensates is confined in the same harmonic trap, where the two components are two hyperfine states of the same species or two different species. Since the discussion of one-component BECs in phase space is similar to the two-component cases here, we do not repeat such a case. The harmonic trap potential is configured as, $V_{har}(\boldsymbol{x}, t) = \frac{1}{2}m(\omega^2 x^2 + \omega_\perp^2(y^2 + z^2))$ with a weak longitudinal trap frequency (ω) and a strong transverse trap frequency ($\omega_\perp > \omega$), so that the BECs are cigar-shaped along the longitudinal direction. Henceforth, the effective 1D two-component

second-quantized Hamiltonian for the system becomes

$$\begin{aligned}\hat{H} &= \sum_{i=A,B}\int d\boldsymbol{x}\hat{\psi}_i^\dagger(\boldsymbol{x})\hat{L}_i\hat{\psi}_i(\boldsymbol{x}) \\ &\quad +\frac{1}{2}\sum_{i=A,B} g_{ii}^{(1D)}\int d\boldsymbol{x}\hat{\psi}_i^\dagger(\boldsymbol{x})\hat{\psi}_i^\dagger(\boldsymbol{x})\hat{\psi}_i(\boldsymbol{x})\hat{\psi}_i(\boldsymbol{x}) \\ &\quad +g_{AB}\int d\boldsymbol{x}\hat{\psi}_A^\dagger(\boldsymbol{x})\hat{\psi}_B^\dagger(\boldsymbol{x})\hat{\psi}_A(\boldsymbol{x})\hat{\psi}_B(\boldsymbol{x}), \end{aligned} \tag{3.1}$$

and the L_i is defined as,

$$L_i = -\frac{\hbar^2\nabla^2}{2m_i} + V_{h,i}(\boldsymbol{x}) + V_{o,i}(\boldsymbol{x},t) - \mu_i. \tag{3.2}$$

Here, we label the first species as 'A' and the second one as 'B'. For each species, m_i is the particle mass, $V_{h,i}(\boldsymbol{x}) = m_i\omega^2 x^2/2$ is an external harmonic trap potential, $V_{o,i}(\boldsymbol{x},t)$ is a time-varying state-dependent optical lattice potential along the axial direction, and μ_i is the chemical potential. Here, we consider the case that the state-dependent lattice is applied to the component A and B differently. Interaction strengths are defined as:

$$\begin{aligned} g_{AA} &= \frac{4\pi\hbar^2 a_{AA}}{m_A}, \\ g_{BB} &= \frac{4\pi\hbar^2 a_{BB}}{m_B}, \\ g_{AB} &= 2\pi\hbar^2 a_{AB}(\frac{1}{m_A}+\frac{1}{m_B}), \end{aligned} \tag{3.3}$$

where g_{AA} and g_{BB} are each intraspecies interaction strength, g_{AB} is an interspecies interaction strength between species A and B, and a_{AA}, a_{BB}, a_{AB} are scattering lengths respectively.

The equation of motion for the state i field operator, $\psi_i(\boldsymbol{x})$, is

$$\begin{aligned} i\frac{d}{dt}\hat{\psi}_i &= \hat{H}_i\hat{\psi}_i \\ &\equiv L_i\hat{\psi}_i + \sum_j g_{ji}\hat{\psi}_j^\dagger\hat{\psi}_j\hat{\psi}_i, \end{aligned} \tag{3.4}$$

which is the two-component Gross-Pitaevskii equation.

3.2 Truncated Wigner Approximation

Now, we focus on the Wigner representation for the BEC in the trap. One of the properties of a Wigner distribution function is that it exists for all density matrices, even though not all of them are easy to find or useful. For example, the Wigner function for a coherent state density operator, $\rho = |\alpha_0\rangle\langle\alpha_0|$, is as follows [16]:

$$W(\alpha,\alpha^*) = \frac{2}{\pi}\exp\big[-2|\alpha-\alpha_0|^2\big], \tag{3.5}$$

and for a thermal state [16],

$$W(\alpha,\alpha^*) = \frac{2}{\pi}\tanh\Big[\frac{\hbar\omega}{2kT}\Big]\exp\Big[-2|\alpha|^2\tanh\big(\frac{\hbar\omega}{2kT}\big)\Big], \tag{3.6}$$

and for a Mott insulator state [72],

$$W_n(\alpha,\alpha^*) = \frac{2(-1)^n}{\pi}\exp\left(-2|\alpha|^2\right)L_n(4|\alpha|^2), \tag{3.7}$$

for the number state $|n\rangle$. Here, L_n is a Laguerre polynomial.

For a BEC, the master equation for a Wigner function is similarly obtained as for the P representation [16]:

$$\begin{aligned}\frac{\partial W(\psi,\psi^*)}{\partial t} &= \int_{-\infty}^{\infty} dx \frac{i}{\hbar}\Big[\frac{\delta}{\delta\psi(x)}\Big\{H_0\psi(x)+g\big(|\psi(x)|^2-1\big)\psi(x)\Big\} \\ &\quad -\frac{1}{4}\frac{\delta^3}{\delta^2\psi^2(x)\delta\psi^*(x)}\psi(x)\Big]W(\psi,\psi^*)+h.c. \end{aligned} \tag{3.8}$$

In the Wigner representation, we can calculate ensemble averages of correlation functions of physical interest, for example, $\langle\hat{a}^\dagger\hat{a}\rangle_{\rm sym}$, $\langle\hat{a}^\dagger\hat{a}^\dagger\hat{a}\hat{a}\rangle_{\rm sym}$, where the averages are taken over a whole set of realizations. More often than not, however, the correlation functions we are interested in are normally ordered, not symmetrically ordered as required for Wigner representation. For simple cases, we can derive a symmetrically ordered correlation function from a normally ordered correlation function as follows. For this purpose, we expand an arbitrary operator into a normally ordered operator,

$$\hat{O}(\hat{a},\hat{a}^\dagger)=\sum_{n,m} c_{nm}\hat{a}^{\dagger n}\hat{a}^m, \tag{3.9}$$

where c_{nm} is an expansion coefficient corresponding to each normally order operator. Then, using the set of coefficients, we find the stochastic average of the correlation function in the Wigner representation [72],

$$\begin{aligned} O_W(\alpha,\alpha^*) &= \langle O(\hat{a},\hat{a}^\dagger)\rangle_{\rm sym} \\ &= \sum_{n,m}(-1)^m\Big(\frac{\partial}{\partial\lambda}+\frac{\lambda^*}{2}\Big)^n\Big(\frac{\partial}{\partial\lambda^*}+\frac{\lambda}{2}\Big)^m e^{\lambda\alpha^*-\lambda^*\alpha}|_{\lambda=\lambda^*=0} \end{aligned} \tag{3.10}$$

However, there is a numerical limit beyond which the truncated Wigner

method does not remain valid. The TWA method must satisfy [72]

$$\frac{M}{2} << N_C. \tag{3.11}$$

In other words, the number of quantum noise modes (M) must be much smaller than the number of particles in the condensate mode (N_C). The factor of 1/2 comes from the fact that in the zero temperature ($T = 0$), the fluctuation width of each quantum noise becomes 1/2 from Eq. 3.6. This condition is satisfied in this work, since the number of Bogoliubov excitation modes is gauged to be much smaller compared to the atom number in the condensate mode ($N_C = 10^3 \sim 10^4$). If this condition should be violated, then the truncated Wigner method is prone to unexpected large excursion in numerical simulations.

The Fokker-Planck equation for the Wigner quasiprobability distribution yields the time evolution equation:

$$\begin{aligned}\frac{\partial W(\boldsymbol{\psi}, \boldsymbol{\psi}^*)}{\partial t} &= \int dz \frac{i}{\hbar} \sum_{i,j=A,B} \Big\{ \frac{\delta}{\delta \psi_i(z)} \big[(L_i \\ &\quad + g_{ij} \big(|\psi_j(z)|^2 - d_{ij} \big) \psi_i(z) \big] \\ &\quad - \frac{g_{ij}}{4} \frac{\delta}{\delta \psi_i(z)} \frac{\delta}{\delta \psi_j(z)} \frac{\delta}{\delta \psi_j^*(z)} \psi_i(z) \Big\} W(\boldsymbol{\psi}, \boldsymbol{\psi}^*) + h.c.,\end{aligned} \tag{3.12}$$

where $\boldsymbol{\psi} = (\psi_A, \psi_B)^T$, and L_i is

$$L_i = -\frac{\hbar^2 \nabla^2}{2m_i} + V_{h,i}(\boldsymbol{x}) + V_{o,i}(\boldsymbol{x}, t) - \mu_i, \tag{3.13}$$

as defined in Eq. 3.2, and $d_{ij} = 1$ (or 1/2) if $i = j$ (or $i \neq j$).

Now we derive the Fokker-Plank equation for the Wigner distribution of two-component BECs. The von Neumann's time-evolution equation for a density operator is

$$\begin{aligned}
\frac{d\hat{\rho}}{dt} &= \frac{1}{i\hbar}[\hat{H},\hat{\rho}] \\
&= \frac{1}{i\hbar}\sum_{i=A,B}\int d^3x\big(\hat{\psi}_i^\dagger(x)\hat{L}_i\hat{\psi}_i(x)\hat{\rho}-\hat{\rho}\hat{\psi}_i^\dagger(x)\hat{L}_i\hat{\psi}_i(x)\big) \\
&\quad +\frac{1}{2i\hbar}\sum_{i=A,B}g_{ii}\int d^3x\big(\hat{\psi}_i^\dagger(x)\hat{\psi}_i^\dagger(x)\hat{\psi}_i(x)\hat{\psi}_i(x)\hat{\rho} \\
&\quad -\hat{\rho}\hat{\psi}_i^\dagger(x)\hat{\psi}_i^\dagger(x)\hat{\psi}_i(x)\hat{\psi}_i(x)\big) \\
&\quad +\frac{1}{i\hbar}g_{AB}\int d^3x\big(\hat{\psi}_A^\dagger(x)\hat{\psi}_B^\dagger(x)\hat{\psi}_A(x)\hat{\psi}_B(x)\hat{\rho} \\
&\quad -\hat{\rho}\hat{\psi}_A^\dagger(x)\hat{\psi}_B^\dagger(x)\hat{\psi}_A(x)\hat{\psi}_B(x)\big). \qquad (3.14)
\end{aligned}$$

Some useful identities are operator correspondence rules for condensate operators,

$$\begin{aligned}
\hat{\psi}_i(x)\hat{\rho} &\Leftrightarrow \left(\psi_i(x)+\frac{1}{2}\frac{\delta}{\delta\psi_i^*(x)}\right)W(\boldsymbol{\psi},\boldsymbol{\psi}^*), \\
\hat{\psi}_i^\dagger(x)\hat{\rho} &\Leftrightarrow \left(\psi_i^*(x)-\frac{1}{2}\frac{\delta}{\delta\psi_i(x)}\right)W(\boldsymbol{\psi},\boldsymbol{\psi}^*), \\
\hat{\rho}\hat{\psi}_i(x) &\Leftrightarrow \left(\psi_i(x)-\frac{1}{2}\frac{\delta}{\delta\psi_i^*(x)}\right)W(\boldsymbol{\psi},\boldsymbol{\psi}^*), \\
\hat{\rho}\hat{\psi}_i^\dagger(x) &\Leftrightarrow \left(\psi_i^*(x)+\frac{1}{2}\frac{\delta}{\delta\psi_i(x)}\right)W(\boldsymbol{\psi},\boldsymbol{\psi}^*), \qquad (3.15)
\end{aligned}$$

and rules of functional derivatives,

$$\frac{\delta}{\delta\psi_j(y)}\psi_i(x) = \delta(x-y)\delta_{ij}, \qquad (3.16)$$

$$\frac{\delta}{\delta\psi_i(y)}\psi_i(x)F(\boldsymbol{\psi}(x)) \;=\; \delta(x-y)F(\boldsymbol{\psi}(x)) + \psi_i(x)\frac{\delta}{\delta\psi_i(y)}F(\boldsymbol{\psi}(x)). \tag{3.17}$$

By defining $c_i \equiv -\frac{\hbar^2}{2m_i}$ and $h_i(x,t) \equiv V_{h,i}(\boldsymbol{x}) + V_{o,i}(\boldsymbol{x},t) - \mu_i$, the first term of Eq. 3.14 becomes

$$\begin{aligned}
& \frac{1}{i\hbar}\sum_{i=A,B}\int d^3x\Big[\psi_i^\dagger(x)\Big(c_i\bigtriangledown^2 + h_i(x,t)\Big)\psi_i(x)\hat{\rho} \\
& -\hat{\rho}\psi_i^\dagger(x)\Big(c_i\bigtriangledown^2 + h_i(x,t)\Big)\psi_i(x)\Big] \\
\Leftrightarrow\; & \frac{1}{i\hbar}\sum_{i=A,B}\int d^3x\Big[\Big(\psi_i^*(x) - \frac{1}{2}\frac{\delta}{\delta\psi_i(x)}\Big) \\
& \Big\{c_i\bigtriangledown^2\Big(\psi_i(x) + \frac{1}{2}\frac{\delta}{\delta\psi_i^*(x)}\Big) + h_i(x,t)\Big(\psi_i(x) + \frac{1}{2}\frac{\delta}{\delta\psi_i^*(x)}\Big)\Big\} \\
& -\Big\{c_i\bigtriangledown^2\Big(\psi_i(x) - \frac{1}{2}\frac{\delta}{\delta\psi_i^*(x)}\Big) + h_i(x,t)\Big(\psi_i(x) - \frac{1}{2}\frac{\delta}{\delta\psi_i^*(x)}\Big)\Big\} \\
& \Big(\psi_i^*(x) + \frac{1}{2}\frac{\delta}{\delta\psi_i(x)}\Big)\Big]W(\boldsymbol{\psi},\boldsymbol{\psi}^*) \\
=\; & \frac{1}{i\hbar}\sum_{i=A,B}\int d^3x\Big[\psi_i^*(x)c_i\bigtriangledown^2\psi_i(x) - \frac{1}{2}\frac{\delta}{\delta\psi_i(x)}c_i\bigtriangledown^2\psi_i(x) \\
& +\frac{1}{2}\psi_i^*(x)\frac{\delta}{\delta\psi_i^*(x)}c_i\bigtriangledown^2 - \frac{1}{4}\frac{\delta}{\delta\psi_i(x)}\frac{\delta}{\delta\psi_i^*(x)}c_i\bigtriangledown^2 \\
& +h_i(x,t)\psi_i^*(x)\Big(\psi_i(x) + \frac{1}{2}\frac{\delta}{\delta\psi_i^*(x)}\Big) \\
& -h_i(x,t)\frac{1}{2}\frac{\delta}{\delta\psi_i(x)}\Big(\psi_i(x) + \frac{1}{2}\frac{\delta}{\delta\psi_i^*(x)}\Big) \\
& -\psi_i^*(x)c_i\bigtriangledown^2\psi_i(x) - \frac{1}{2}c_i\bigtriangledown^2\psi_i(x)\frac{\delta}{\delta\psi_i(x)} \\
& +\frac{1}{2}\frac{\delta}{\delta\psi_i^*(x)}c_i\bigtriangledown^2\psi_i^*(x) + \frac{1}{4}\frac{\delta}{\delta\psi_i(x)}\frac{\delta}{\delta\psi_i^*(x)}c_i\bigtriangledown^2 \\
& -h_i(x,t)\Big(\psi_i(x) - \frac{1}{2}\frac{\delta}{\delta\psi_i^*(x)}\Big)\psi_i^*(x)
\end{aligned}$$

$$
\begin{aligned}
& -h_i(x,t)\Big(\psi_i(x) - \frac{1}{2}\frac{\delta}{\delta\psi_i^*(x)}\Big)\frac{1}{2}\frac{\delta}{\delta\psi_i(x)}\Big]W(\boldsymbol{\psi},\boldsymbol{\psi}^*) \\
= \quad & \frac{1}{i\hbar}\sum_{i=A,B}\int d^3x\Big(-\frac{\delta}{\delta\psi_i(x)}\Big)\Big[c_i\bigtriangledown^2 + h_i(x,t)\Big]\psi_i(x)W(\boldsymbol{\psi},\boldsymbol{\psi}^*) \\
& + h.c., \qquad (3.18)
\end{aligned}
$$

and the second term in Eq. 3.14 is

$$
\begin{aligned}
& \frac{1}{i\hbar}\frac{g_{ii}}{2}\sum_{i=A,B}\int d^3x\big(\psi_i^\dagger(x)\psi_i^\dagger(x)\psi_i(x)\psi_i(x)\hat{\rho} - \hat{\rho}\psi_i^\dagger(x)\psi_i^\dagger(x)\psi_i(x)\psi_i(x)\big) \\
\Leftrightarrow \quad & \frac{1}{i\hbar}\frac{g_{ii}}{2}\sum_{i=A,B}\int d^3x\Big[\Big(\psi_i^*(x) - \frac{1}{2}\frac{\delta}{\delta\psi_i(x)}\Big)\Big(\psi_i^*(x) - \frac{1}{2}\frac{\delta}{\delta\psi_i(x)}\Big) \\
& \Big(\psi_i(x) + \frac{1}{2}\frac{\delta}{\delta\psi_i^*(x)}\Big)\Big(\psi_i(x) + \frac{1}{2}\frac{\delta}{\delta\psi_i^*(x)}\Big) \\
& -\Big(\psi_i(x) - \frac{1}{2}\frac{\delta}{\delta\psi_i^*(x)}\Big)\Big(\psi_i(x) - \frac{1}{2}\frac{\delta}{\delta\psi_i^*(x)}\Big) \\
& \Big(\psi_i^*(x) + \frac{1}{2}\frac{\delta}{\delta\psi_i(x)}\Big)\Big(\psi_i^*(x) + \frac{1}{2}\frac{\delta}{\delta\psi_i(x)}\Big)\Big]W(\boldsymbol{\psi},\boldsymbol{\psi}^*) \\
= \quad & \frac{1}{i\hbar}\frac{g_{ii}}{2}\sum_{i=A,B}\int d^3x\Big[\psi_i^*(x)\psi_i^*(x)\psi_i(x)\psi_i(x) \\
& -\frac{1}{2}\frac{\delta}{\delta\psi_i(x)}\psi_i^*(x)\psi_i(x)\psi_i(x) - \frac{1}{2}\psi_i^*(x)\frac{\delta}{\delta\psi_i(x)}\psi_i(x)\psi_i(x) \\
& +\frac{1}{2}\psi_i^*(x)\psi_i^*(x)\frac{\delta}{\delta\psi_i^*(x)}\psi_i(x) + \frac{1}{2}\psi_i^*(x)\psi_i^*(x)\psi_i(x)\frac{\delta}{\delta\psi_i^*(x)} \\
& +\frac{1}{4}\frac{\delta}{\delta\psi_i(x)}\frac{\delta}{\delta\psi_i(x)}\psi_i(x)\psi_i(x) - \frac{1}{4}\frac{\delta}{\delta\psi_i(x)}\psi_i^*(x)\frac{\delta}{\delta\psi_i^*(x)}\psi_i(x) \\
& -\frac{1}{4}\frac{\delta}{\delta\psi_i(x)}\psi_i^*(x)\psi_i(x)\frac{\delta}{\delta\psi_i^*(x)} - \frac{1}{4}\psi_i^*(x)\frac{\delta}{\delta\psi_i(x)}\frac{\delta}{\delta\psi_i^*(x)}\psi_i(x) \\
& -\frac{1}{4}\psi_i^*(x)\frac{\delta}{\delta\psi_i(x)}\psi_i(x)\frac{\delta}{\delta\psi_i^*(x)} + \frac{1}{4}\psi_i^*(x)\psi_i^*(x)\frac{\delta}{\delta\psi_i^*(x)}\frac{\delta}{\delta\psi_i^*(x)} \\
& +\frac{1}{8}\frac{\delta}{\delta\psi_i(x)}\frac{\delta}{\delta\psi_i(x)}\frac{\delta}{\delta\psi_i^*(x)}\psi_i(x) + \frac{1}{8}\frac{\delta}{\delta\psi_i(x)}\frac{\delta}{\delta\psi_i(x)}\psi_i(x)\frac{\delta}{\delta\psi_i^*(x)} \\
& -\frac{1}{8}\frac{\delta}{\delta\psi_i(x)}\psi_i^*(x)\frac{\delta}{\delta\psi_i^*(x)}\frac{\delta}{\delta\psi_i^*(x)} - \frac{1}{8}\psi_i^*(x)\frac{\delta}{\delta\psi_i(x)}\frac{\delta}{\delta\psi_i^*(x)}\frac{\delta}{\delta\psi_i^*(x)}
\end{aligned}
$$

$$
\begin{aligned}
&+\frac{1}{16}\frac{\delta}{\delta\psi_i(x)}\frac{\delta}{\delta\psi_i(x)}\frac{\delta}{\delta\psi_i^*(x)}\frac{\delta}{\delta\psi_i^*(x)}\\
&-\psi_i(x)\psi_i(x)\psi_i^*(x)\psi_i^*(x)\\
&+\frac{1}{2}\frac{\delta}{\delta\psi_i^*(x)}\psi_i(x)\psi_i^*(x)\psi_i^*(x)+\frac{1}{2}\psi_i(x)\frac{\delta}{\delta\psi_i^*(x)}\psi_i^*(x)\psi_i^*(x)\\
&-\frac{1}{2}\psi_i(x)\psi_i(x)\frac{\delta}{\delta\psi_i(x)}\psi_i^*(x)-\frac{1}{2}\psi_i(x)\psi_i(x)\psi_i^*(x)\frac{\delta}{\delta\psi_i(x)}\\
&-\frac{1}{4}\frac{\delta}{\delta\psi_i^*(x)}\frac{\delta}{\delta\psi_i^*(x)}\psi_i^*(x)\psi_i^*(x)+\frac{1}{4}\frac{\delta}{\delta\psi_i^*(x)}\psi_i(x)\frac{\delta}{\delta\psi_i(x)}\psi_i^*(x)\\
&+\frac{1}{4}\frac{\delta}{\delta\psi_i^*(x)}\psi_i(x)\psi_i^*(x)\frac{\delta}{\delta\psi_i(x)}+\frac{1}{4}\psi_i(x)\frac{\delta}{\delta\psi_i^*(x)}\frac{\delta}{\delta\psi_i(x)}\psi_i^*(x)\\
&+\frac{1}{4}\psi_i(x)\frac{\delta}{\delta\psi_i^*(x)}\psi_i^*(x)\frac{\delta}{\delta\psi_i(x)}-\frac{1}{4}\psi_i(x)\psi_i(x)\frac{\delta}{\delta\psi_i(x)}\frac{\delta}{\delta\psi_i(x)}\\
&-\frac{1}{8}\frac{\delta}{\delta\psi_i^*(x)}\frac{\delta}{\delta\psi_i^*(x)}\frac{\delta}{\delta\psi_i(x)}\psi_i^*(x)-\frac{1}{8}\frac{\delta}{\delta\psi_i^*(x)}\frac{\delta}{\delta\psi_i^*(x)}\psi_i^*(x)\frac{\delta}{\delta\psi_i(x)}\\
&+\frac{1}{8}\frac{\delta}{\delta\psi_i^*(x)}\psi_i(x)\frac{\delta}{\delta\psi_i(x)}\frac{\delta}{\delta\psi_i(x)}+\frac{1}{8}\psi_i(x)\frac{\delta}{\delta\psi_i^*(x)}\frac{\delta}{\delta\psi_i(x)}\frac{\delta}{\delta\psi_i(x)}\\
&-\frac{1}{16}\frac{\delta}{\delta\psi_i^*(x)}\frac{\delta}{\delta\psi_i^*(x)}\frac{\delta}{\delta\psi_i(x)}\frac{\delta}{\delta\psi_i(x)}\Bigg]W(\boldsymbol{\psi},\boldsymbol{\psi}^*). \qquad (3.19)
\end{aligned}
$$

In the above equation, the zeroth-order and fourth-order derivative terms cancel out. The first-order derivative terms are

$$
\begin{aligned}
&\frac{1}{i\hbar}\frac{g_{ii}}{2}\sum_{i=A,B}\int d^3x\Bigg[-\frac{\delta}{\delta\psi_i(x)}\psi_i^*(x)\psi_i(x)\psi_i(x)+\psi_i^*(x)\psi_i^*(x)\frac{\delta}{\delta\psi_i^*(x)}\psi_i(x)\\
&+\frac{\delta}{\delta\psi_i^*(x)}\psi_i(x)\psi_i^*(x)\psi_i^*(x)-\psi_i(x)\psi_i(x)\frac{\delta}{\delta\psi_i(x)}\psi_i^*(x)\Bigg]W(\boldsymbol{\psi},\boldsymbol{\psi}^*)\\
=\;&\frac{1}{i\hbar}\frac{g_{ii}}{2}\sum_{i=A,B}\int d^3x\Bigg[-\frac{\delta}{\delta\psi_i(x)}\psi_i^*(x)\psi_i(x)\psi_i(x)+\frac{\delta}{\delta\psi_i^*(x)}\psi_i(x)\psi_i^*(x)\psi_i^*(x)\\
&-2\delta(x-x)\psi_i(x)\psi_i^*(x)\\
&+\frac{\delta}{\delta\psi_i^*(x)}\psi_i(x)\psi_i^*(x)\psi_i^*(x)-\frac{\delta}{\delta\psi_i(x)}\psi_i^*(x)\psi_i(x)\psi_i(x)\\
&+2\delta(x-x)\psi_i^*(x)\psi_i(x)\Bigg]W(\boldsymbol{\psi},\boldsymbol{\psi}^*)
\end{aligned}
$$

$$= \frac{1}{i\hbar} g_{ii} \sum_{i=A,B} \int d^3x \Big[- \frac{\delta}{\delta\psi_i(x)} \psi_i^*(x)\psi_i(x)\psi_i(x) \Big] W(\boldsymbol{\psi}, \boldsymbol{\psi}^*) + h.c., \quad (3.20)$$

and the second-order terms in Eq. 3.19 are

$$\begin{aligned}
&\frac{1}{i\hbar}\frac{g_{ii}}{4}\frac{1}{2}\sum_{i=A,B}\int d^3x \Big[2\delta(x-x)\delta(x-x) + 4\delta(x-x)\psi_i(x)\frac{\delta}{\delta\psi_i(x)} \\
&+\psi_i(x)\psi_i(x)\frac{\delta}{\delta\psi_i(x)}\frac{\delta}{\delta\psi_i(x)} - 4\delta(x-x)\psi_i^*(x)\frac{\delta}{\delta\psi_i^*(x)} \\
&-4\psi_i^*(x)\psi_i(x)\frac{\delta}{\delta\psi_i(x)}\frac{\delta}{\delta\psi_i^*(x)} + \psi_i^*(x)\psi_i^*(x)\frac{\delta}{\delta\psi_i^*(x)}\frac{\delta}{\delta\psi_i^*(x)} \\
&-2\delta(x-x)\delta(x-x) - 4\delta(x-x)\psi_i^*(x)\frac{\delta}{\delta\psi_i^*(x)} \\
&-\psi_i^*(x)\psi_i^*(x)\frac{\delta}{\delta\psi_i^*(x)}\frac{\delta}{\delta\psi_i^*(x)} + 4\delta(x-x)\psi_i(x)\frac{\delta}{\delta\psi_i(x)} \\
&+4\psi_i^*(x)\psi_i(x)\frac{\delta}{\delta\psi_i(x)}\frac{\delta}{\delta\psi_i^*(x)} - \psi_i(x)\psi_i(x)\frac{\delta}{\delta\psi_i(x)}\frac{\delta}{\delta\psi_i(x)} \Big] W(\boldsymbol{\psi}, \boldsymbol{\psi}^*) \\
= \; & \frac{1}{i\hbar} g_{ii} \sum_{i=A,B} \int d^3x \left[\frac{\delta}{\delta\psi_i(x)} \delta(x-x)\psi_i(x) \right] W(\boldsymbol{\psi}, \boldsymbol{\psi}^*) + h.c., \quad (3.21)
\end{aligned}$$

and the third-order terms in Eq. 3.19 are

$$\begin{aligned}
&\frac{1}{i\hbar}\frac{g_{ii}}{8}\frac{1}{2}\sum_{i=A,B}\int d^3x \Big[2\frac{\delta}{\delta\psi_i(x)}\frac{\delta}{\delta\psi_i(x)}\frac{\delta}{\delta\psi_i^*(x)}\psi_i(x) \\
&-2\Big(\frac{\delta}{\delta\psi_i^*(x)}\frac{\delta}{\delta\psi_i^*(x)}\frac{\delta}{\delta\psi_i(x)}\psi_i^*(x) - 2\delta(x-x)\frac{\delta}{\delta\psi_i(x)}\frac{\delta}{\delta\psi_i^*(x)}\Big) \\
&-2\frac{\delta}{\delta\psi_i^*(x)}\frac{\delta}{\delta\psi_i^*(x)}\frac{\delta}{\delta\psi_i(x)}\psi_i^*(x) \\
&+2\Big(\frac{\delta}{\delta\psi_i(x)}\frac{\delta}{\delta\psi_i(x)}\frac{\delta}{\delta\psi_i^*(x)}\psi_i(x) - 2\delta(x-x)\frac{\delta}{\delta\psi_i(x)}\frac{\delta}{\delta\psi_i^*(x)}\Big) \Big] W(\boldsymbol{\psi}, \boldsymbol{\psi}^*) \\
= \; & \frac{1}{i\hbar}\frac{g_{ii}}{4}\sum_{i=A,B}\int d^3x \left[\frac{\delta}{\delta\psi_i(x)}\frac{\delta}{\delta\psi_i(x)}\frac{\delta}{\delta\psi_i^*(x)}\psi_i(x) \right] W(\boldsymbol{\psi}, \boldsymbol{\psi}^*) + h.c. \quad (3.22)
\end{aligned}$$

Finally, the last term in Eq. 3.14, which corresponds to interspecies inter-

action, is

$$
\begin{aligned}
& \frac{g_{AB}}{i\hbar}\int d^3x\big(\psi_A^\dagger(x)\psi_B^\dagger(x)\psi_A(x)\psi_B(x)\hat\rho-\hat\rho\psi_A^\dagger(x)\psi_B^\dagger(x)\psi_A(x)\psi_B(x)\big)\\
\Leftrightarrow\quad & \frac{g_{AB}}{i\hbar}\int d^3x\Big[\Big(\psi_A^*(x)-\frac{1}{2}\frac{\delta}{\delta\psi_A(x)}\Big)\Big(\psi_B^*(x)-\frac{1}{2}\frac{\delta}{\delta\psi_B(x)}\Big)\\
& \Big(\psi_A(x)+\frac{1}{2}\frac{\delta}{\delta\psi_A^*(x)}\Big)\Big(\psi_B(x)+\frac{1}{2}\frac{\delta}{\delta\psi_B^*(x)}\Big)\\
& -\Big(\psi_B(x)-\frac{1}{2}\frac{\delta}{\delta\psi_B^*(x)}\Big)\Big(\psi_A(x)-\frac{1}{2}\frac{\delta}{\delta\psi_A^*(x)}\Big)\\
& \Big(\psi_B^*(x)+\frac{1}{2}\frac{\delta}{\delta\psi_B(x)}\Big)\Big(\psi_A^*(x)+\frac{1}{2}\frac{\delta}{\delta\psi_A(x)}\Big)\Big]W(\boldsymbol{\psi},\boldsymbol{\psi}^*)\\
= \quad & \frac{g_{AB}}{i\hbar}\int d^3x\Big[\psi_A^*(x)\psi_B^*(x)\psi_A(x)\psi_B(x)\\
& -\frac{1}{2}\frac{\delta}{\delta\psi_A(x)}\psi_B^*(x)\psi_A(x)\psi_B(x)-\frac{1}{2}\psi_A^*(x)\frac{\delta}{\delta\psi_B(x)}\psi_A(x)\psi_B(x)\\
& +\frac{1}{2}\psi_A^*(x)\psi_B^*(x)\frac{\delta}{\delta\psi_A^*(x)}\psi_B(x)+\frac{1}{2}\psi_A^*(x)\psi_B^*(x)\psi_A(x)\frac{\delta}{\delta\psi_B^*(x)}\\
& +\frac{1}{4}\frac{\delta}{\delta\psi_A(x)}\frac{\delta}{\delta\psi_B(x)}\psi_A(x)\psi_B(x)-\frac{1}{4}\frac{\delta}{\delta\psi_A(x)}\psi_B^*(x)\frac{\delta}{\delta\psi_A^*(x)}\psi_B(x)\\
& -\frac{1}{4}\frac{\delta}{\delta\psi_A(x)}\psi_B^*(x)\psi_A(x)\frac{\delta}{\delta\psi_B^*(x)}-\frac{1}{4}\psi_A^*(x)\frac{\delta}{\delta\psi_B(x)}\frac{\delta}{\delta\psi_A^*(x)}\psi_B(x)\\
& -\frac{1}{4}\psi_A^*(x)\frac{\delta}{\delta\psi_B(x)}\psi_A(x)\frac{\delta}{\delta\psi_B^*(x)}+\frac{1}{4}\psi_A^*(x)\psi_B^*(x)\frac{\delta}{\delta\psi_A^*(x)}\frac{\delta}{\delta\psi_B^*(x)}\\
& +\frac{1}{8}\frac{\delta}{\delta\psi_A(x)}\frac{\delta}{\delta\psi_B(x)}\frac{\delta}{\delta\psi_A^*(x)}\psi_B(x)+\frac{1}{8}\frac{\delta}{\delta\psi_A(x)}\frac{\delta}{\delta\psi_B(x)}\psi_A(x)\frac{\delta}{\delta\psi_B^*(x)}\\
& -\frac{1}{8}\frac{\delta}{\delta\psi_A(x)}\psi_B^*(x)\frac{\delta}{\delta\psi_A^*(x)}\frac{\delta}{\delta\psi_B^*(x)}-\frac{1}{8}\psi_A^*(x)\frac{\delta}{\delta\psi_B(x)}\frac{\delta}{\delta\psi_A^*(x)}\frac{\delta}{\delta\psi_B^*(x)}\\
& +\frac{1}{16}\frac{\delta}{\delta\psi_A(x)}\frac{\delta}{\delta\psi_B(x)}\frac{\delta}{\delta\psi_A^*(x)}\frac{\delta}{\delta\psi_B^*(x)}\\
& -\psi_B(x)\psi_A(x)\psi_B^*(x)\psi_A^*(x)\\
& +\frac{1}{2}\frac{\delta}{\delta\psi_B^*(x)}\psi_A(x)\psi_B^*(x)\psi_A^*(x)+\frac{1}{2}\psi_B(x)\frac{\delta}{\delta\psi_A^*(x)}\psi_B^*(x)\psi_A^*(x)\\
& -\frac{1}{2}\psi_B(x)\psi_A(x)\frac{\delta}{\delta\psi_B(x)}\psi_A^*(x)-\frac{1}{2}\psi_B(x)\psi_A(x)\psi_B^*(x)\frac{\delta}{\delta\psi_A(x)}
\end{aligned}
$$

$$
\begin{aligned}
&-\frac{1}{4}\frac{\delta}{\delta\psi_B^*(x)}\frac{\delta}{\delta\psi_A^*(x)}\psi_B^*(x)\psi_A^*(x)+\frac{1}{4}\frac{\delta}{\delta\psi_B^*(x)}\psi_A(x)\frac{\delta}{\delta\psi_B(x)}\psi_A^*(x)\\
&+\frac{1}{4}\frac{\delta}{\delta\psi_B^*(x)}\psi_A(x)\psi_B^*(x)\frac{\delta}{\delta\psi_A(x)}+\frac{1}{4}\psi_B(x)\frac{\delta}{\delta\psi_A^*(x)}\frac{\delta}{\delta\psi_B(x)}\psi_A^*(x)\\
&+\frac{1}{4}\psi_B(x)\frac{\delta}{\delta\psi_A^*(x)}\psi_B^*(x)\frac{\delta}{\delta\psi_A(x)}-\frac{1}{4}\psi_B(x)\psi_A(x)\frac{\delta}{\delta\psi_B(x)}\frac{\delta}{\delta\psi_A(x)}\\
&-\frac{1}{8}\frac{\delta}{\delta\psi_B^*(x)}\frac{\delta}{\delta\psi_A^*(x)}\frac{\delta}{\delta\psi_B(x)}\psi_A^*(x)-\frac{1}{8}\frac{\delta}{\delta\psi_B^*(x)}\frac{\delta}{\delta\psi_A^*(x)}\psi_B^*(x)\frac{\delta}{\delta\psi_A(x)}\\
&+\frac{1}{8}\frac{\delta}{\delta\psi_B^*(x)}\psi_A(x)\frac{\delta}{\delta\psi_B(x)}\frac{\delta}{\delta\psi_A(x)}+\frac{1}{8}\psi_B(x)\frac{\delta}{\delta\psi_A^*(x)}\frac{\delta}{\delta\psi_B(x)}\frac{\delta}{\delta\psi_A(x)}\\
&-\frac{1}{16}\frac{\delta}{\delta\psi_B^*(x)}\frac{\delta}{\delta\psi_A^*(x)}\frac{\delta}{\delta\psi_B(x)}\frac{\delta}{\delta\psi_A(x)}\Big]W(\boldsymbol{\psi},\boldsymbol{\psi}^*). \qquad (3.23)
\end{aligned}
$$

In the above equation, the zeroth-order and fourth-order derivative terms cancel out, and the first-order derivative terms are

$$
\begin{aligned}
&\frac{g_{AB}}{i\hbar}\frac{1}{2}\int d^3x\Big[-\frac{\delta}{\delta\psi_A(x)}\psi_B^*(x)\psi_B(x)\psi_A(x)-\frac{\delta}{\delta\psi_B(x)}\psi_A^*(x)\psi_A(x)\psi_B(x)\\
&+\frac{\delta}{\delta\psi_A^*(x)}\psi_B^*(x)\psi_B(x)\psi_A^*(x)-\delta(x-x)\psi_B^*(x)\psi_B(x)\\
&+\frac{\delta}{\delta\psi_B^*(x)}\psi_A^*(x)\psi_A(x)\psi_B^*(x)-\delta(x-x)\psi_A^*(x)\psi_A(x)\\
&+\frac{\delta}{\delta\psi_B^*(x)}\psi_A^*(x)\psi_A(x)\psi_B^*(x)+\frac{\delta}{\delta\psi_A^*(x)}\psi_B^*(x)\psi_B(x)\psi_A^*(x)\\
&-\frac{\delta}{\delta\psi_B(x)}\psi_A^*(x)\psi_A(x)\psi_B(x)+\delta(x-x)\psi_A^*(x)\psi_A(x)\\
&-\frac{\delta}{\delta\psi_A(x)}\psi_B^*(x)\psi_B(x)\psi_A(x)+\delta(x-x)\psi_B^*(x)\psi_B(x)\Big]W(\boldsymbol{\psi},\boldsymbol{\psi}^*)\\
=\;&\frac{g_{AB}}{i\hbar}\int d^3x\Big[-\frac{\delta}{\delta\psi_A(x)}\psi_B^*(x)\psi_B(x)\psi_A(x)\\
&-\frac{\delta}{\delta\psi_B(x)}\psi_A^*(x)\psi_A(x)\psi_B(x)\Big]W(\boldsymbol{\psi},\boldsymbol{\psi}^*)+h.c., \qquad (3.24)
\end{aligned}
$$

and the second-order terms in Eq. 3.23 are

$$
\begin{aligned}
&\frac{1}{i\hbar}\frac{g_{AB}}{4}\int d^3x\Bigg[\frac{\delta}{\delta\psi_A(x)}\frac{\delta}{\delta\psi_B(x)}\psi_A(x)\psi_B(x)\\
&-\frac{\delta}{\delta\psi_A(x)}\psi_A(x)\Big(\frac{\delta}{\delta\psi_B^*(x)}\psi_B^*(x)-\delta(x-x)\Big)\\
&-\frac{\delta}{\delta\psi_B(x)}\psi_B(x)\Big(\frac{\delta}{\delta\psi_A^*(x)}\psi_A^*(x)-\delta(x-x)\Big)\\
&+\Big(\frac{\delta}{\delta\psi_A^*(x)}\psi_A^*(x)-\delta(x-x)\Big)\Big(\frac{\delta}{\delta\psi_B^*(x)}\psi_B^*(x)-\delta(x-x)\Big)\\
&-\frac{\delta}{\delta\psi_B^*(x)}\frac{\delta}{\delta\psi_A^*(x)}\psi_B^*(x)\psi_A^*(x)\\
&+\frac{\delta}{\delta\psi_B^*(x)}\psi_B^*(x)\Big(\frac{\delta}{\delta\psi_A(x)}\psi_A(x)-\delta(x-x)\Big)\\
&+\frac{\delta}{\delta\psi_A^*(x)}\psi_A^*(x)\Big(\frac{\delta}{\delta\psi_B(x)}\psi_B(x)-\delta(x-x)\Big)\\
&-\Big(\frac{\delta}{\delta\psi_B(x)}\psi_B(x)-\delta(x-x)\Big)\Big(\frac{\delta}{\delta\psi_A(x)}\psi_A(x)-\delta(x-x)\Big)\Bigg]W(\boldsymbol{\psi},\boldsymbol{\psi}^*)\\
=\;&\frac{1}{i\hbar}\frac{g_{AB}}{2}\int d^3x\Bigg[\frac{\delta}{\delta\psi_A(x)}\delta(x-x)\psi_A(x)\\
&+\frac{\delta}{\delta\psi_B(x)}\delta(x-x)\psi_B(x)\Bigg]W(\boldsymbol{\psi},\boldsymbol{\psi}^*)+h.c.,
\end{aligned}
\tag{3.25}
$$

and the third-order terms are

$$
\begin{aligned}
&\frac{1}{i\hbar}\frac{g_{AB}}{8}\int d^3x\Bigg[\frac{\delta}{\delta\psi_A(x)}\frac{\delta}{\delta\psi_B(x)}\frac{\delta}{\delta\psi_A^*(x)}\psi_B(x)\\
&+\frac{\delta}{\delta\psi_A(x)}\frac{\delta}{\delta\psi_B(x)}\frac{\delta}{\delta\psi_B^*(x)}\psi_A(x)\\
&-\frac{\delta}{\delta\psi_A(x)}\frac{\delta}{\delta\psi_A^*(x)}\frac{\delta}{\delta\psi_B^*(x)}\psi_B^*(x)+\delta(x-x)\frac{\delta}{\delta\psi_A(x)}\frac{\delta}{\delta\psi_A^*(x)}\\
&-\frac{\delta}{\delta\psi_B(x)}\frac{\delta}{\delta\psi_A^*(x)}\frac{\delta}{\delta\psi_B^*(x)}\psi_A^*(x)+\delta(x-x)\frac{\delta}{\delta\psi_B(x)}\frac{\delta}{\delta\psi_B^*(x)}\\
&-\frac{\delta}{\delta\psi_B^*(x)}\frac{\delta}{\delta\psi_A^*(x)}\frac{\delta}{\delta\psi_B(x)}\psi_A^*(x)-\frac{\delta}{\delta\psi_B^*(x)}\frac{\delta}{\delta\psi_A^*(x)}\frac{\delta}{\delta\psi_A(x)}\psi_B^*(x)
\end{aligned}
$$

$$
\begin{aligned}
&+\frac{\delta}{\delta\psi_B^*(x)}\frac{\delta}{\delta\psi_B(x)}\frac{\delta}{\delta\psi_A(x)}\psi_A(x)-\delta(x-x)\frac{\delta}{\delta\psi_B^*(x)}\frac{\delta}{\delta\psi_B(x)}\\
&+\frac{\delta}{\delta\psi_A^*(x)}\frac{\delta}{\delta\psi_B(x)}\frac{\delta}{\delta\psi_A(x)}\psi_B(x)-\delta(x-x)\frac{\delta}{\delta\psi_A^*(x)}\frac{\delta}{\delta\psi_A(x)}\Big]W(\boldsymbol{\psi},\boldsymbol{\psi}^*)\\
=\;&\frac{1}{i\hbar}\frac{g_{AB}}{4}\int d^3x\Big[\frac{\delta}{\delta\psi_A(x)}\frac{\delta}{\delta\psi_B(x)}\frac{\delta}{\delta\psi_B^*(x)}\psi_A(x)\\
&+\frac{\delta}{\delta\psi_B(x)}\frac{\delta}{\delta\psi_A(x)}\frac{\delta}{\delta\psi_A^*(x)}\psi_B(x)\Big]W(\boldsymbol{\psi},\boldsymbol{\psi}^*)+h.c. \qquad (3.26)
\end{aligned}
$$

Therefore, collecting the terms in Eq. 3.18, 3.20, 3.21, 3.22, 3.24, 3.25, 3.26, we obtain the Fokker-Plank equation for the two-component BECs' quasiprobability function, Eq. 3.12.

The phase degree of freedom of the Wigner functional is integrated out over the global phase of the classical field,

$$
W(\psi_i,\psi_i^*)=\int\frac{d\theta}{2\pi}W_0(\exp^{-i\theta}\psi_i,\exp^{i\theta}\psi_i^*), \qquad (3.27)
$$

and the phase operator corresponding to the global phase is unimportant so that it enables us to choose an arbitrary constant phase factor for an initial Wigner functional.

The approximation made in the TWA is now to neglect the third-order derivative term which is a non-analytic term making the equation difficult to solve [17]. In this functional form of the TWA, expectation values of those classical fields, $\prod_{i,j}\psi_i^*(x_i)\psi_j^*(x_j)$ follow from expectation values of quantum operators that are symmetrically ordered with a Wigner distribution function, where the latter, $W(\psi,\psi^*)$, is obtained from the corresponding density operator as discussed in this chapter 4. For example, the expectation value of two

creation field operator is:

$$\langle \prod_{i,j} \psi_i^\dagger(x_i)\psi_j^\dagger(x_j)\rangle_W = \int \prod_k d^2\psi_k W(\psi,\psi^*) \prod_{i,j} \psi_i^*(x_i)\psi_j^*(x_j). \tag{3.28}$$

Using the above Fokker-Planck equation and the definition of expectation values of observables, one can find the stochastic differential equation for the classical Wigner fields, $\psi_i(x)$:

$$\begin{aligned} i\hbar\frac{\partial\psi_{W,A}(x,t)}{\partial t} &= \Big[L_A + g_{AA}(|\psi_{W,A}(x,t)|^2 - 1) \\ &\quad + g_{AB}\big(|\psi_{W,B}(x,t)|^2 - \frac{1}{2}\big)\Big]\psi_{W,A}(x,t), \\ i\hbar\frac{\partial\psi_{W,B}(x,t)}{\partial t} &= \Big[L_B + g_{BB}(|\psi_{W,B}(x,t)|^2 - 1) \\ &\quad + g_{AB}\big(|\psi_{W,A}(x,t)|^2 - \frac{1}{2}\big)\Big]\psi_{W,B}(x,t). \end{aligned} \tag{3.29}$$

Since there is no second-order derivative term corresponding to a diffusion matrix in Eq. 3.12, stochastic noises during time evolution are absent. Nevertheless, an initial state has a stochastic noise determined by the Wigner distribution. Therefore, given an initial random point in phase space for each realization, the classical field, $\psi_i(x)$, evolves under the above deterministic trajectory which looks similar to the Gross-Pitaevskii equation, except the offset by a single particle wavefunction that becomes negligible compared to a condensate field as the number of bosons in the condensate field is large ($N_C >> 1$).

This TWA method was used in [58] to study a dephasing effect after splitting a BEC into two subcondensates.

3.3 A Hybrid Method for Bose Einstein Condensates

As a last discussion of phase space representations, we now turn our interest to a hybrid model [49, 73], which is a combination of a condensate mode and an excited mode, each of which is projected by different representations: the condensate mode by the TWA, and the noncondensate mode by the positive P representation. We now study the model for one-component BECs only. The rationale of this model is that the condensate mode is a highly occupied state so it can be safely described by a mean-field theory neglecting a small quantum effect, whereas the noncondensate mode is unoccupied on average (for zero temperature), or low-occupied (for low temperature) so its quantum effects are more evident and dynamical. These two modes are treated separately in different representations and combined together in calculations of observables.

With respect to dynamics in phase space, the TWA is similar to the mean-field theory in the sense that quantum noises in time evolution are neglected and so its dynamics is almost classical except the fact that the initial state in the TWA has a quantum noise unlike the mean-field theory. On the other hand, the positive P representation is not an approximation method, so it has more potential to describe the quantum mechanical effects that might be present in the mode.

The disadvantage of using the TWA is that as noted above, it is not appropriate for a mode with strong quantum noises. The weakness of positive P representation lies on its weak or absent convergence for some paths in a phase space. That is because some trajectories in phase space unexpectedly detour

a lot from their mean-path in the positive P representation. In that case, it requires integration of a large sampling set, and it would not be plausible to implement it in numerical simulations. This is especially true for highly occupied modes such as condensate modes, so it is not applicable to the condensate mode.

By noting these two kinds of pros and cons for each representation, we approach the problem in a different way, treating two modes separately by the two different representations: the TWA for the condensate mean field, the positive P representation for noncondensate modes.

The characteristic functional of this hybrid model [74] is,

$$\begin{aligned}
\chi[\xi_C, \xi_C^\dagger, \xi_{NC}, \xi_{NC}^\dagger] &= \mathrm{Tr}\big[\hat{\rho}\hat{\Omega}(\xi_{\mathrm{C}}, \xi_{\mathrm{C}}^\dagger, \xi_{\mathrm{NC}}, \xi_{\mathrm{NC}}^\dagger)\big], && (3.30)\\
\hat{\Omega} &= \prod \hat{\Omega}_C \hat{\Omega}_{NC}, && (3.31)\\
\hat{\Omega}_C &= \mathrm{Exp}\Big[\int \mathrm{d}\boldsymbol{x}\mathrm{i}\big\{\xi_{\mathrm{C}}(\boldsymbol{x})\hat{\psi}_{\mathrm{C}}^\dagger(\boldsymbol{x}) + \xi_{\mathrm{C}}^\dagger(\boldsymbol{x})\hat{\psi}_{\mathrm{C}}(\boldsymbol{x})\big\}\Big]\\
\hat{\Omega}_{NC} &= \mathrm{Exp}\Big[\int \mathrm{d}\boldsymbol{x}\mathrm{i}\big\{\xi_{\mathrm{NC}}(\boldsymbol{x})\hat{\psi}_{\mathrm{NC}}^\dagger(\boldsymbol{x})\big\}\Big]\\
&\quad \times \mathrm{Exp}\Big[\int \mathrm{d}\boldsymbol{x}\mathrm{i}\big\{\xi_{\mathrm{NC}}^\dagger(\boldsymbol{x})\hat{\psi}_{\mathrm{NC}}(\boldsymbol{x})\big\}\Big], && (3.32)
\end{aligned}$$

where the transformation operator $\hat{\Omega}$ is a product of that for the condensate mode in the TWA and that for the noncondensate in the positive P representation for each component. As discussed in Chapter 2, a derivative with respect to ξ_C or $\xi_{NC}^\dagger$, etc., evaluated at zero generates moments (expectation values of the products of classical fields, $\psi_C(\boldsymbol{x})^\dagger$ or $\psi_{NC}(\boldsymbol{x})$, etc.). The quasi-probability function can be obtained through the reverse transformation of the following definition of characteristic function [74].

We now derive the stochastic time evolution of classical fields in this hybrid (TWA + positive P) representation [74]. The Ito stochastic differential equation for the condensate field $\psi_C(\boldsymbol{x},t)$ is

$$\begin{aligned} i\hbar\frac{\partial}{\partial t}\psi_C(\boldsymbol{x},t) &= -\frac{\hbar^2}{2m}\bigtriangledown^2\psi_C(\boldsymbol{x}) + V(\boldsymbol{x})\psi_C(\boldsymbol{x}) \\ &+g\big[|\psi_C(\boldsymbol{x})|^2 - |\phi(\boldsymbol{x})|^2\big]\psi_C(\boldsymbol{x}) \\ &+g\big[2|\psi_C(\boldsymbol{x})|^2 - N|\phi(\boldsymbol{x})|^2\big]\psi_{NC}(\boldsymbol{x}) \\ &+g(\psi_C(\boldsymbol{x}))^2\psi^\dagger_{NC}(\boldsymbol{x}) \\ &+2g|\psi_{NC}(\boldsymbol{x})|^2\psi_C(\boldsymbol{x}) + g(\psi_{NC}(\boldsymbol{x}))^2\psi^\dagger_C(\boldsymbol{x}) \\ &+\frac{\partial}{\partial t}G_C(\psi(\boldsymbol{x}),\Gamma(\boldsymbol{x})), \end{aligned} \tag{3.33}$$

where $G_C(\psi(\boldsymbol{x}),\Gamma(\boldsymbol{x}))$ is a noise field [75], and $\phi(\boldsymbol{x})$ is a solution to the Gross-Pitaevskii equation:

$$i\hbar\frac{\partial\phi(\boldsymbol{x})}{\partial t} = \Big[-\frac{\hbar^2\nabla^2}{2m} + V_h(\boldsymbol{x}) + V_o(\boldsymbol{x},t) + g|\phi(x)|^2\Big]\phi(x). \tag{3.34}$$

The first line and the second line on the right hand side are nothing but the time-dependent Gross-Pitaevskii type term except the presence of a depletion term by one single particle field ($|\phi(\boldsymbol{x})|^2$), and the third and fourth line are a sum of coupling terms linear in two independent noncondensate fields, $\psi_{NC}(\boldsymbol{x}),\psi^\dagger_{NC}(\boldsymbol{x})$. In comparison, the fifth line is coupling terms that are linear in the condensate field, $\psi_C(\boldsymbol{x})$, and its conjugate field, $\psi^\dagger_C(\boldsymbol{x})$.

The corresponding equation for the noncondensate field, $\psi_{NC}(\boldsymbol{x})$ is,

$$i\hbar\frac{\partial}{\partial t}\psi_{NC}(\boldsymbol{x},t) = -\frac{\hbar^2}{2m}\bigtriangledown^2\psi_{NC}(\boldsymbol{x}) + V(\boldsymbol{x})\psi_{NC}(\boldsymbol{x})$$

$$
\begin{aligned}
&+g\big[2|\psi_C(\boldsymbol{x})|^2 - |\phi(\boldsymbol{x})|^2\big]\psi_{NC}(\boldsymbol{x}) \\
&+g(\psi_C(\boldsymbol{x}))^2\psi^\dagger_{NC}(\boldsymbol{x}) \\
&+g\big[|\psi_C(\boldsymbol{x})|^2 - N|\phi(\boldsymbol{x})|^2\big]\psi_C(\boldsymbol{x}) \\
&+\frac{\partial}{\partial t}G_{NC}(\psi(\boldsymbol{x}),\Gamma(\boldsymbol{x})),
\end{aligned}
\tag{3.35}
$$

and similarly for the field, $\psi^\dagger_{NC}(\boldsymbol{x})$ [75]. This equation has a similarity with the well-known Bogoliubov equation: The first, second, and third line are the time-dependent Bogoliubov equation for the noncondensate field except that there is a depletion term as in the equation for the condensate field. Note that the coefficient of coupling terms with the condensate field in the second line, is 2 not 1 as usual for the Bogoliubov equation. The fourth line is similarly a coupling term with the condensate field and the last line is another independent noise term.

The above equations are stochastic coupled differential equations in which all fields are implicitly dependent on each other, which are difficult to solve analytically. We now instead focus on an approximation to this approach. First, we take a look at Eq. 3.33 for $\psi_N(\boldsymbol{x},t)$. We note that the third, fourth, and fifth line of the equation are on the order of $|\psi_{NC}(\boldsymbol{x})|$, or $|\psi_{NC}(\boldsymbol{x})|^2$, which are a few orders of magnitude smaller compared to nonlinear terms in the second line ($\sqrt{N} \gg |\psi_{NC}(\boldsymbol{x})|$), since we assume that the fraction of noncondensate fields is very small. As they are in higher order in $\sqrt{N}^{-1}$ or N^{-1}, they are neglected in our approximation. Furthermore, we discard the noise term, because the noise is small compared to the condensate mean field.

Concerning the equation of noncondensate fields, Eq. 3.35, its fourth line

is taken to be zero, since the classical mean-field for the condensate mode is $\psi_C(\boldsymbol{x}) \simeq \sqrt{N}\phi(\boldsymbol{x})$ and its quantum fluctuation is assumed to be small. All diffusion matrix elements in the noncondensate fields are zero except diagonal noise terms, $D_{NC-,NC-}$ and $D_{NC+,NC+}$:

$$\begin{aligned}
&\overline{\Big(\frac{\partial}{\partial t}G_{NC}\big(\psi(\boldsymbol{x}_1),\Gamma(\boldsymbol{x})\big)\Big)\Big(\frac{\partial}{\partial t}G_{NC}\big(\psi(\boldsymbol{x}_2),\Gamma(\boldsymbol{x})\big)\Big)} \\
&\qquad = \overline{D_{NC-,NC-}(\psi(\boldsymbol{x}_1),\boldsymbol{x}_1,\psi(\boldsymbol{x}_2),\boldsymbol{x}_2)}\delta(t_1,t_2), \\
&\overline{\Big(\frac{\partial}{\partial t}G^{\dagger}_{NC}\big(\psi(\boldsymbol{x}_1),\Gamma(\boldsymbol{x})\big)\Big)\Big(\frac{\partial}{\partial t}G^{\dagger}_{NC}\big(\psi(\boldsymbol{x}_2),\Gamma(\boldsymbol{x})\big)\Big)} \\
&\qquad = \overline{D_{NC+,NC+}(\psi(\boldsymbol{x}_1),\boldsymbol{x}_1,\psi(\boldsymbol{x}_2),\boldsymbol{x}_2)}\delta(t_1,t_2). \qquad (3.36)
\end{aligned}$$

For both the condensate mode and the noncondensate mode, the single particle field, $\phi(\boldsymbol{x},t)$ can be neglected for a large N of particles, so we discard it for our current approximation. In summary, the condensate field evolves as

$$\begin{aligned}
i\hbar\frac{\partial}{\partial t}\psi_C(\boldsymbol{x},t) &= -\frac{\hbar^2}{2m}\bigtriangledown^2\psi_C(\boldsymbol{x}) + V(\boldsymbol{x})\psi_C(\boldsymbol{x}) \\
&\quad +g|\psi_C(\boldsymbol{x})|^2\psi_C(\boldsymbol{x}), \qquad (3.37)
\end{aligned}$$

which is a TWA for the condensate field only. The noncondensate field, on the other hand, evolves as

$$\begin{aligned}
i\hbar\frac{\partial}{\partial t}\psi_{NC}(\boldsymbol{x},t) &= -\frac{\hbar^2}{2m}\bigtriangledown^2\psi_{NC}(\boldsymbol{x}) + V(\boldsymbol{x})\psi_{NC}(\boldsymbol{x}) \\
&\quad +2g|\psi_C(\boldsymbol{x})|^2\psi_{NC}(\boldsymbol{x}) \\
&\quad +g(\psi_C(\boldsymbol{x}))^2\psi^{\dagger}_{NC}(\boldsymbol{x}) \\
&\quad +\frac{\partial}{\partial t}G_{NC}(\psi(\boldsymbol{x}),\Gamma(\boldsymbol{x})), \qquad (3.38)
\end{aligned}$$

and similarly for $\psi^{\dagger}_{NC}(\boldsymbol{x},t)$. One of the important aspects in the positive P representation is that these two modes, $\psi_{NC}(\boldsymbol{x},t)$ and $\psi^{\dagger}_{NC}(\boldsymbol{x},t)$, are independent fields following similar-looking different stochastic differential equations, though in other representations they are treated as just conjugate fields. This idea is called, 'doubling phase space', that makes it different from a normal P representation. The normal P representation has a distribution function that may sometimes produce negative values. On the other hand, the 'positive' P representation gets rid of such a problem by treating the conjugate field as independent, so doubling the phase space.

For the above equation, a noise field $\eta^{-}(\boldsymbol{x},t)$ is defined as in [76]:

$$\begin{aligned}\frac{\partial}{\partial t}G_{NC}(\psi(\boldsymbol{x}),\Gamma(t)) &= \sqrt{\frac{i}{\hbar}g(\psi_C(\boldsymbol{x}))^2}\eta^{-}_{NC}(\boldsymbol{x},t),\\ \frac{\partial}{\partial t}G^{\dagger}_{NC}(\psi(\boldsymbol{x}),\Gamma(t)) &= \sqrt{-\frac{i}{\hbar}g(\psi^{\dagger}_C(\boldsymbol{x}))^2}\eta^{+}_{NC}(\boldsymbol{x},t),\end{aligned} \tag{3.39}$$

and the other noise field, $\eta^{+}(\boldsymbol{x},t)$ is an independent noise field for $\psi^{\dagger}_{NC}(\boldsymbol{x},t)$. These two stochastic terms are all multiplicative noises, and they follow the Gaussian-Markov process that satisfies:

$$\eta^{i}_{NC}(\boldsymbol{x}_1,t_1)\eta^{j}_{NC}(\boldsymbol{x}_2,t_2)=\delta^3(\boldsymbol{x}_1-\boldsymbol{x}_2)\delta(t_1-t_2)\delta_{ij} \qquad (i,j=-,+). \tag{3.40}$$

3.4 Sampling Initial States

Having discussed various representations, we now discuss how to prepare an initial state, since it contains quantum noises which are not normal in classical dynamics. We consider an initial state composed of a mixture of two

Bose-Einstein condensates in thermal equilibrium and in a harmonic trap confinement. For sufficiently low temperatures ($T \ll T_c$), the Bogoliubov quasiparticle description (for collective excitations in BECs, see [17, 77, 78]) for a noncondensate field combined with a condensate field is a suitable approximation to exact many-body dynamics of the system, provided that the number of noncondensate particles (N_{ex}) is sufficiently smaller than that of condensate bosons ($N_c \gg N_{ex}$). The rigorous Particle Number Conserving(PNC) formalism was studied by [79, 80] where a GPE naturally arises. The Bogoliubov quasiparticle method in an optical lattice was developed by Oosten et al. [81] and it was applied to the superfluid-Mott insulator transition [82]. In Bogoliubov approximation, noncondensate operators creating small quasiparticles are added to the condensate field operator.

$$\begin{aligned} \hat{\psi}_A(x) &= \psi_{0A}(x)\hat{\alpha}_{A0} + \sum_{\mu>0}(u_{A\mu}(x)\hat{\alpha}_\mu - v_{A\mu}(x)\hat{\alpha}_\mu^\dagger) \\ \hat{\psi}_B(x) &= \psi_{0B}(x)\hat{\alpha}_{B0} + \sum_{\mu>0}(u_{B\mu}(x)\hat{\alpha}_\mu - v_{B\mu}(x)\hat{\alpha}_\mu^\dagger). \end{aligned} \tag{3.41}$$

Here, $\hat{\alpha}_{i0}$ is a ground state annihilation operator for the component i, whereas $\hat{\alpha}_\mu$ is a quasiparticle annihilation operator in the mode μ. These operators satisfy the bosonic commutation relation, $[\hat{\alpha}_{i0}, \hat{\alpha}_{j0}^\dagger] = \delta_{ij}$. The normalization conditions for a single-particle condensate amplitude and for a Bogoliubov quasiparticle mode amplitude are,

$$\int dx \psi_{0A}^*(x)\psi_{0A}(x) = \int dx \psi_{0B}^*(x)\psi_{0B}(x) = 1 \tag{3.42}$$

$$\int dx \big[u_{A\mu}^*(x)u_{A\nu}(x) + u_{B\mu}^*(x)u_{B\nu}(x)$$

$$-v^*_{A\mu}(x)v_{A\nu}(x) - v^*_{B\mu}(x)v_{B\nu}(x)\big] = \delta_{\mu\nu}. \tag{3.43}$$

An expectation value of a number operator is the population in the condensate mode and in the noncondensate modes for each component.

$$\langle \alpha^\dagger_{i0}\alpha_{i0}\rangle = N_{i0}, \tag{3.44}$$

$$\langle \alpha^\dagger_{\mu}\alpha_{\mu}\rangle = N_{\mu} = \frac{1}{\exp\left(\epsilon_\mu/k_BT\right)-1}, \tag{3.45}$$

if the quasiparticle noncondensate fields are in thermal equilibrium with temperature T.

A quasiparticle mode amplitude function should satisfy the two-component Bogoliubov-de Gennes equation using a 4×4 matrix form:

$$\begin{pmatrix} H_A + g_{AA}N_A|\psi_A|^2 & g_{AB}\sqrt{N_AN_B}\psi_A\psi_B^* & -g_{AA}N_A\psi_A^2 & -g_{AB}\sqrt{N_AN_B}\psi_A\psi_B \\ g_{AB}\sqrt{N_AN_B}\psi_A^*\psi_B & H_B + g_{BB}N_B|\psi_B|^2 & -g_{AB}\sqrt{N_AN_B}\psi_A\psi_B & -g_{BB}N_B\psi_B^2 \\ -g_{AA}N_A(\psi_A^*)^2 & -g_{AB}\sqrt{N_AN_B}\psi_A^*\psi_B^* & H_A + g_{AA}N_A|\psi_A|^2 & g_{AB}\sqrt{N_AN_B}\psi_A^*\psi_B \\ -g_{AB}\sqrt{N_AN_B}\psi_A^*\psi_B^* & -g_{BB}N_B(\psi_B^*)^2 & g_{AB}\sqrt{N_AN_B}\psi_A\psi_B^* & H_B + g_{BB}N_B|\psi_B|^2 \end{pmatrix} \times \begin{pmatrix} u_{A\mu} \\ u_{B\mu} \\ v_{A\mu} \\ v_{B\mu} \end{pmatrix}$$

$$= \begin{pmatrix} \epsilon_\mu u_{A\mu} \\ \epsilon_\mu u_{B\mu} \\ -\epsilon_\mu v_{A\mu} \\ -\epsilon_\mu v_{B\mu} \end{pmatrix}.$$

(3.46)

As noted above, we generate stochastic fields of an initial state by taking samples from the corresponding Wigner distribution function and we obtain the dynamics of the state by averaging the ensemble of individual event trajectories. The expectation values of operators that are symmetrically ordered are calculated by the weighted average of stochastic fields with the Wigner quasi-probability function, $W(\psi_W, \psi_W^*)$.

The field amplitudes $\psi_{0i}(\boldsymbol{x})$ are multiplied by stochastic complex c-numbers, $\alpha_{A0}, \alpha_{B0}, \alpha_\mu$ corresponding to quantum operators, $\hat{\alpha}_{A0}, \hat{\alpha}_{B0}, \hat{\alpha}_\mu$ in Eq. 3.41. Since operators for condensate modes and for quasiparticle modes are uncorrelated, and the component A and the component B are uncorrelated too, we independently sample the above random numbers. As explained in Chapter 2 for a superfluid initial state, we approximate the two-component condensate state as an independent coherent state for which each coherent state keeps its own phase coherence. The Wigner function is given similarly as in Eq. 3.5,

$$\begin{aligned} W_{A0}(\alpha_{A0}, \alpha_{A0}^*) &= \frac{2}{\pi} \exp\left[-2|\alpha_{A0} - \sqrt{N_{A0}}|^2\right], \\ W_{B0}(\alpha_{B0}, \alpha_{B0}^*) &= \frac{2}{\pi} \exp\left[-2|\alpha_{B0} - \sqrt{N_{B0}}|^2\right], \end{aligned} \tag{3.47}$$

where $\langle \alpha_{i0} \rangle = \sqrt{N_{i0}}$ and $\langle \alpha_{i0}^* \alpha_{i0} \rangle = N_{i0} + \frac{1}{2}$.

For a coherent state, the distribution function has a Gaussian profile in a complex phase space with a finite width of 1/2. For a large number of atoms ($N_{i0} \gg 1$), the quantum fluctuation corresponding to this width around the mean classical field becomes small, since $\Delta N_{i0}/N_{i0} = 1/\sqrt{\langle N_{i0} \rangle}$. Thus, we can

think of the initial state as a classical field with a small fluctuation in phase space.

Even though the condensate mode has a nonzero expectation value for the operator, α_{i0}, the noncondensate mode has a zero expectation value for the quasiparticle excitation operator, $\alpha_{i\mu}$, for which the Wigner distribution function is a product of uncorrelated Wigner function for each mode(Eq. 3.6).

$$\begin{aligned} W_\mu(\alpha_\mu, \alpha_\mu^*) &= \frac{2}{\pi} \tanh\big(\frac{\epsilon_\mu}{k_B T}\big) \exp\Big[-2|\alpha_\mu|^2 \tanh\big(\frac{\epsilon_\mu}{k_B T}\big)\Big], \\ W_{BG}(\alpha, \alpha^*) &= \prod_\mu W_\mu(\alpha_\mu, \alpha_\mu^*), \end{aligned} \tag{3.48}$$

where $W_{BG}(\alpha, \alpha^*)$ is the Wigner function of Bogoliubov quasiparticles, and $W_\mu(\alpha_\mu, \alpha_\mu^*)$ is the Wigner function for mode μ. The Wigner expectation values of quasiparticle modes satisfy the condition that they have the zero mean value and finite widths of Gaussian distribution, in which the widths broaden as the temperature increases:

$$\langle \alpha_\mu \rangle_W = \langle \alpha_\mu^* \rangle_W = 0, \tag{3.49}$$

$$\langle \alpha_\mu^* \alpha_\nu \rangle_W = \delta_{\mu\nu}\Big[n_\nu + \frac{1}{2}\Big]. \tag{3.50}$$

For one-component BECs in the hybrid model, the positive P distribution function for the noncondensate mode is in a different form:

$$\begin{aligned} P_\mu(\alpha_\mu, \alpha_\mu^*) &= \frac{1}{\pi n_\mu} \exp\Big(-\frac{|\alpha_\mu|^2}{n_\mu}\Big), \\ P_{BG}(\alpha, \alpha^*) &= \prod_\mu P_\mu(\alpha_\mu, \alpha_\mu^*), \end{aligned} \tag{3.51}$$

where $P_{BG}(\alpha, \alpha^*)$ is the positive P distribution of Bogoliubov quasiparticles, and $P_\mu(\alpha_\mu, \alpha_\mu^*)$ is the positive P function for mode μ. The corresponding expectation values of quasiparticle modes in the positive P representation are,

$$\langle \alpha_\mu \rangle_P = \langle \alpha_\mu^* \rangle_P = 0, \tag{3.52}$$

$$\langle \alpha_\mu^* \alpha_\nu \rangle_P = \delta_{\mu\nu} n_\nu, \tag{3.53}$$

For the model we consider, we assume that a system does not have a loss mechanism - a condensate in a trap does not lose its particles through two-body collisions or etc., nor recombines into another form through three-body collisions.

Chapter 4

Numerical Methods for Phase Space Representations

4.1 Monte Carlo Method

Efficient numerical methods are required to generate sufficiently well-behaved noises to achieve better convergence. Such quantum noise needs to have sufficient 'randomness', since the residual effects of a regular pattern of numerical set-up must not appear during numerical integrations. A Monte Carlo method is one of the efficient numerical algorithms suitable to generating random noises needed for initial states or intermediate states. Usual computational algorithms rely on integration on a regular lattice, whereas Monte Carlo methods select grid points on a random basis.

A general algorithm of Monte Carlo methods consists of the following steps:

1. Determine an appropriate range (D$\prime$) of space for input states.
2. Define a (quasi-)probability distribution function of states in the range.

3. Generate random inputs following such a distribution function.

4. Implement a deterministic (or stochastic if necessary) calculation of each initial input using suitable numerical algorithms.

5. Accumulate outputs from the simulation and average the result out with a weight factor.

A normal way of integration, for example, a Riemann-Stieltjes integral, begins with dividing the space of states into a grid. For a n-dimension-al definite integral,

$$M = \int_{i_1}^{f_1} \int_{i_2}^{f_2} ... \int_{i_n}^{f_n} \Pi_{k=1}^{n} dx_k f(x_1, x_2, ..., x_n) = \int_V f(\boldsymbol{x}) d\boldsymbol{x}. \tag{4.1}$$

A Monte Carlo integration selects N′ random points over a predetermined domain (D′) in the step 1 larger than the integration domain (D) of volume V and then filters it through the integration domain (D) by checking whether it belongs to the integration domain. Then we evaluate the deterministic function ($f(x_i)$). If the number of filtered points is N, then an estimate for the integral is

$$M \simeq Q = \frac{V}{N} \sum_{i=1}^{N} f(x_i) = V \langle f \rangle, \tag{4.2}$$

and an unbiased estimate of variance of the integral is

$$\text{var(f)} = \sigma^2 \;\; = \;\; \frac{1}{N-1} \sum_{i=1}^{N} \left[f(x_i) - \langle f \rangle \right]^2$$

$$= \frac{1}{N-1}\Big[\sum_{i=1}^{N} f^2(x_i) - \langle f\rangle^2\Big], \tag{4.3}$$

and a variance of the estimate of the integral is

$$\mathrm{var(Q)} = \frac{\mathrm{V}^2}{\mathrm{N}}\mathrm{var(f)} = \frac{\mathrm{V}^2}{\mathrm{N}}\sigma^2. \tag{4.4}$$

Therefore, the function f is estimated as follows:

$$M \simeq V\langle f\rangle \pm V\sqrt{\frac{\langle f^2\rangle - \langle f\rangle^2}{N}}. \tag{4.5}$$

4.1.1 Systematic Sampling

An initial state sampling process for a Gaussian distribution first requires a sample of uniform distribution. That is because a Gaussian distribution can be transformed from a uniform distribution by some algorithms such as the Box Muller algorithm. Before we deal with more exact methods, we discuss a convenient way of sampling a uniform distribution for a Monte Carlo method.

Sometimes, it happens that more efficient and less resource-consuming generation of random numbers is requested in frequent high-load Monte Carlo simulations. However, a plain Monte Carlo sampling is not efficient to achieve a high degree of uniformness quickly. For completely-random selection procedures, sub-populations vary between sub-domains in the same size. In fact, there exist more efficient methods that can benefit from the uniformness property of the distribution. Before we discuss those methods, we look at a simple systematic sampling [83, 84] method which modifies a plain random sampling method by selecting systematically an element from a sample domain. The

process is engineered for efficiency by adopting a pre-designed pattern of selection, while not affecting the statistics of the distribution.

A simple way is that it draws every i^{th} element in a finite sample set or an element at a regular interval in a given continuous domain. For a continuous domain, $[I_a, I_b]$,

$$\begin{aligned} I_i &= I_1 + \frac{i-1}{N}, \\ I_a \leq I_1 &< I_a + \frac{I_b - I_a}{N}, \end{aligned} \tag{4.6}$$

where N is the size of the sample.

One of the requirements for this sampling method is that a corresponding distribution should be uniform, since selected elements represent a local group near the element. The group of drawn samples is then homogeneous and it has a regular interval, so the distribution should be homogeneous too. By a similar reasoning, there must not be any pattern left behind the region not selected, since otherwise it might distort the output severely. For example, if we choose $2^{th}, 5^{th}, 8^{th}, ...$ elements from a group, then any hidden fluctuations present in $4^{th}, 7^{th}, 10^{th}, ..$ elements will not be revealed, thus generating false expectation values.

With regard to the issue of randomness, this method still endows randomness to the sampling process even though the sampling is planned ahead, since the starting point, I_1 is randomly generated before any designed sampling structure begins to be applied to later points. The initial point generated by a random process needs not to be the smallest element of a group for an ordered distribution, and it can be any point in the domain of interest.

After the initial random point is obtained, all other sample points except the initial point are placed at a regular interval during the sampling process. A problem might arise when the size of population domain is not divisible by the number of samples. For example, when a finite set of elements with a size of N is to be extracted from a population (M) and $\mathrm{mod}(\mathrm{M}, \mathrm{N}) \neq 0$, then there remains a residue, $\mathrm{mod}(\mathrm{M}, \mathrm{N})$, after N elements are drawn. The solution to detour this problem is that we use a noninteger interval (M/N) instead of an integer interval as one period and choose each point as close as possible to an exact noninteger interval points.

While this method might be used for this work and other high-volume Monte Carlo simulations for efficiency enhancement, it might become a little bit flawed in some cases. For it might produce erroneous outputs with regard to dynamics, resulting from a hidden pattern imprinted on unselected regular intervals. Therefore, we alter this method to reveal hidden physical patterns or to remove any residual pattern of numerical round-off errors. We will discuss more effective calibration mechanisms for variance reduction in the following sections.

4.1.2 Stratified Sampling

As explained in the previous section, an initial state sampling process begins with a sample of uniform distribution. To be more specific, any kind of choices for the range of uniform domain is acceptable, though the unit domain, $[0, 1]$, is adopted for this work. As it is not uncommon to perform more than 1000 runs in a Monte Carlo method for this distribution, the goal here is to

minimize the number of samples to be drawn for simulations and to reduce variance across different sampling procedures like the systematic sampling, but to remove unwanted patterns unlike it.

Stratified sampling is a variance reduction method to improve the precision of estimates from samples of the given size. The mechanism of stratified sampling [83, 85] is to divide the sampling domain into mutually-exclusive subdomains and select random elements in proportion to its subdomain's distribution (probability) such that the total domain becomes more homogeneous across subgroups (or stratum) than a plain randomized sampling do. The process of random sampling is applied independently in each subdomain after the process of stratification. Since each element of a domain belongs to only one subdomain, no overlap is allowed. This method also works effectively for a uniform distribution too.

Suppose we now have a non-homogeneous distribution. For example, suppose that there are four local potential wells in a region of interest: an upper left (A), an upper right (B), a lower left (C), and a lower right well (D). The probability of finding a particle in upper wells and lower wells is 60% and 40% and the probability of finding it in left wells and right wells are 30% and 70%, respectively. The probability for each well is 18% (A), 42% (B), 12% (C), and 28% (D) respectively. The strategy of stratified sampling is applied now that if projection of 100 samples onto this space is planned for a simulation, then a fraction of the samples is allocated to each stratum in proportion to the population of the stratum so that the proportionate fractions follow the given probability. With the above example at hand, 18 samples are forced to be allocated in the upper left well, 42 samples in the upper right, 12 samples

in the lower left, and 28 samples in the lower right. In contrast to plain Monte Carlo methods, we utilize the information about the probability distribution that we know before an actual simulation occurs.

The advantage of this extra work is that for the foremost part, the stratification achieves more precise coverage of a true distribution than a plain random sampling method. The reason for this is that it is based on the 'a priori' knowledge about the population of the true distribution. Second, it is more efficient than the plain random sampling by the similar reasoning. In general, it is possible to achieve in less time a similar variance of an expected mean-value from samples, since the stratification allows for a weighted average with each weight based on the probability of the stratum. For example, only four samples are required for a simulation in the above four well problem, if the strata are perfectly homogeneous within each stratum, since we calculate quantities of interest once for each subgroup. On the other hand, in random sampling, it is unexpected how large a sample size is required to arrive at acceptable convergence.

Therefore, this algorithm is beneficial unless it is difficult to find the 'a priori' knowledge of a distribution function. However, there are possibilities of other kinds of obstacles. In some cases, it is not an easy task to determine representative subgroups, or sample points might not be obtained because of absence of analytic distribution functions.

The unit domain $I = [0, 1]$, mainly used in this work, is supposed to be homogeneous all across the domain. Even in this flat population region, adopting the stratified sampling method is advantageous. For it generates an output of even more homogeneous sample with the number of samples given,

by forcing the homogeneity. We apply the strategy of the stratified sampling in the following way:

1. Divide the interval, $I = [0, 1]$ into n consecutive segments of intervals, $I_i = (\frac{i-1}{n}, \frac{i}{n}]$ for i=1,. . ., n.

2. Perform generation of m random numbers (m is divisible by n, $m = nq$) $u_i \in [0, 1], i = 1, ..., m$

3. Allocate q numbers of generated random numbers into every subinterval while rescaling them by a factor of $1/n$

To be specific, in the case that $n = m$ when each segment contains only one random element, the stratified sampling variable $\hat{u}_i$ is,

$$\hat{u}_i = \frac{u_i}{n} + \frac{i-1}{n}, \tag{4.7}$$

where $\hat{u}_i$'s are the resulting sample elements that we will use later.

After this modification, we are guaranteed to have a random number for each segment. Otherwise, the plain random sampling might generate a vacancy or an overflow in certain subdomains so that it becomes less homogeneous compared to stratification. The high degree of homogeneity translates into a more exact approximation to the mean and the variance.

4.1.3 Antithetic Variate Method

The antithetic variates method developed by [86] is another variance reduction mechanism by adding an equally–likely sample but having negative correlation to the original one. To be more precise, if a sample is going to be drawn from a normal distribution with a mean 0 and a variance 1, and

we have actually drawn a sample, 1.3 from the distribution, then it is equally probable to choose -1.3 as another sample, and adding it to the set reduces the variance. Formally, when there is given a sample $u_1, u_2, ..., u_n$, the antithetic variate strategy takes their antithetic points in the sampling space, $-u_1, -u_2, ..., -u_n$. Therefore, if n independent random sample paths are generated at first, the estimation of values counts 2n samples.

In Monte Carlo methods, the convergence of simulated calculations usually depends on the number of realizations, which is proportional to the square root of the sample number. In comparison with other general numerical methods which converge linearly on the number of runs, a plain Monte Carlo method converges very slowly. On the other hand, the antithetic sampling method can be especially useful in reducing the variance of samples, thereby gaining an efficiency improvement. The rationale is that a pair of two opposite samples in the sample path space is negatively correlated. Therefore, appending antithetic samples to original selections reduce the variance of expected values.

An advantage of this method is that it requires less generation of random numbers ($< n$) for sampling of n points. It also improves the accuracy of a result per number of samples drawn. Furthermore, since the analysis about the structure of distribution as required for the stratified sampling method is not required, it is more conveniently implemented. However, it does not play a role in reducing the error of a mean.

To see the effect of adding an antithetic variable to a sample, suppose that a set of samples, $\{x_i\}$, is prepared. For each x_i, generate an antithetic variable, $\bar{x}_i$, which does not have to be equal to x_i in magnitude but have to be negatively correlated. In other words, $\mathrm{cov}(\mathrm{x_i}, \bar{\mathrm{x}}_\mathrm{i}) < 0$. Then, the unbiased

estimate of average of this pair is simply,

$$\hat{\theta} = \frac{x_i + \bar{x_i}}{2}, \tag{4.8}$$

and a variance of this estimate is

$$\mathrm{var}(\hat{\theta}) = \frac{\mathrm{var(x_i)} + \mathrm{var(\hat{x}_i)} + 2\mathrm{cov(x_i, \bar{x}_i)}}{4}. \tag{4.9}$$

Since x_i and $\bar{x}_i$ are identically drawn from the same distribution, $\mathrm{var(x_i)} = \mathrm{var(\bar{x}_i)}$,

$$\mathrm{var}(\hat{\theta}) = \frac{\mathrm{var(x_i)}}{2} + \frac{\mathrm{cov(x_i, \bar{x}_i)}}{2}. \tag{4.10}$$

For a pair of independent samples, $\mathrm{cov(x_i, x_i\prime)} = 0$, thereby,

$$\mathrm{var}(\theta) = \frac{\mathrm{var(x_i)}}{2}. \tag{4.11}$$

On the other hand, for a pair of correlated samples $\{x_i, \bar{x}_i\}$, the variance can be larger or smaller than the above, depending on whether the pair is positively correlated ($\mathrm{cov(x_i, \bar{x}_i)} > 0$) or negatively correlated ($\mathrm{cov(x_i, \bar{x}_i)} < 0$). For a negatively correlated pair, the variance becomes smaller than a pair of independent samples.

The antithetic variate algorithm for a uniform random number $u_i \in [0, 1]$ is the following:

1. Generate for each u_i a negatively correlated sample, $1 - u_i$.

2. Suppose that we want to estimate an expectation value of $\mathbf{X}$,

$$\theta = E[\mathbf{X}] = E[h(\mathbf{U})], \tag{4.12}$$

where $\mathbf{U}^{(i)} = \{\mathbf{U}_1^{(i)}, \mathbf{U}_2^{(i)}, ..., \mathbf{U}_m^{(i)}\}$ is a set of random elements to be used for the construction of one nonuniform variable x_i. $\mathbf{U} = \{\mathbf{U}^{(i)}\}$, and h is a transformation function from a set $\mathbf{U}^{(i)}$ to an element x_i. Thus, set $x_i = h(\mathbf{U}^{(i)})$ and $\bar{x}_i = h(1 - \mathbf{U}^{(i)})$

3. Set $\theta_i = (x_i + \bar{x}_i)/2$

4. Average θ_i over all n elements,

$$\hat{\theta}_n = \sum_{i=1}^{n} \frac{\theta_i}{n}, \tag{4.13}$$

then by the strong law of numbers, $\hat{\theta}_n \to \theta$ as $n \to \infty$.

The strategy of implementing this algorithm into numerical simulations of this work is based on the preparation of antithetic points in a complex space. A generation of random complex numbers, α_i for a coherent state, consists of drawing two real random numbers, $\mathrm{Re}(\alpha_\mathrm{i}), \mathrm{Im}(\alpha_\mathrm{i})$. In this work, the moduli of samples, $|\alpha_i|$, are normally distributed with a mean m and a variance σ^2, and that the phases, ϕ_i are uniformly distributed over the cyclic unit phase interval, $[0, 2\pi]$. Therefore, for each $\alpha_i = |\alpha_i|e^{i\phi_i}$, $(i = 1, \ldots, n)$ which is randomly generated, its antithetic point is $\bar{\alpha}_i = |\alpha_i|e^{-i\phi_i}$ in the complex plane. Then carrying both points into a set of samples makes the algorithm more efficient.

4.2 Numerical Methods for Time Evolution of Wavefunctions

Analytical and numerical analysis of physical systems demand identification and initialization of states of interest to start with. Here, the first thing to be done is therefore finding a ground state wavefunction of a system. We obtain ground states by the imaginary Split-Operator method combined with the Discrete Variable Representation method (DVR, Appendix B). For imaginary-time evolution algorithms applied to Bose-Einstein condensates, see [87]. A numerical method for time evolution of a wavefunction is the second and essential part of analysis of dynamical systems.

In Monte Carlo methods, successive and repetitive calculations of evolution with a small time step are the major time-consuming factor in integration. Therefore, searching for an optimized algorithm for this problem is widely regarded as the most important step to begin with before constructing an algorithm routine in detail.

The split operator method is a candidate for numerical solutions to the time-dependent Schrödinger equation, whose mechanism is splitting noncommutative operators (a kinetic operator and a potential operator) into parts. It provides sufficient accuracy for calculation of time evolution of wavefunctions.

The time-dependent Schrödinger equation with its physical units set to one ($\hbar = 1, m = 1$) is,

$$\begin{aligned} i\frac{\partial\psi(\boldsymbol{x},t)}{\partial t} &= -\frac{\nabla^2}{2}\psi(\boldsymbol{x},t) + V(\boldsymbol{x})\psi(\boldsymbol{x},t) \\ &= H\psi(\boldsymbol{x},t), \end{aligned} \tag{4.14}$$

where $V(\boldsymbol{x})$ is an arbitrary potential and, $\bigtriangledown^2$ is the Laplacian, which is in Cartesian coordinates

$$\bigtriangledown^2 = \frac{\partial^2}{\partial x^2} + \frac{\partial^2}{\partial y^2} + \frac{\partial^2}{\partial z^2}, \tag{4.15}$$

and $H = T + V$ is the Hamiltonian.

A general solution to the Schrödinger equation is one in which an exponential Hamiltonian operator is applied to the wavefunction in an operator sense:

$$\begin{aligned} \psi(\boldsymbol{x}, t) &= e^{iHt}\psi(\boldsymbol{x}, 0) \\ &= e^{i(T+V)t}\psi((x), 0). \end{aligned} \tag{4.16}$$

A naive expansion of the above exponential operator into a kinetic term and a potential term,

$$\begin{aligned} \psi(\boldsymbol{x}, t) &= e^{iTt}e^{iVt}\psi(\boldsymbol{x}, 0) \\ &\text{or} \quad e^{iVt}e^{iTt}\psi(\boldsymbol{x}, 0) \end{aligned} \tag{4.17}$$

does not work, since the kinetic operator (T) and the potential operator (V) do not commute with each other ($[T, V] \neq 0$). Therefore, we are led to think about how to expand these operators correctly in order.

The split operator method uses a more accurate way for advancing the wavefunction forward in time. The wavefunction propagated forward in a time

step, $h = \Delta t$, is written in this method as symmetrically in the operators:

$$\begin{aligned}\psi(\boldsymbol{x}, t+\Delta t) &\simeq e^{i\Delta tT/2} e^{i\Delta tV} e^{i\Delta tT/2} \psi(\boldsymbol{x}, t) \\ &= \exp\left(\frac{i\Delta t}{4} \bigtriangledown^2\right) \exp\left(i\Delta tV\right) \exp\left(\frac{i\Delta t}{4} \bigtriangledown^2\right) + O[(\Delta t^3)] \\ &. \end{aligned} \tag{4.18}$$

The order of the kinetic operator and the potential operator can be reversed interchangeably:

$$\begin{aligned}\psi(\boldsymbol{x}, t+\Delta t) &\simeq e^{i\Delta tT/2} e^{i\Delta tV} e^{i\Delta tT/2} \psi(\boldsymbol{x}, t) \\ \text{or} \quad & e^{i\Delta tV/2} e^{i\Delta tT} e^{i\Delta tV/2} \psi(\boldsymbol{x}, t). \end{aligned} \tag{4.19}$$

The key point of this algorithm is the 'symmetric' decomposition of operators which are successively applied to a wavefunction for one evolution step. Using the first kind of orderings in Eq. 4.19, the strategy of split operator applications in this work proceeds as the following:

1. A wavefunction ($\psi(\boldsymbol{x}, t)$) in configuration space is transformed to the corresponding wavefunction ($\psi(\boldsymbol{k}, t)$) in momentum space, in order to calculate the Laplacian, which might be difficult to do in configuration space but easy to do in momentum space. This is accomplished by applying a Fast Fourier Transform (FFT) forward to the wavefunction:

$$\Psi_0(\boldsymbol{k}, t) = \mathrm{FFT}(\psi_0(\boldsymbol{x}, \mathrm{t})). \tag{4.20}$$

2. Multiply the wavefunction by the exponential kinetic operator, $e^{i\Delta tT/2}$ from

the left:

$$\Psi_1(\boldsymbol{k},t) = e^{i\Delta t k^2/2}\Psi_0(\boldsymbol{k},t). \tag{4.21}$$

3. Transform the wavefunction ($\Psi_1(\boldsymbol{k},t)$) backward to wavefunction ($\psi_1(\boldsymbol{x},t)$) in configuration space:

$$\psi_1(\boldsymbol{x},t) = \mathrm{FFT}^{-1}(\Psi_1(\boldsymbol{k},\mathrm{t})). \tag{4.22}$$

4. Multiply it by the exponential potential operator, $e^{i\Delta tV}$:

$$\psi_2(\boldsymbol{x},t) = e^{i\Delta tV}\psi_1(\boldsymbol{x},t). \tag{4.23}$$

5. Transform $\psi_2(\boldsymbol{x},t)$ once again into the momentum space ($\Psi_2(\boldsymbol{k},t)$):

$$\Psi_2(\boldsymbol{k},t) = \mathrm{FFT}(\psi_2(\boldsymbol{x},\mathrm{t})). \tag{4.24}$$

6. Multiply it by the kinetic operator with the remaining half-time interval:

$$\Psi_3(\boldsymbol{k},t) = e^{i\Delta t k^2/2}\Psi_2(\boldsymbol{k},t). \tag{4.25}$$

7. Transform it ($\Psi_3(\boldsymbol{k},t)$) back into the configuration space to obtain the final result,$\psi(\boldsymbol{x},t+\Delta t)$:

$$\psi(\boldsymbol{x},t+\Delta t) = \mathrm{FFT}^{-1}(\Psi_3(\boldsymbol{k},\mathrm{t})). \tag{4.26}$$

This sequence of steps completes one cycle of time evolution of the wave-

function. Since this series of propagation is repeated continuously to reach the final wavefunction,

$$\begin{aligned}\psi(\boldsymbol{x}, t+\Delta t) &= e^{iH\Delta t}\psi(\boldsymbol{x}, t) \\ &= \underbrace{e^{\frac{iH\Delta t}{n}} e^{\frac{iH\Delta t}{n}} ... e^{\frac{iH\Delta t}{n}}}_{n} \psi(\boldsymbol{x}, t), \end{aligned} \tag{4.27}$$

the above procedure can be shortened in such a way that for intermediate steps, the final backward FFT (step 7) of a previous cycle and the initial forward FFT (step 1) of a next cycle is combined to be canceled each other. In succession, the step 6 of the previous cycle and the step 2 of the next cycle are combined to give a one-full time step evolution of the kinetic operator:

$$\begin{aligned}\Psi_{1,next}(\boldsymbol{k}, t+\Delta t) &= e^{i\Delta t k^2/2}\Psi_{3,previous}(\boldsymbol{k}, t) \\ &= e^{i\Delta t k^2/2} e^{i\Delta t k^2/2}\Psi_{2,previous}(\boldsymbol{k}, t) \\ &= e^{i\Delta t k^2}\Psi_{2,previous}(\boldsymbol{k}, t). \end{aligned} \tag{4.28}$$

So far, we have discussed the Schrödinger equation that contains operators linear in a wavefunction. However, the time-dependent Gross-Pitaevskii equation,

$$i\hbar\frac{\partial}{\partial t}\psi(\boldsymbol{x}, t) = \Big[-\frac{\hbar^2}{2m}\bigtriangledown^2 + V(\boldsymbol{x}, t) + g|\psi(\boldsymbol{x}, t)|^2)\Big]\psi(\boldsymbol{x}, t) \tag{4.29}$$

contains nonlinear interaction terms so that it needs further careful consideration into the expansion of operators, since the operator algebra used in the previous split operator method might no longer work with nonlinearity. The

nonlinear term is not an independent external potential, but a function of time-varying wavefunctions.

Fortunately, it turns out [88] that this new potential problem with a split operator method for the Gross-Pitaevskii equation is resolved by simple modification to the intermediate step 4, the step of applying potential energy containing the nonlinear term. The potential term $V(\boldsymbol{x},t)+g|\psi(\boldsymbol{x},t)|^2$ has a nonlinear term which remains to be specified in detail with respect to time. Then, the solution is to use the most recent wavefunction ($\psi_1(\boldsymbol{x},t)$) for the nonlinear term [88] instead of the initial wavefunction ($\psi_0(\boldsymbol{x},t)$) at the beginning of the time step:

$$V'(\boldsymbol{x},t) \equiv V(\boldsymbol{x},t)+g|\psi_1(\boldsymbol{x},t)|^2. \tag{4.30}$$

To be more specific, the step 4 is slightly modified to:

$$\begin{aligned} \psi_2(\boldsymbol{x},t) &= e^{i\Delta t V'}\psi_1(\boldsymbol{x},t) && (4.31)\\ &= \exp\left[i\Delta t\big(V(\boldsymbol{x},t)+g|\psi_1(\boldsymbol{x},t)|^2\big)\right]\psi_1(\boldsymbol{x},t). && (4.32) \end{aligned}$$

This change keeps the order of time stepping error ($\mathrm{O}(\Delta t^3)$) as the traditional split operator method does.

The above split operator method has a third order numerical round-off error. If we note that the kinetic operators and the potential operators are alternately applied to a wavefunction, we can guess how to reduce the stepping error: it is by repeating the interchange of operator applications more frequently. In fact, it is possible to enhance the accuracy of evolution to $\mathrm{O}(\Delta t^4)$

and $O(\Delta t^5)$ [88].

Generalizing the split operator method to higher order precision, the wave-function is propagated in the following way,

$$\psi(\boldsymbol{x}, t+\Delta t) = e^{i\Delta t\beta_n} e^{i\Delta t\alpha_n} ... e^{i\Delta t\beta_1} e^{i\Delta t\alpha_1} \psi(\boldsymbol{x}, t+\Delta t). \tag{4.33}$$

For the precision within $O(\Delta t^4)$,

$$\begin{aligned}
\alpha_1 &= 1 - \tfrac{3\gamma - \frac{4}{3} \mp \Gamma}{2\gamma(\gamma \mp \Gamma)}, & \beta_1 &= \tfrac{\gamma \mp \Gamma}{2}, \\
\alpha_2 &= \tfrac{3-4\gamma}{2(2-3\gamma)}, & \beta_2 &= \tfrac{\gamma \pm \Gamma}{2}, \\
\alpha_3 &= \tfrac{4/3 - \gamma \pm \Gamma}{2\gamma(\gamma \pm \Gamma)}, & \beta_3 &= 1 - \gamma,
\end{aligned}$$

$$\Gamma = \sqrt{\frac{16 - 48\gamma + 45\gamma^2 - 12\gamma^3}{9 - 12\gamma}}, \tag{4.34}$$

where γ is chosen such that Γ does not become an imaginary number. We can easily see that neither the ordering nor the coefficients are symmetric. For the precision up to $O(\Delta t^5)$,

$$\begin{aligned}
\alpha_1 &= \tfrac{1}{2}\xi, & \beta_1 &= \xi, \\
\alpha_2 &= \tfrac{1-\sqrt[3]{2}}{2}\xi, & \beta_2 &= -\sqrt[3]{2}\xi, \\
\alpha_3 &= \tfrac{1-\sqrt[3]{2}}{2}\xi, & \beta_3 &= \xi, \\
\alpha_4 &= \tfrac{1}{2}\xi,
\end{aligned}$$

$$\xi = \frac{1}{2 - \sqrt[3]{2}}, \tag{4.35}$$

which is implemented for some cases in this work along with the third order split operator above.

4.3 Numerical Conversion

For every numerical calculation of a physical system, it is required to have an appropriate dimensionless system in order to implement it into a program. Here, we discuss a setup for numerical simulations used in this work: a dimensionless Gross-Pitaevskii equation in both the Truncated Wigner Approximation and the positive P representation.

4.3.1 The One-Dimensional GPE

First, we derive the one-dimensional Gross-Pitaevskii equation from the three-dimensional Gross-Pitaevskii equation:

$$i\hbar\frac{\partial}{\partial t}\bar{\psi}(\boldsymbol{x},t) = \big[-\frac{\hbar^2}{2m}\bigtriangledown^2 + V(\boldsymbol{x},t) + g_{3D}|\bar{\psi}(\boldsymbol{x},t)|^2\big]\bar{\psi}(\boldsymbol{x},t), \tag{4.36}$$

where the external potential $V(\boldsymbol{x},t)$ and the three-dimensional interaction coefficient g_{3D} are defined as,

$$V(\boldsymbol{x},t) = \frac{1}{2}m\big(\omega_\rho^2\bar{\rho}^2 + \omega_z^2\bar{z}^2\big) + \bar{s}\sin^2(k\bar{z}), \tag{4.37}$$

$$g_{3D} = \frac{4\pi\hbar^2 a}{m}. \tag{4.38}$$

We use the cylindrical coordinates for the Laplacian,

$$i\hbar\frac{\partial}{\partial t}\bar{\psi}(\boldsymbol{x},t) = \Big[-\frac{\hbar^2}{2m}\Big\{\frac{\partial^2}{\partial\bar{z}^2} + \frac{1}{\bar{\rho}}\frac{\partial^2}{\partial\bar{\phi}^2} + \frac{1}{\bar{\rho}}\frac{\partial}{\partial\bar{\rho}}\bar{\rho}\frac{\partial}{\partial\bar{\rho}}\Big\}$$
$$+\frac{1}{2}m(\omega_\rho^2\bar{\rho}^2 + \omega_z^2\bar{z}^2) + \bar{s}\sin^2(k\bar{z}) + \frac{4\pi\hbar^2 a}{m}|\bar{\psi}(\boldsymbol{x},t)|^2\Big]\bar{\psi}(\boldsymbol{x},t). \tag{4.39}$$

Suppose the wavefunction is separated by variables,

$$\psi(\boldsymbol{x},z) = \psi_{\bar{\rho}}(\bar{\rho})\psi_{\bar{\phi}}(\bar{\phi})\psi_{\bar{z}}(\bar{z}), \tag{4.40}$$

and the wavefunction has no dependence on the angular coordinate so we can assume the following function with a proper normalization,

$$\psi_{\bar{\phi}}(\bar{\phi}) = \frac{1}{\sqrt{2\pi}},$$
$$\int_0^{2\pi} d\bar{\phi}|\psi_{\bar{\phi}}(\bar{\phi})|^2 = 1. \tag{4.41}$$

With regard to the radial coordinate $\bar{\rho}$,

$$H_{\bar{\rho}}\psi_{\bar{\rho}}(\bar{\rho}) \;=\; \Big[-\frac{\hbar^2}{2m}\frac{1}{\bar{\rho}}\frac{\partial}{\partial\bar{\rho}}\bar{\rho}\frac{\partial}{\partial\bar{\rho}} + \frac{1}{2}m\omega_\rho^2\bar{\rho}^2\Big]\psi(\bar{\rho})(\bar{\rho}) = \bar{\epsilon}_{\bar{\rho}}\psi_{\bar{\rho}}(\bar{\rho}). \tag{4.42}$$

Dividing both sides by $\hbar^2/2m$,

$$\Big[-\frac{1}{\bar{\rho}}\frac{\partial}{\partial\bar{\rho}}\bar{\rho}\frac{\partial}{\partial\bar{\rho}} + \frac{\bar{\rho}^2}{\bar{\alpha}_\rho^4}\Big]\psi(\bar{\rho})(\bar{\rho}) = \frac{2m}{\hbar^2}\bar{\epsilon}_{\bar{\rho}}\psi_{\bar{\rho}}(\bar{\rho}), \tag{4.43}$$

where $\bar{\alpha}_\rho^2$ is defined as

$$\bar{\alpha}_\rho = \sqrt{\frac{\hbar}{m\omega_\rho}}, \tag{4.44}$$

which is the characteristic length of a simple harmonic oscillator in the radial direction.

Then, the solution to the above equation is

$$\psi_{\bar{\rho}}(\bar{\rho}) = \eta_\rho e^{-\bar{\rho}^2/2\bar{\alpha}_\rho^2}, \tag{4.45}$$

where the normalization condition requires that

$$\int_0^\infty \bar{\rho} d\bar{\rho} |\psi_{\bar{\rho}}(\bar{\rho})|^2 = 1, \tag{4.46}$$

$$\eta_\rho = \frac{\sqrt{2}}{\bar{\alpha}_\rho}, \bar{\epsilon}_{\bar{\rho}} = \frac{\hbar^2}{m\bar{\alpha}_\rho^2}, \tag{4.47}$$

such that the above equation becomes,

$$\Big[-\frac{\hbar^2}{2m}\frac{\partial^2}{\partial \bar{z}^2} + \frac{1}{2}m\omega_z^2 \bar{z}^2 + \bar{s}\sin^2(k\bar{z}) + \frac{4\pi\hbar^2 a}{m}|\psi(\boldsymbol{x},t)|^2 \Big] \psi_{\bar{\rho}}(\bar{\rho})\psi_{\bar{\phi}}(\bar{\phi})\psi_{\bar{z}}(\bar{z}) = (\bar{\mu} - \bar{\epsilon}_{\bar{\rho}})\psi_{\bar{\rho}}(\bar{\rho})\psi_{\bar{\phi}}(\bar{\phi})\psi_{\bar{z}}(\bar{z}). \tag{4.48}$$

We multiply this equation by $\psi_{\bar{\rho}}(\bar{\rho})\psi_{\bar{\phi}}(\bar{\phi})$ from the left and integrate over the $\bar{\rho}, \bar{\phi}$ coordinates,

$$[-\frac{\hbar^2}{2m}\frac{\partial^2}{\partial \bar{z}^2} + \frac{1}{2}m\omega_z^2 \bar{z}^2 + \bar{s}\sin^2(k\bar{z}) + \frac{2\hbar^2 a}{m\bar{\alpha}_\rho^2}|\psi_{\bar{z}}(\bar{z},t)|^2)]\psi_{\bar{z}}(\bar{z})$$

$$= (\bar{\mu} - \bar{\epsilon}_{\bar{\rho}})\psi_{\bar{z}}(\bar{z}). \tag{4.49}$$

Here, we note that

$$\int_0^{2\pi} d\phi |\psi_{\bar{\phi}}(\bar{\phi})|^2 = 1, \qquad \int_0^{\infty} \bar{\rho} d\bar{\rho} |\psi_{\bar{\rho}}(\bar{\rho})|^2 = 1,$$
$$\int_0^{2\pi} d\bar{\phi} |\psi_{\bar{\phi}}(\bar{\phi})|^4 \int_0^{\infty} \bar{\rho} d\bar{\rho} |\psi_{\bar{\rho}}(\bar{\rho})|^4 = \frac{1}{2\pi} \frac{4}{\bar{\alpha}_\rho^4} \int_0^{\infty} \bar{\rho} d\bar{\rho} e^{-2\bar{\rho}^2/\bar{\alpha}_\rho^2} = \frac{1}{2\pi\bar{\alpha}_\rho}. \tag{4.50}$$

Putting the definition of $\bar{\alpha}_\rho$, we finally get the one-dimensional Gross-Pitaevskii equation,

$$\Big[-\frac{\hbar^2}{2m}\frac{\partial^2}{\partial \bar{z}^2} + \frac{1}{2} m\omega_z^2 \bar{z}^2 + \bar{s}\sin^2(k\bar{z}) + 2\hbar\omega_\rho a |\psi_{\bar{z}}(\bar{z}, t)|^2) \Big] \psi_{\bar{z}}(\bar{z})$$
$$= (\bar{\mu} - \bar{\epsilon}_{\bar{\rho}})\psi_{\bar{z}}(\bar{z}). \tag{4.51}$$

4.3.2 Numerical Conversion

We now convert the Eq. 4.51 to a dimensionless equation. The first thing we can easily do is to scale the coordinates by the factor of wavelengths of the optical lattice:

$$\bar{z} = \frac{z}{k}, \bar{\alpha}_\rho = \frac{\alpha_\rho}{k}, \bar{\alpha}_z = \frac{\alpha_z}{k}, \tag{4.52}$$
$$k = 2\pi/\lambda, \tag{4.53}$$

where z is a dimensionless rescaled coordinate, and α_ρ, α_z are dimensionless characteristic lengths of a harmonic oscillator in the transverse and the longitudinal direction, respectively.

At the same time, we rescale the wavefunction using the normalization

condition:

$$\begin{aligned} 1 &= \int d\bar{z}|\bar{\psi}(\bar{z})|^2 \\ &= \frac{1}{k}\int dz|\bar{\psi}(\bar{z})|^2 \\ &= \int dz|\psi(z)|^2, \end{aligned} \tag{4.54}$$

thus

$$\bar{\psi}(\bar{z},t) = \sqrt{k}\psi(z,t). \tag{4.55}$$

Now, we convert the one-dimensional GPE, Eq. 4.51 into a dimensionless one, by dividing it by the recoil energy,

$$E_R = \frac{\hbar^2 k^2}{2m}. \tag{4.56}$$

We have then

$$\big[-\frac{\partial^2}{\partial z^2} + \frac{z^2}{\alpha_z^4} + s\sin^2(z) + \frac{4ka}{\alpha_\rho}|\psi_z(z,t)|^2)\big]\psi_z(z,t) = (\mu - \epsilon_\rho)\psi_z(z,t), \tag{4.57}$$

where $\bar{s} = E_R s, \bar{\mu} = E_R\mu, \bar{\epsilon}_{\bar{\rho}} = E_R\epsilon_\rho$, and

$$\frac{2m}{\hbar^2 k^2}2\hbar\omega_\rho a = \frac{4m\omega_\rho a}{\hbar k} = \frac{4ka}{\alpha_\rho}. \tag{4.58}$$

The dimensionless time-dependent GPE is obtained similarly. We first

scale the time step as the following,

$$\bar{t} \;=\; \frac{\hbar}{E_R}t = \frac{1}{\omega_R}t. \tag{4.59}$$

Using the scaled time coordinate t, we obtain from the dimensionful time-dependent GPE,

$$\begin{aligned}\big[-\frac{\hbar^2}{2m}\frac{\partial^2}{\partial\bar{z}^2} + \frac{1}{2}m\omega_z^2\bar{z}^2 + \bar{s}\sin^2(k\bar{z}) + 2\hbar\omega_\rho a|\psi_{\bar{z}}(\bar{z},t)|^2)\big]\psi_{\bar{z}}(\bar{z}) \\ = i\hbar\frac{\partial}{\partial\bar{t}}\psi_{\bar{z}}(\bar{z}),\end{aligned} \tag{4.60}$$

and the dimensionless time-dependent GPE is

$$\big[-\frac{\partial^2}{\partial z^2} + \frac{z^2}{\alpha_z^4} + s\sin^2(z) + \frac{4ka}{\alpha_\rho}|\psi_z(z,t)|^2)\big]\psi_z(z,t) = i\frac{\partial}{\partial t}\psi_z(z,t). \tag{4.61}$$

The time-dependent evolution equation of a noncondensate wavefunction in the positive P representation is similarly obtained with a noise term added.:

$$\begin{aligned} i\hbar\frac{\partial}{\partial\bar{t}}\bar{\psi}_{NC}(\bar{z},\bar{t}) \;&=\; -\frac{\hbar^2}{2m}\bigtriangledown^2\bar{\psi}_{NC}(\bar{z},\bar{t}) + V(\bar{z})\bar{\psi}_{NC}(\bar{z},\bar{t}) \\ &\quad +2g|\bar{\psi}_C(\bar{z},\bar{t})|^2\bar{\psi}_{NC}(\bar{z},\bar{t}) + g(\bar{\psi}_C(\bar{z}))^2\bar{\psi}^\dagger_{NC}(\bar{z},\bar{t}) \\ &\quad +\sqrt{\frac{i}{\hbar}g(\bar{\psi}_C(\boldsymbol{x}))^2}\bar{\eta}_{NC}(\bar{z},\bar{t}), \end{aligned} \tag{4.62}$$

$$\bar{\eta}^i_{NC}(\bar{z}_1,\bar{t}_1)\bar{\eta}^j_{NC}(\bar{z}_2,\bar{t}_2) \;=\; \delta(\bar{z}_1-\bar{z}_2)\delta(\bar{t}_1-\bar{t}_2)\delta_{ij} \qquad (i,j=-,+). \tag{4.63}$$

We now use the same unit as in the above for the condensate wavefunction

and the noncondensate wavefunction:

$$\bar{\psi}_C(\bar{z},\bar{t}) = \sqrt{k}\psi_C(z,t),$$
$$\bar{\psi}_{NC}(\bar{z},\bar{t}) = \sqrt{k}\psi_{NC}(z,t), \tag{4.64}$$

and the normalization for the noise field is

$$\bar{\eta}^i_{NC}(\bar{z},\bar{t}) = \sqrt{\omega_R k}\eta^i_{NC}(z,t), \tag{4.65}$$

since

$$\begin{aligned}\delta_{ij} &= \int d\bar{z}d\bar{t}\bar{\eta}^i_{NC}(\bar{z}_1,\bar{t}_1)\bar{\eta}^j_{NC}(\bar{z}_2,\bar{t}_2) = \frac{1}{\omega_R k}\int dzdt\bar{\eta}^i_{NC}(\bar{z}_1,\bar{t}_1)\bar{\eta}^j_{NC}(\bar{z}_2,\bar{t}_2) \\ &= \int dzdt\eta^i_{NC}(z_1,t_1)\eta^j_{NC}(z_2,t_2). \end{aligned}\tag{4.66}$$

Then, dividing Eq. 4.62 by E_R and $\sqrt{k}$, the dimensionless equation is obtained as,

$$\begin{aligned}i\frac{\partial}{\partial t}\psi_{NC}(z,t) &= -\frac{\partial^2}{\partial z^2}\psi_{NC}(z,t) + V(z,t)\psi_{NC}(z,t) \\ &\quad + \frac{8ka}{\alpha_\rho}|\psi_C(z,t)|^2\psi_{NC}(z,t) + \frac{4ka}{\alpha_\rho}(\psi_C(z,t))^2\psi^\dagger_{NC}(z,t) \\ &\quad + \sqrt{i\frac{4ka}{\alpha_\rho}(\psi_C(z,t))^2}\eta^i_{NC}(z,t), \end{aligned}\tag{4.67}$$

where the nontrivial coefficient of the noise term is calculated as

$$\frac{1}{E_R}\sqrt{i\hbar(2\hbar\omega_\rho a)\bar{\psi}_C(\bar{z},\bar{t})^2}\bar{\eta}_{NC}(\bar{z},\bar{t}) =$$

$$\sqrt{i\hbar(\frac{2m}{\hbar^2k^2})^2 2\hbar\frac{\hbar}{m}(\frac{k}{\alpha_\rho})^2 ak\omega_R k\frac{1}{k}}\psi_C(z,t)\eta^i_{NC}(z,t)$$
$$= \sqrt{i\frac{4ka}{\alpha_\rho}(\psi_C(z,t))^2}\eta^i_{NC}(z,t). \tag{4.68}$$

Chapter 5

Phase Coherence of One- and Two-Component BECs

5.1 Configuration of Systems

The systems we study include one-component and two-component 1D BEC confined by a harmonic trap with state-dependent optical lattices at zero or low temperature. The two-components might be two hyperfine states of the same species or two states from two different species, where they have interspecies interaction between the states. Here, we assume that the condensate is of the former type consisting of Rubidium atoms, and we choose $F = 1, m_F = -1$ or $F = 2, m_F = -2$ for those one-component or two-component BECs. Even though they are of the same species, we will call intraspecies and interspecies interactions among the states, instead of intra-component and inter-component interactions. One can calculate a phase diagram using Density Matrix Renormalization Group (DMRP) for one-component systems [89] or for two- com-

ponent systems [26, 90].

We choose these two states for this work, since they have almost identical intraspecies and interspecies interaction strengths. Therefore, we assume that the two atoms have the same intraspecies interaction strength ($a_{AA} = a_{BB} = 5.5nm$) and they share the same interspecies interaction strength equal to the intraspecies interaction ($a_{AB} = a_{AA} = a_{BB}$).

For one-component BECs, the condensation of cigar-shaped atomic clouds is achieved in the harmonic trap with the tight confinement along the radial direction ($\omega_\rho = 2\pi \times 500Hz$) and the shallow confinement along the axial direction ($\omega_z = 2\pi \times 100Hz$). In this work, the total number of atoms ranges from 10^3 to 10^4. The chemical potential is $1.27E_R$ for $N = 10^4$, $1.16E_R$ for $N = 8 \times 10^3$. For two-component BECs, the trap frequencies are $\omega_\rho = 2\pi \times 2kHz$, $\omega_z = 2\pi \times 100Hz$, and the chemical potential is $2.9E_R$ for $N = 5 \times 10^3$. The optical lattices are generated by a blue-detuned off-resonant laser with wavelength $\lambda = 1064$ nm, so that the period is $d = \lambda/2$, and the recoil frequency is $\omega_R/2\pi = (\hbar/2m)(2\pi/\lambda)^2 = 2\pi \times 2.03$ kHz.

The numerical preparation of initial states requires calculations of ground state wavefunctions, Bogoliubov quasiparticle excited modes, and probability distributions governed by selected phase space representations. We find the ground state wavefunctions by numerically integrating the GPE in imaginary time with a time step of $\omega_R \delta t = 0.005$ or less and with 2048 or 3072 spatial grid points. We utilize the split-operator method to integrate the time evolution of wavefunctions. Using the ground state solutions of the GPE, we obtain quasiparticle wavefunctions for energy, ϵ_μ by the diagonalization of the Bogoliubov-de Gennes equation [Eq. 3.46].

The dimensionless coupling strength of interaction energies in this work is $\gamma = mg_{1D}/\hbar^2 n_{1D} \lesssim 1.5 \times 10^{-3}$ and the reduced temperature for most cases is $\tau = 2mk_BT/\hbar^2 n_{1D}^2 = 0$ unless stated otherwise. Therefore, the 1D Bose gas can be effectively described by the Gross-Pitaevskii equation in the regime ($\tau^2 \lesssim \gamma \lesssim 1$) far from the Tonks-Girardeau regime ($\gamma \gtrsim 1$). The nonlinearity $g_{1D}N/\hbar\omega_z l_z$ [16] ranges from 200 to 1500.

We calculate the ensemble average of stochastic fields along the trajectory and find their coherence. Stochastic quantum fluctuations are appended to the initial mean-field state for the generation of the ensemble of Wigner-distributed or P-distributed initial states, in which step we perform the Gaussian random variable generation of order parameters $(\alpha_{i0}, \alpha_\mu)$ for both components. For the condensate mode, the mean of α_{io} is $\sqrt{N_{i0}}$ and its width of deviation is $\sqrt{1/2}$. For the Bogoliubov quasiparticle mode, the mean of α_μ is zero for both the Wigner and the positive P representations, whereas the width is $\sqrt{n_\mu + 1/2}$ in the Wigner representation, $\sqrt{n_\mu}$ in the positive P representations. A single sample of stochastic fields, $\psi_W(x)$ is obtained by configuring the wavefunction profiles with the generated stochastic order parameters.

The condition for numerical validity of the TWA method in the Bogoliubov theory is that the condensate mode must be highly populated compared to the noncondensate mode so that the quantum fluctuation is small being dominated by the order of condensate field. In other words, the TWA in the mean-field theory is valid with a relatively small number of excited modes compared to the number of condensate particles in the system, $N \gg M/2$, where N is the total number of atoms, M is the number of Bogoliubov quasiparticles [72]. This is a regime different from other exact numerical methods, for example,

the Time Evolving Block Decimation(TEBD) method or the Density Matrix Renormalization Group (DMRG) with the Bose Hubbard Model, in which cases each site is limited to a low filling factor since the Hilbert space increases exponentially with the number of atoms and the number of sites.

This validity condition means that quantum noises in the initial state should not be greater than the number of atoms in a system in the TWA method. In the hybrid model to be compared with the TWA, we also require the same validity condition for the system, since time evolution of wavefunctions with dominating noncondensate quasiparticles in the positive P representation used to be divergent being subject to large excursion in phase space.

In pursuit of sufficient convergence in Monte Carlo methods, we typically perform simulations with an ensemble of states consisting of 500 samples with the TWA or the hybrid distribution. The time evolution of ensembles has usually a time step given by $\omega_R \delta t = 0.005$, i.e. $\delta t = 0.4\mu s$, or less.

We study phase coherence properties of a system as we apply state-dependent time-varying optical lattice along the axial direction to one-component or two-component BECs, which will eventually lead to phase decoherence. We are especially interested in the short-range non-local coherence of subcondensates between neighboring sites, since these terms will mimic the visibility of the interference patterns observed in experiments in which the condensates in the lattice are released. Long-range coherence is not considered, since the condensate of finite size is not uniform in the presence of a harmonic trap, which might affect long-range coherence. The effect due to fluctuation in local phases is ignored, since local phase diffusion is averaged out for each well as follows. We define a subcondensate projection operator for each site l as in

[71],

$$\hat{a}_{il}(t) = \int_{l^{th}site} dz \bar{\psi}_{GP}(z,t)\hat{\psi}_{W,i}(z,t), \tag{5.1}$$

where a_{il} is the annihilation operator for component i in the l^{th} well, $\bar{\psi}_{GP}(z,t)$ the solution of the GPE for each fixed time t, normalized to one, $\hat{\psi}_i(x,t)$ is a single realization of the field following a stochastic path by the TWA or the hybrid representation. The definitions of the site positions are different for two components as explained below. This operator is defined as a stochastic field operator whose amplitudes are projected over the ground state of each condensate mode. The projection method allows us to avoid the complicated calculations of symmetrically-ordered multimode fields.

The initial wavefunction under an external harmonic potential is shown in Fig. 5.1. In addition to the trap, for one-component BECs, we apply a sinusoidal lattice potential with a local maximum at the center, $V_o = sE_R \cos^2(k\bar{z})$, where s is the scale of lattice height and $E_R = \hbar^2 k^2/2m$ is the recoil energy. For two-component BECs in this work, the lattices applied are state-dependent:

$$\begin{aligned} V_{o,A} &= s_A E_R \cos^2(k\bar{z}), \\ V_{o,B} = 0 \quad \text{or} \quad V_{o,B} &= s_B E_R \sin^2(k\bar{z}), \end{aligned} \tag{5.2}$$

where s_i is the lattice height for the component i. The optical lattice for component B is absent or a half-period mismatch potential if present.

Here, the stationary ground state wavefunction of both one-component and two-component BECs become symmetric with respect to the origin because

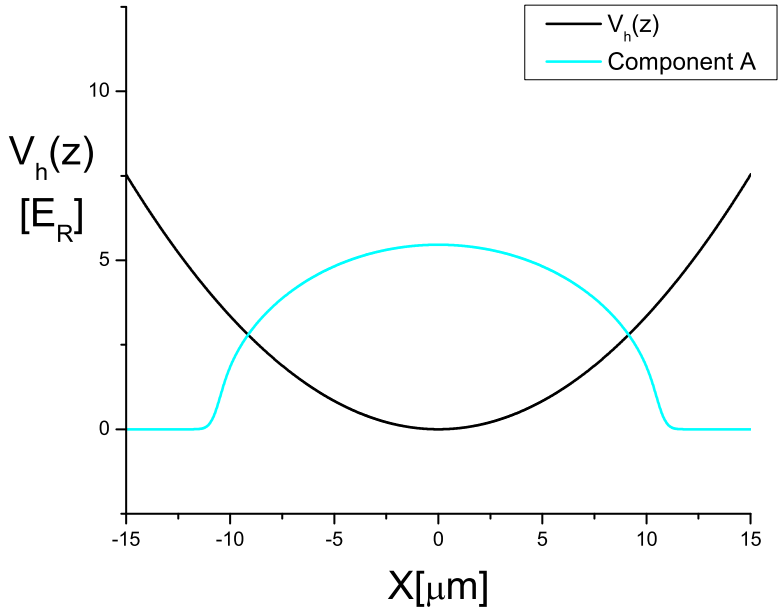

Figure 5.1: The shape of a harmonic trap potential with no lattice and a ground state wavefunction, which is obtained by imaginary time evolution under GPE: the black line (harmonic trap), the blue line (ground state wavefunction, arbitrarily scaled).

the $\cos^2(k\bar{z})$ and $\sin^2(k\bar{z})$ are even functions. For each component, we denote the well closest to the minimum of the harmonic trap ($z = 0$) as the center well (0^{th} well) and the wells adjacent to the center well in the outward direction as the 1^{st} well, 2^{nd} well, and so on.

For now, we focus on two-component BECs with a state-dependent lattice effective to component A only. Even though the external potential for the component B does not include an optical lattice ($V_{o,B} = 0$), the component B is not unaffected by the presence of the optical lattice for A. If the density of the condensate A sufficiently dominates the density of the condensate B and the condensate A experiences a deep lattice, the interspecies interaction term in the GPE, which is proportional to the density of condensate A provides an effective atomic mean-field lattice potential to the component B, since the interaction strength periodically varies over space because of the field A's modulational variation. As the condensate A becomes localized at each well of the optical lattice when the lattice is ramped up, the condensate B becomes localized too, but to the wells formed by variation of the component A's modulus.

Here, the distance between two sites for component B is the same as for the component A, but the positions of each well is shifted by $d/2$, where d is the period of the optical lattice. In other words, each i^{th} well for the component B is located amidst the two adjacent wells for the component A, as shown in Fig. 5.2 and Fig. 5.3. ψ_A and ψ_B are localized at the odd sites $z = \pm(2n + 1)d/2$, at the even sites $z = \pm 2nd/2$ ($n = 0, 1, 2, ...$), respectively. Repulsive interspecies interactions repel component B atoms from the localization sites of the component A. Also, we selectively define the projection operators of the component A and B only for the odd and even sites in Eq. 5.1.

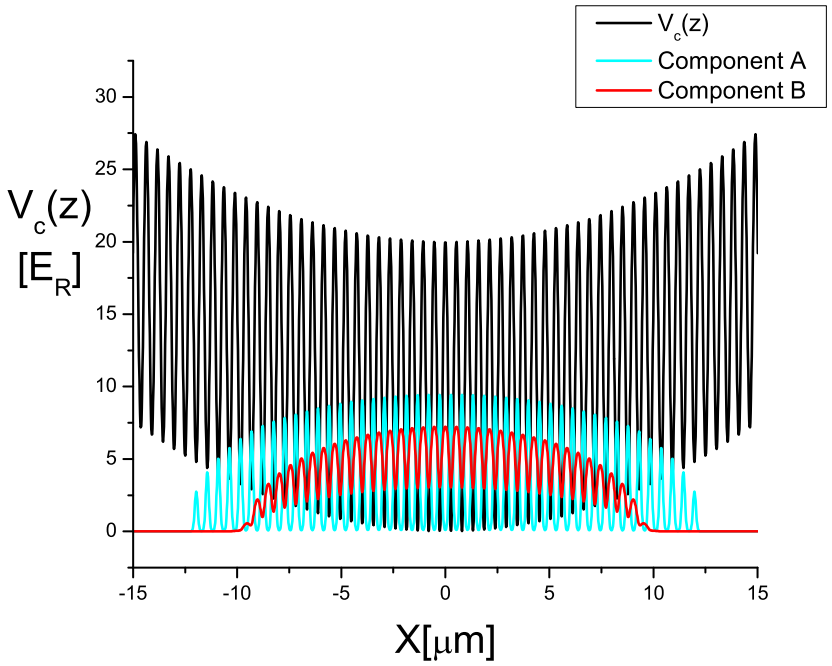

Figure 5.2: The ground state wavefunctions of the component A (the blue line) and the component B (the red line) under a harmonic trap plus an optical lattice effective to component A only (the black line), $V_c(z) = V_h(z) + V_{o,A}(z)$. The wavefunctions are arbitrarily scaled to this figure.

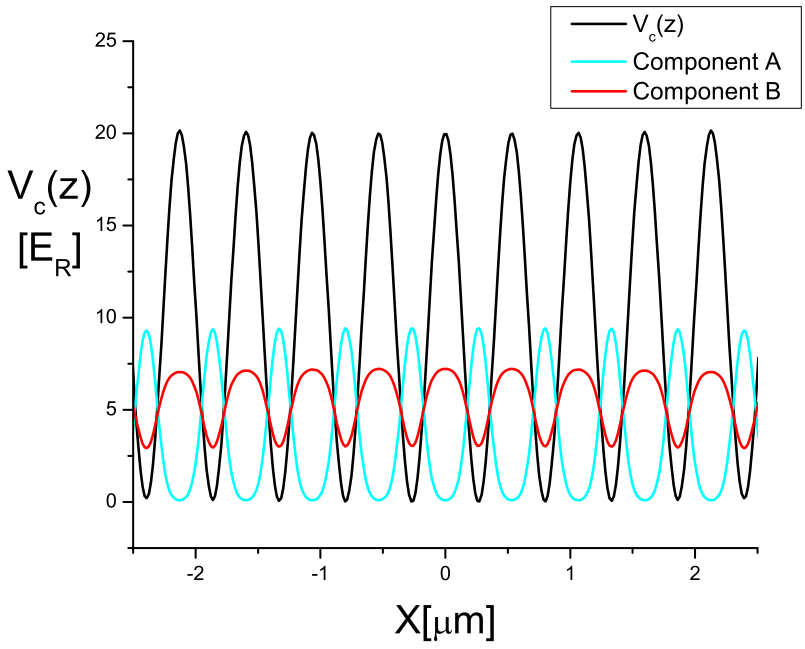

Figure 5.3: Fig. 5.2 rescaled.

We now consider the moments of operators of interest. First, the occupation number of component i in the l^{th} site is

$$n_{il} = \langle \hat{a}_{il}^{\dagger} \hat{a}_{il} \rangle = \langle \hat{a}_{il}^{\dagger} \hat{a}_{il} \rangle_W - \frac{1}{2}. \tag{5.3}$$

For the BEC with a large number of atoms, the transformation offset $1/2$ between the symmetrically-ordered operators and the normally-ordered operators can be disregarded. A more interesting observable is the degree of coherence. The general n^{th} order correlation function is defined as

$$g^{(n)} = \frac{\langle \hat{a}_1^{\dagger}(t_1) \hat{a}_2^{\dagger}(t_2) ... \hat{a}_n^{\dagger}(t_n) \hat{a}_n(t_n) ... \hat{a}_2(t_2) \hat{a}_1(t_1) \rangle}{\prod_i^n \langle \hat{a}_i^{\dagger}(t_i) \hat{a}_i(t_i) \rangle^{1/2}}, \tag{5.4}$$

where $\hat{a}_i$ denotes any projection operator. The equal-time first-order coherence is the phase coherence of component i between two sites at the time t:

$$\begin{aligned} g_i^{(1)} \equiv C_{i;ll'}(t) &= \frac{|\langle \hat{a}_{il}^\dagger(t)\hat{a}_{il'}(t)\rangle|}{(\langle \hat{a}_{il}^\dagger(t)\hat{a}_{il}(t)\rangle\langle \hat{a}_{il'}^\dagger(t)\hat{a}_{il'}(t)\rangle)^{1/2}} \\ &= \frac{|\langle \hat{a}_{il}^\dagger\hat{a}_{il'}\rangle|}{\sqrt{n_{il}n_{il'}}}, \end{aligned} \tag{5.5}$$

where in the last equation the notation is simplified via Eq. 5.3. This coherence is directly related to the visibility of interference peaks if the system is released from the optical lattice. For brevity, we now omit the time dependence from the expectation values of the condensate mode operators.

The above discussion was related to the number operator and the coherence factor. On the other hand, the construction of a phase operator is more demanding, since no complete phase operator has been found, though there are many excellent attempts [91–95]. Instead, we can work with an exponential form of such a phase operator, which is known to be Hermitian making the theoretical model consistent. We divide an expectation value of $\hat{a}_i = |\hat{a}_i|e^{i\hat{\phi}_i}$ operator into two parts: the modulus part ($|\hat{a}_i|$) and the phase part ($e^{i\hat{\phi}_i}$). Then the relative phase coherence between two wells, D_{ij} is

$$D_{ij} = |e^{i\hat{\phi}_i - i\hat{\phi}_j}|. \tag{5.6}$$

5.2 Phase Coherence of One-Component BEC

5.2.1 Phase Decoherence by Increased Lattice Height

Before discussing phase coherence of two-component BECs, we first investigate one-component cases. In this section, we show that phase coherence is lost depending on the final maximum lattice height, when we linearly turn on the optical lattice up to a certain level and then maintain it at that level. All other considerations, for example, change in variance of number, dependence of coherence loss on temperature and interaction strength, etc. are discussed in [16, 68]. The Bose-Hubbard Hamiltonian (for the extended Bose Hubbard model, see [96]) that describes on-site interaction energies and tunneling amplitudes between wells based on tight-binding approximation is

$$H = \frac{U}{2}\sum_i \hat{a}_i^\dagger \hat{a}_i^\dagger \hat{a}_i \hat{a}_i - J\sum_{i\neq j} \hat{a}_i^\dagger \hat{a}_j + \sum_i \epsilon_i \hat{a}_i^\dagger \hat{a}_i, \tag{5.7}$$

where U is the on-site interaction strength and J is the strength of tunneling from site to site. As the lattice height is increased, the overlap of wavefunctions between adjacent wells is decreasing, reducing the tunneling strength. Therefore, the BEC changes from the superfluid phase ($U/J \to 0$) to the Mott-insulator phase ($U/J \to \infty$). Eventually, the relative phase coherence between adjacent sites is lost, since the tunneling time becomes longer. The quantum phase fluctuation plays an important role in the quantum phase transition [58, 97]. A ground state of Mott insulator phase has a zero number fluctuation ($\Delta n = 0$) and uncorrelated phases between wells ($\Delta\phi = \phi_1 - \phi_2$ becomes uncertain).

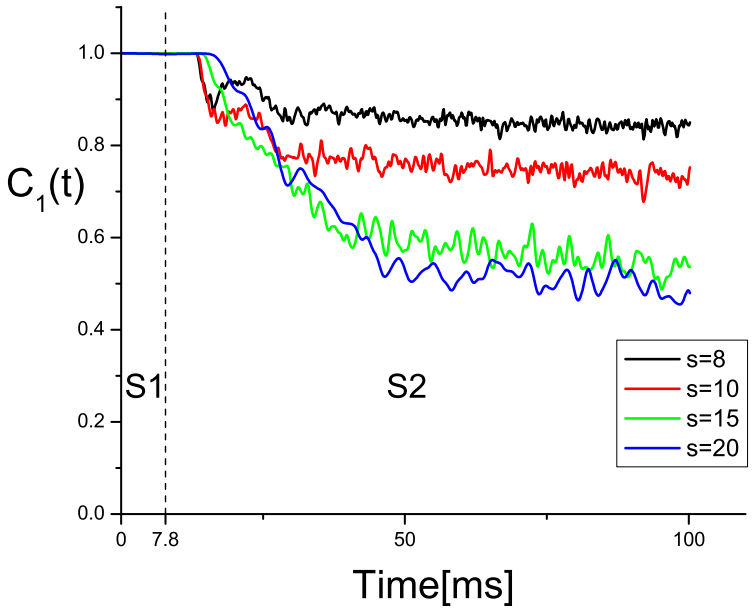

Figure 5.4: Phase coherence of one-component BEC depending on final lattice heights (s): the black line ($s = 8$), the red line ($s = 10$), the green line ($s = 15$), and the blue line ($s = 20$). The period of ramping up the optical lattice is denoted by 'S1' and the period of keeping the lattice height constant is denoted by 'S2'.

In general, the ground state in the Mott insulator is difficult to obtain since it requires long relaxation time because of small tunneling strength. Therefore, in an experiment it is necessary for the ramping-up of a lattice to be sufficiently adiabatic to keep unwanted excitation from occurring to a condensate.

We show phase coherence between the center well and i^{th} adjacent wells, C_i in later plots of this section. The number of atoms is 10^4 and we gradually ramp up the lattice in 7.8ms, and after the ramp-up, the lattice and the harmonic trap are kept constant until the end of simulations. It is expected that coherence is lost as the lattice height is increased and the tunneling prob-

abilities between wells become decreased. In Fig. 5.4, the change in phase coherence is shown as a function of time depending on the final lattice heights. The coherence is plotted from when the lattice begins to turn on to the end of calculations. The initial state is supposed to have the maximal coherence of 1. Thus, the period of ramping up the lattice is denoted by 'S1', and the next period of maintaining the maximum lattice height is denoted by 'S2'. We will keep using this notation for later plots in this section.

The coherence does not immediately drop after the lattice height is fully increased, but it begins to decrease after spending a certain amount of time while staying at the final lattice height. Coherences converge to some intermediate values at 100ms. The initial coherences, however, are not completely lost at final states, since the lattice heights are not high enough to block the tunneling between sites. The degree of phase coherence remaining at the final stages depends on final lattice heights. For the higher lattice height, less coherence is left in the system as can be seen in Fig. 5.4. The phase decoherence is stronger for longer-range phase coherence between distant wells (for example, compare Fig. 5.5 and Fig. 5.6), so that the phase coherence would eventually converge to zero for distant wells.

It was shown in [98] that Beliaev and Landau damping at a finite temperature are gradually suppressed as the superfluid phase enters into the Mott insulator regime. Therefore, the relaxation time to the ground state becomes longer as we go to the Mott insulator phase and accordingly the process of phase transition becomes more nonadiabatic. There are some discussions with two extreme ways of ramping up the lattice (sudden loading and adiabatic loading) in [99]. To understand better nonadiabatic excitations that might be

involved in the loading of the lattice with intermediate speeds, we calculate the dependence of phase decoherence on finite ramp-up speeds in the next section.

5.2.2 Nonadiabaticity: Coherence Loss and Revival

The superfluid-to-Mott-insulator transition is a process of reversible phase transitions. However, nonadiabatic excitations are generated as an external optical lattice is quickly applied to the stationary system in consideration, unless it follows the adiabatic path. Therefore, if the lattice is quickly ramped up and it is reversely ramped down, initial coherence might not be completely recovered at the completion of the cycle, even if we ramp down the lattice adiabatically. This aspect was experimentally examined for one-component cases by Orzel et al. [14]. Here, we show numerical simulations of the similar setup with the TWA. There also exist numerical simulations based on the Bose-Hubbard Model with the Time-Evolving Block Decimation (TEBD, [100]) [101].

We control the optical lattice such that its variation of height in time has four steps. The first step is increasing the lattice at different rates. The second step ($7.8ms$) is keeping the maximum lattice height to wait for the system to stabilize. The third step is ramping down the lattice slowly ($78ms$) and the potential in the final period has only a harmonic trap which is the same as the initial situation. The number of atoms is $N_A = 10^4$, and the trap frequencies for the transverse direction and the longitudinal direction are $500Hz$ and $100Hz$, respectively. The maximum lattice height is $s = V_{ol,max} =$

10 or $20E_R$.

In Fig. 5.5, we show phase coherence between the center well and the adjacent well ($C_1(t)$) for $s = 20E_R$. The labels 'S2, S3, and S4' in Fig. 5.5 and Fig. 5.6 denote the second period of the constant maximum lattice heights, the third period of lattice ramp-down, and the final period of no lattice, exemplified for the case of $\tau_{RU} = 7.8ms$. The plot displays how phase coherence changes as a function of time depending on ramp-up rates. For all cases, phase coherence is lost due to the ramp-up of lattice and recovered due to the ramp-down of lattice. The coherence for the slow ramp-up time ($78ms$) is not changed too much until 110ms. However, the condensate subject to faster ramp-up time seems to yield excitations.

The point is that phase coherences at the final stage, S4 do not converge to 1, though condensates are driven to initial conditions with no lattice applied. Note that the superfluid-Mott insulator phase transition is a reversible process, so after one complete adiabatic cycle, the condensate is expected to be in the superfluid phase which has a phase coherence of 1. Since the coherences are not fully recovered, there might be nonadiabatic excitations imprinted on condensates. In addition to that, faster ramp-up rates appear to induce more excitations, since their final coherences are converging to lower values.

There are other aspects to note in this plot. First, the condensate under faster ramp-up times has its coherence starting to lose at earlier times. Second, maximal coherence losses during evolutions are greater for condensates under faster ramp-up times. Third, the coherences are recovered later on, but coherence recoveries are slower than the rates of coherence losses, presumably because the time for ramp-down (78ms) is longer than ramp-up times.

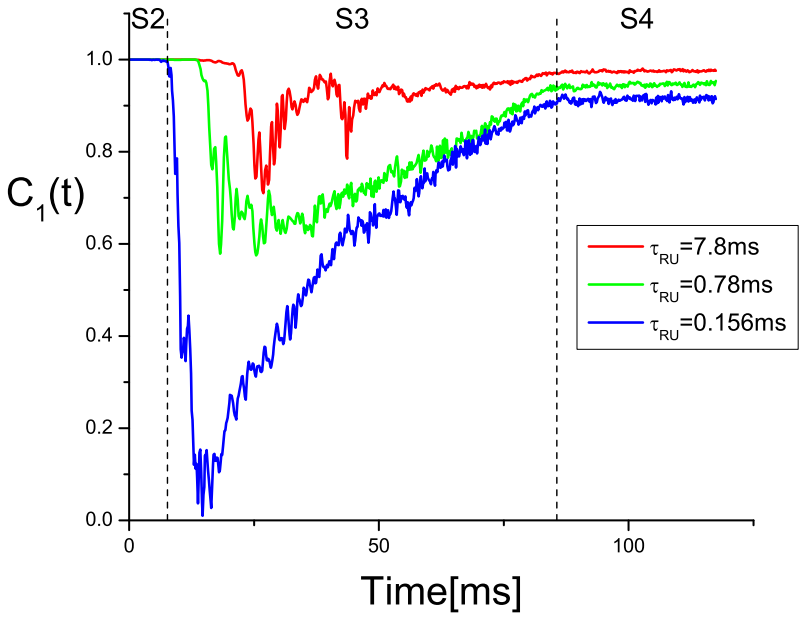

Figure 5.5: The loss and revival of phase coherence $C_1(t)$ when $s = 20E_R$. The lattice is ramped up with different speeds given by the following: the red line ($7.8ms$), the green line ($0.78ms$), and the blue line ($0.156ms$). The label 'S2' indicates the step of maximum lattice heights, 'S3' the step of ramp-down, and 'S4' the step of no lattice, all indicating the $\tau_{RU} = 7.8ms$ case only.

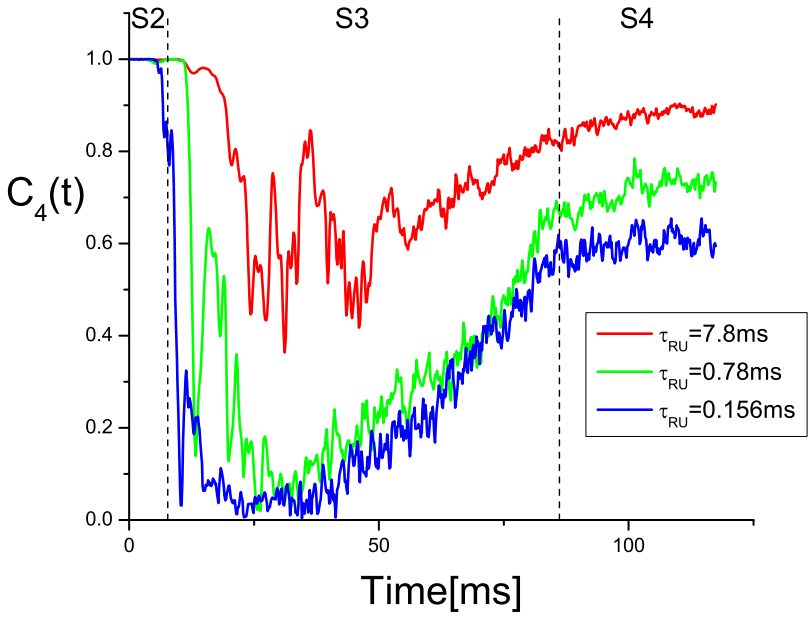

Figure 5.6: The loss and revival of phase coherence $C_4(t)$ when $s = 20E_R$. The lattice is ramped up with different speeds specified by the following: the red line ($7.8ms$), the green line ($0.78ms$), and the blue line ($0.156ms$).

So far, we have discussed coherences between adjacent wells, but we can also calculate longer-range phase coherence between distant wells. Coherences between the center well and the fourth-adjacent well for the above set-up are shown in Fig. 5.6. On the one hand, patterns similar to the ones in Fig. 5.6 can be observed. Here, however, the magnitude and longevity of coherence drop for long-range coherence is greater than for short-range coherence, meaning that long-range coherences are lost earlier and recovered later than coherences at proximity. Also, less phase coherence is left at the end of this process.

Another case is shown in Fig. 5.7 ($C_1(t)$) and Fig. 5.8 ($C_4(t)$) for the same set-up as above but with a different lattice height $s = 10E_R$. Since the lattice height is reduced compared to the previous case, the magnitude of coherence loss at each instance of time is reduced, and all the properties found in the previous case are observed in this case too. One thing that changed in this case, however, is when the green line and the blue line cross each other in both figures. It seems that phase coherence loss for initial drops under faster ramp-up time (0.156ms) is not greater than that with slower ramp-up time (0.78ms). It might be due to that the lattice ramped down before the gradual ramp-up of the lattice induces phase decoherence to the BEC for faster ramp-up. It is still true that faster ramp-up rates induce more excitations as observed in the end of calculations, since their final coherences are converging to lower values.

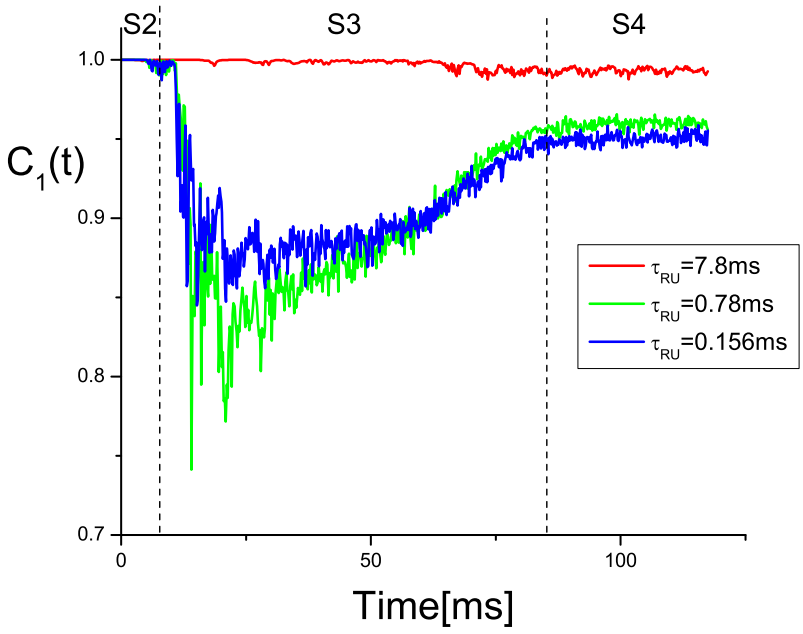

Figure 5.7: Phase coherence $C_1(t)$ loss and its revival at $s = 10E_R$. A lattice is ramped up with different speeds given by the following: the red line ($7.8ms$), the green line ($0.78ms$), and the blue line ($0.156ms$).

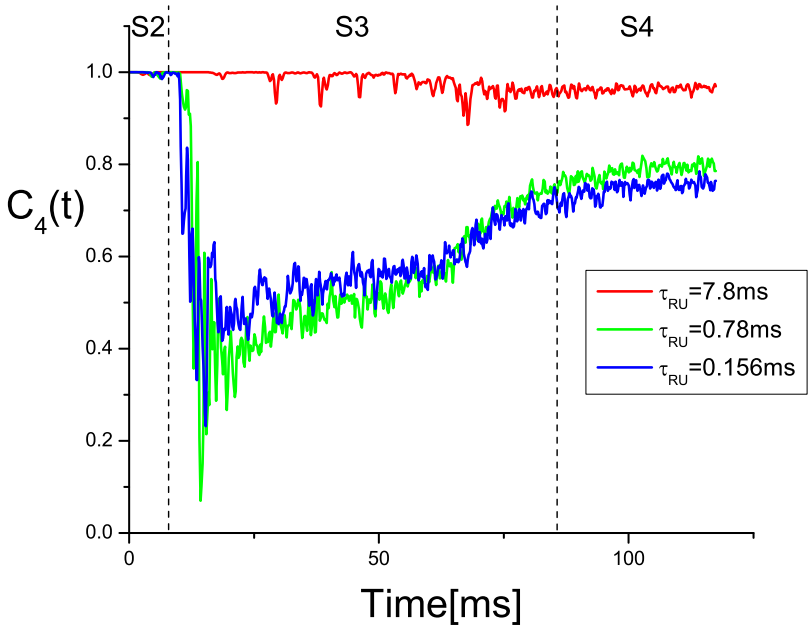

Figure 5.8: Phase coherence $C_4(t)$ loss and its revival at $s = 10E_R$. A lattice is ramped up with different speeds given by the following: the red line ($7.8ms$), the green line ($0.78ms$), and the blue line ($0.156ms$).

5.2.3 Comparison between the TWA Model and the Hybrid Model

Up to this point, we have implemented the TWA method for time evolution of systems. From now on, we study the hybrid model that uses the TWA for time evolution of a condensate mode and adopts the positive P representation for time evolution of a noncondensate mode as discussed in Chapter 3.

The systems we deal with are one-component BECs with the same parameters as condensates as in Section 5.2.1 but at $T = 30nK$. We have $N = 10^4$ of atoms with the same interaction strength and we ramp up an optical lattice up to $20E_R$ in 7.8ms. We numerically integrate 500 samples for both methods. In Fig. 5.9, we show the time evolution of phase coherence of BECs that begin with the same initial conditions of $\psi_C(z,t)$ and $\psi_{NC}(z,t)$, but we utilize three different methods for time evolution: the TWA method as usual, the hybrid method without a noise field ($\eta_{NC}(z,t)$), and the complete hybrid method including such quantum noise fields.

First, we compare the TWA model and the hybrid model without noise. In the TWA method, the phase coherence gradually decreases after phase decoherence suddenly starts, until the coherence loss becomes very slow. In contrast to the TWA, the no-noise hybrid method reveals more abrupt change in coherence for shorter time. In other words, it begins to lose phase coherence later than the one by TWA does, though it suddenly drops to the converging level earlier than the one by TWA does.

In addition to that, there are amplitude fluctuations in phase coherence by the no-noise hybrid method as the coherence drops after ramping up the

lattice. After this period of coherence loss, the variations are washed out in size. During the final stages, the variations in phase coherence become similar in both methods. The coherence loss observed at 50ms in the no-noise hybrid method seems a little larger than by the TWA, but it converges to the same value at the final state as by the TWA.

We now compare the above no-noise hybrid method with the complete hybrid one. In both methods, the initial trajectories of phase coherence until coherence losses are bounded (up to 50ms) are almost identical, but after that period, their trajectories separate each other. This is because effects of noise fields slowly creep into the coherence properties of the entire BEC field, and so it becomes gradually more effective as the states evolve in time. Nonetheless, the coherence on average is not affected by such noise fields, and its amplitude fluctuations are not noticeably changed from the no-noise hybrid model.

In Fig. 5.10, we show another results with a different number of atoms ($N = 8 \times 10^3$) with all other parameters the same as before. The above analysis is valid again for these results. In this case too, it is evident that coherence loss at the final state is similar between both methods whether it follows from the sudden drop of coherence (Hybrid) or from the slow drop (TWA).

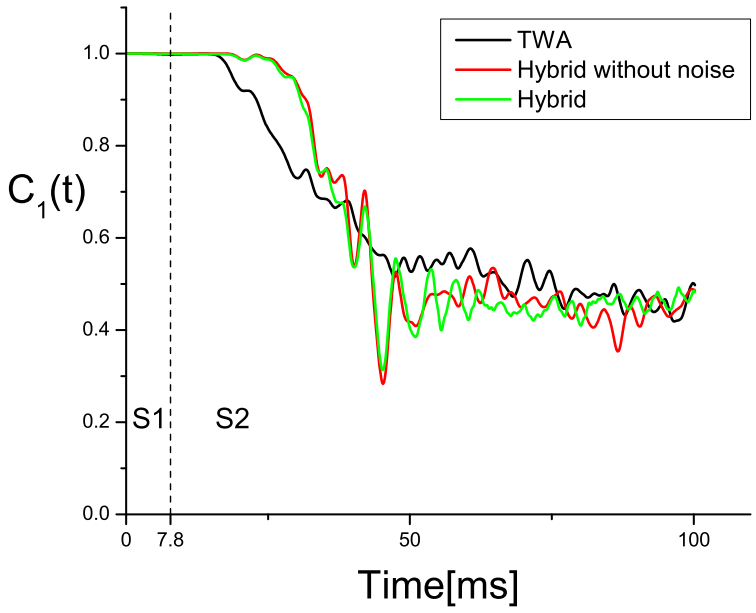

Figure 5.9: We compare the time evolution of phase coherence between by the TWA method and by the hybrid methods, for the BEC with $N = 10^4$: the black line is by the TWA method, the red line by the hybrid method without noises, the blue line by the original hybrid method including stochastic quantum noises.

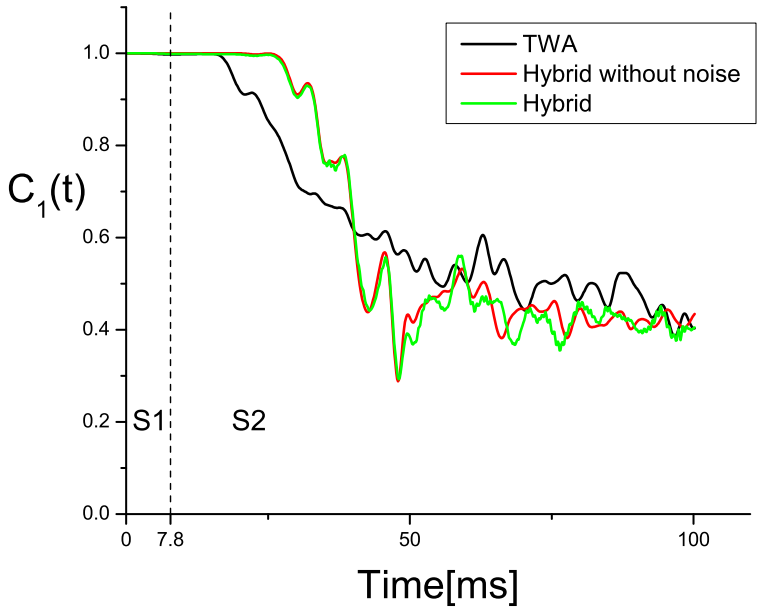

Figure 5.10: We continue to compare the time evolution of phase coherence between by the TWA method and by the hybrid methods, for the similar BEC with $N = 8 \times 10^3$: the black line is by the TWA method, the red line by the hybrid method without noises, the blue line by the complete hybrid method including stochastic noises.

5.3 Phase Coherence of Two-Component BEC

5.3.1 Increasing Fragmentation of A Atoms, Decreasing Fragmentation of B Atoms as the B Fraction is Raised.

We now examine the phase decoherence patterns of two-component BECs at $T = 0$, driven by a single state-selective optical lattice. Both components are trapped by the same anisotropic harmonic potential. Without loss of generality, component A in this work is placed in an optical lattice whereas no external lattice is applied to component B. In this subsection, we fix the total atom number and the ramp-up time, and vary the number ratio of A to B atoms. Both species fragment as the A lattice is applied, but with more B atoms, the B atom fragmentation is much reduced.

Having prepared the initial state of superfluid BECs placed in the harmonic trap, we linearly turn on the optical lattice up to the final height of $s_{max,A} = 10$ in the ramp-up time of $\omega_R \tau_{RU} = 250$ (τ_{RU}=20 ms), then maintain the height until the end of simulations:

$$\begin{aligned} V_{o,A}(z,t) &= s_A(t) E_R \cos^2(kz), \\ V_{o,B}(z,t) &= 0, \end{aligned} \tag{5.8}$$

where $s_A(t) = s_{max,A} t/\tau_{RU}$, $0 \le t \le \tau_{RU}$.

We fix the total number of atoms, $N_{tot} = 5 \times 10^3$ ($\mu = 2.9 E_R$), and vary the fractions of components A and B, f_A and $f_B = 1 - f_A$, in order to see

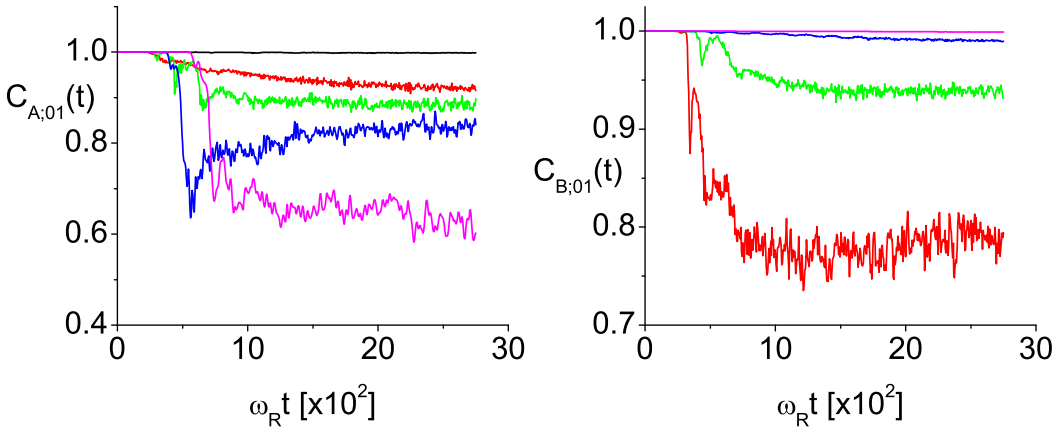

Figure 5.11: Phase coherence of component A (on left) and component B (on right) for various populational fractions ($0 \leq f_B \leq 1$), for $N = 5 \times 10^3$, $\tau_{RU} = 1/250\Omega_R = 20$ms for ^{87}Rb. The numerical simulation shows the results from when lattice loading begins. The fractions of component B, f_B, and the line colors are (in the large t limit, top to bottom on the left; bottom to top on the right): 0, black (for left side only); 0.1, red; 0.2, green; 0.4, blue; 0.6 pink. (online in color)

the effects of interspecies interaction and imbalanced populations on phase decoherence. The number of lattice sites with a filling factor of 1 or more varies depending on the populations, ranging from 30 to 80 along the axial direction. As the periodic lattice rises into the BEC cloud, the regions occupied by the lattice peaks are locally avoided by ground state component A and the wavefunctions are eventually fragmented to some degree. The interaction energies increase and the tunneling rate of the wavefunctions between the adjacent sites is reduced so that the fluctuation in each subcondensate breaks the long-range phase coherence.

Figure 5.11 shows the change in phase coherence between the center and nearest neighbor well, $C_{i;01}$, for component A (left) and B (right) from the time the lattice begins to ramp up, to a large time limit. The coherence changes

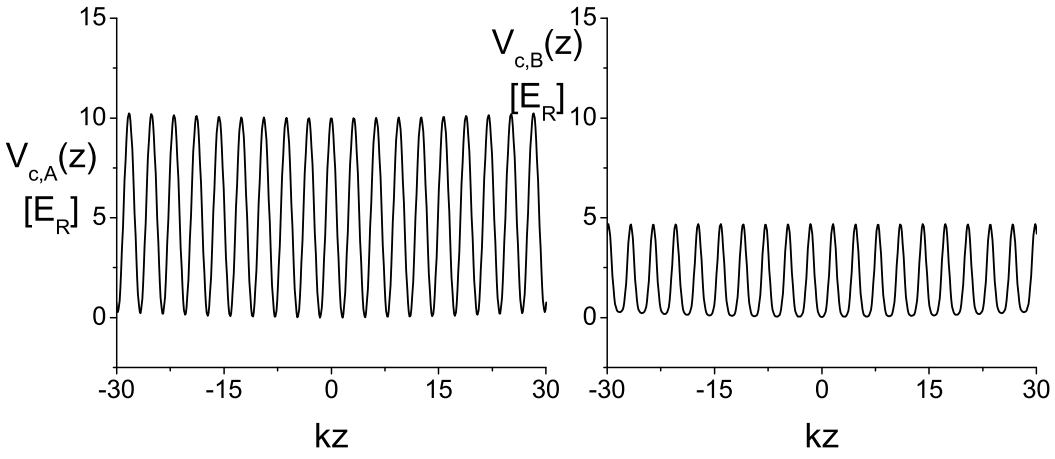

Figure 5.12: The profile of combined potential for the component A, $V_{c,A}(z) = V_{har,A}(z) + V_{ol,A}(z)$ with $s_{max,A} = 10$ and for the component B, $V_{c,B}(z) = V_{har,B}(z) + g_{AB}|\psi_A(z)|^2$. The population ratio ($q$) is 4 and $N_A = 4 \times 10^3$, $N_B = 1 \times 10^3$.

for other distant wells ($C_{i;02}, C_{i;03}, C_{i;04}$, etc.) exhibit a similar pattern, but with more coherence loss at a given time. The first-order correlation functions between sites are closely related to the visibilities of the interference pattern when the atoms are released under gravity [3, 102]. For one-component BEC cases, a complete loss of phase coherence would imply a transition to the Mott insulator state. In these calculations, the maximum lattice height does not reach the Mott insulator regime, as indicated by the observation that in Fig. 5.11, $C_{A;01}$ remains very close to unity if $f_A = 1$. However, as f_B increases, component A exhibits decoherence.

A new feature in this two-component case is the reduction of phase coherence of component B, which is induced as for component A but with the role of the optical lattice replaced by the atomic mean-field potential formed by

component A's periodic localization. In the GPE for the component B,

$$i\hbar\frac{\partial\psi_B(z,t)}{\partial t} = \left[L_B + g_{BB}|\psi_B(z,t)|^2 + g_{AB}|\psi_A(z,t)|^2\right]\psi_B(z,t), \tag{5.9}$$

this is expressed by the term $g_{AB}|\psi_A(x,t)|^2$. In Fig. 5.12, we show the optical lattice with the harmonic trap, which directly affects coherence properties of component A, and the mean-field lattice of A with the same harmonic trap, acting on component B, for the case $N = 5\times10^3$,$N_A = 4\times10^3$. The distortion by the harmonic trap potential is almost negligible around the center. The depth of the optical lattice and the interaction strength of the mean-field lattice are comparable $((I_{al,A}(z)|_{max} - I_{al,A}(z)|_{min})/(V_{o,A}(z,t)|_{max} - V_{o,A}(z,t)|_{min}) \simeq 0.6)$ for $f_B \to 0$ as can be verified by Fig. (5.12), for which

$$I_{al,A}(z) = g_{AB}|\psi_A(z)|^2. \tag{5.10}$$

Due to the presence of the mean-field lattice, the tunneling amplitude between the localization sites for component B is reduced, resulting in coherence loss, as shown on the right of Fig. 5.11.

The phase decoherence of component A is greater in the presence of component B than without component B, and increases as f_B increases. Note also that the mean-field potential from B atoms acting on A atoms is in phase with the optical lattice, and thus effectively raises the periodic potential that A atoms see, therefore contributing to the loss of coherence of the A atoms. However, comparison with the degree of coherence for A atoms alone as a func-

tion of lattice height shown in the next section, elevation of the effective lattice acting on A atoms does not explain fully the decrease of coherence shown in Fig. 5.11 (left side). Evidently the stochastic nature of the atom distributions also plays a role.

The experiment in [20] has shown a similar dependency but with two in-phase state-dependent optical lattices in order to place two components at the same lattice site.

To gain another perspective on this process, we expand the wavefunctions in an array of Wannier-like orbitals, $w_i(z)$,

$$\hat{\psi}_i(z) = \sum_l \hat{a}_{il} w_i(z - R_{il}), \tag{5.11}$$

where the single particle wavefunction, $w_i(z - R_{il})$ is centered at $R_{Al} = (2l + 1)d/2$, $R_{Bl} = 2ld/2$ for each component, and the operators $\hat{a}_{il}$ satisfy the bosonic commutation relation, $[\hat{a}_{il}, \hat{a}^\dagger_{jl'}] = \delta_{ij}\delta_{ll'}$. The variationally minimum solution of orbital wavefunctions implicitly depends on the occupation per site. Putting this set of orbitals into the Hamiltonian in Eq. 3.1, we obtain

$$\begin{aligned} H &= -\sum_{i;ll'} J_{i;ll'}(\hat{a}^\dagger_{il}\hat{a}_{il'} + \hat{a}^\dagger_{il'}\hat{a}_{il}) + \sum_{i;l} U_{ii}\hat{a}^\dagger_{il}\hat{a}^\dagger_{il}\hat{a}_{il}\hat{a}_{il} \\ &\quad + \sum_{i;l} U_{AB}\hat{a}^\dagger_{Al}\hat{a}^\dagger_{Bl}\hat{a}_{Al}\hat{a}_{Bl} + \sum_{i;l} \epsilon_{il}\hat{a}^\dagger_{il}\hat{a}_{il}, \end{aligned} \tag{5.12}$$

where

$$J_{i;ll'} = -\int dz w_i(z - R_{il})$$

$$\left[-\frac{\hbar^2}{2m_i} \bigtriangledown^2 + V_{h,i}(z) + V_{o,i}(z,t) \right] w_i(z - R_{il'}),$$

$$U_{ij} = g \int dz w_i^2(z - R_{il}) w_j^2(z - R_{jl}) \tag{5.13}$$

In the tight-binding regime, the Wannier functions can be written as Gaussian functions [103]. When the tight-binding limits are achieved, i.e. $(V_{o,A}(z,t)|_{max} - V_{o,A}(z,t)|_{min}) \gg E_R$ and $(I_{al,A}(z)|_{max} - I_{al,A}(z)|_{min}) \gg E_R$, the profile of each component can be well described by the ground state, the Gaussian wavefunction. Starting from the initial trial state of infinite 1D BECs ($V_{i,h} = 0$) in the periodic state-dependent optical lattice, we employ the Gaussian variational ansatz for single-particle orbitals placed on each site, $w_i(z - R_{il}) = (1/\pi\sigma_i^2)^{1/4} \exp(-(z - R_{il})^2/2\sigma_i^2)$, with the density of atoms per site equal to the average density of the center site calculated from the GPE ($n_{il} = n_{i0}^{(GPE)}$). Here, the widths of Gaussian wavefunctions are variational parameters, as in [104–107]

Within the Gaussian approximation, we obtain the minimized Gross-Pitaevskii energy functional, where the interaction energies and the tunneling amplitudes can be calculated from variational parameters. The local single-band Gaussian state is known to be accurate for the calculation of on-site interaction energies even for shallow lattices ($\sim 3E_R$) with the overlap between the true Wannier function and the Gaussian wavefunction nearly equal to 1.0 [108]. Since the Gaussian ansatz is not quite precise for the calculation of tunneling amplitudes because of the tail of Gaussian functions [108, 109], however, we concentrate on calculating on-site interaction energies.

In Fig. 5.13, we show on-site interaction energies for component A and B

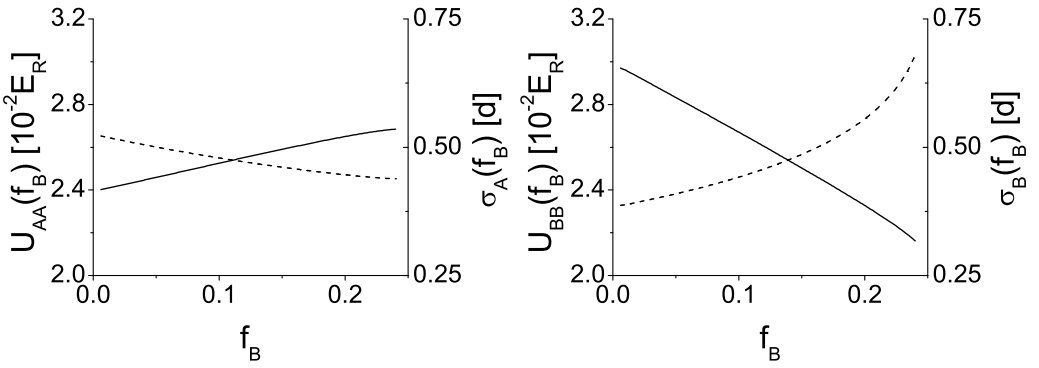

Figure 5.13: The on-site interaction energies, U_{ii} (solid line) and the widths of single-particle wavefunctions, σ_i (dashed line) for component A (left) and for component B (right), showing opposite changes as the impurity component B populates increasingly. Here $s_{A,max}$=10, $N_{tot} = 5 \times 10^3$.

as a function of the fraction of component B (f_B) using the same parameters as in the TWA simulations, $s_{max,A} = 10$ and $N_{tot} = 5 \times 10^3$. Higher on-site energies, U_{ii} correspond to greater localization, (smaller σ_i) and reduced coherence, $C_{i,01}$.

The bosonic mixture with the high population ratio, $q \gg 1$ ($f_A \simeq 1$), can be approximated by the foreground component A with a B impurity. Within the first-order approximation, the average strength of interspecies interaction ($\sim g_{AB} f_A N$) over its spatial variation, is greater than when $f_A < 1$. The interaction strength varies over space because of the component A's modulational variance and the points of localization sites for two components differ by $d/2$ because of repulsive interaction. Therefore, we can qualitatively interpret the strengthened phase decoherence of component B for high q (large N_A/N_B) by the increased strength of the mean-field lattice formed by the component A.

On the other hand, the larger phase decoherence of component A as $f_A \to 0$ can be understood by the combined effects of a larger number of B atoms and

also of the broadening of component B distribution in each B well and the narrowing of the A distribution in each A well. Due to the contact-interaction property of interspecies interaction, the minimized Hamiltonian is found in the balance between reducing the spatial overlap of the two components' amplitudes and weakening the intraspecies interaction energies of each component. The competition between the interaction strengths of two components generates one component's localization and the other component's delocalization as the population ratio q changes.

5.3.2 Increased Fragmentation of Both A and B atoms when the Optical Lattice Height is Raised

In this section, we fix the fractions of the two components and show how the phase coherences change as a function of time and on the final lattice height for component A. As in Sec. 5.3.1, $V_{o,B}(z,t) = 0$, but now the atom numbers are fixed at $N_A = 4.0 \times 10^3, N_B = 1.0 \times 10^3$. As before, the optical lattice for component A linearly increases up to the indicated value of $s_{max,A}$: the ramping-up time is $\omega_R \tau_{RU} = 100$ in this case.

The changes in phase coherences, $C_{i;01}$, are shown in Fig. 5.14 for component A and B. As the lattice becomes deeper, the phase coherence of component A decreases as expected, since it is fragmented by the external lattice height increase even without consideration of interspecies effect. Decoherence of component B is enhanced as well because of the growth of the mean-field lattice from component A. In Fig. 5.15, the on-site interaction energies are displayed for both components in the regime where the two components are

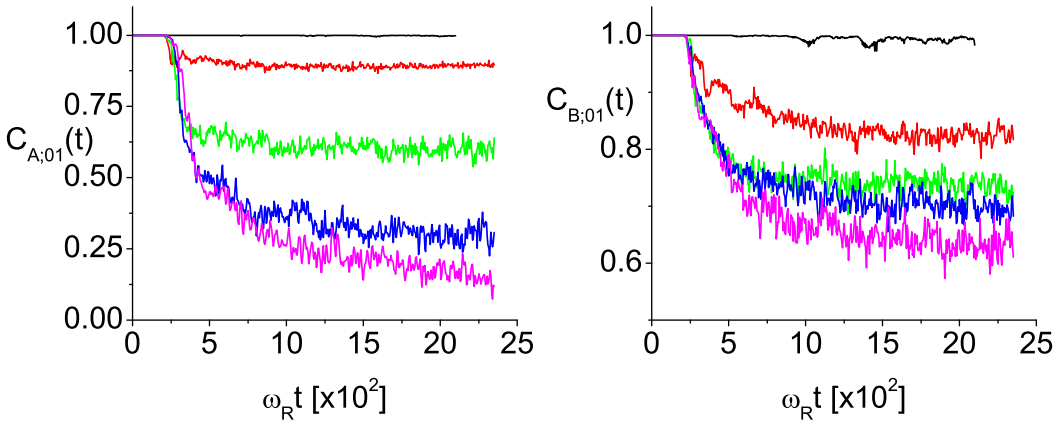

Figure 5.14: The effect of final optical lattice heights on phase coherence of component A (on left) and component B (on right). The final lattice height (s_A) for each curve is following: the black line (3), the red line (6.5), the green line (10), the blue line (13.5), and the pink line (17).

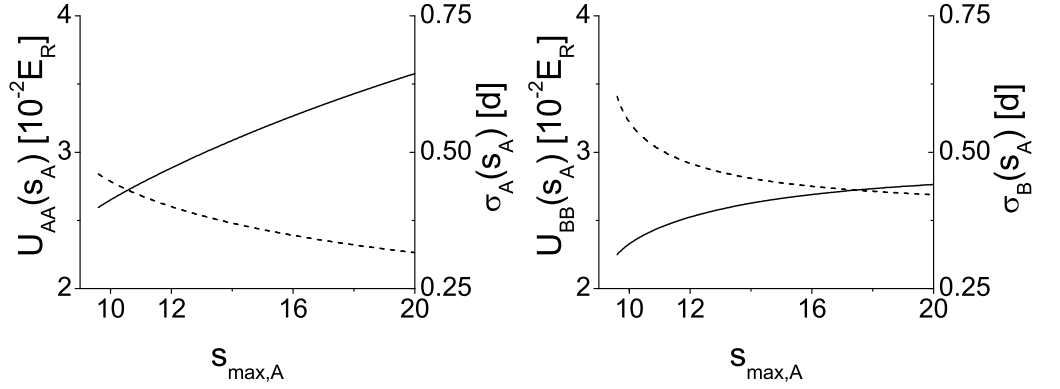

Figure 5.15: The on-site interaction energies, U_{ii} (solid line) and the widths of single-particle wavefunctions, σ_i (dashed line) for component A (U_{AA} on left) and for component B (U_{BB} on right) for $N_{tot} = 5 \times 10^3$. Both components become more fragmented as the state-dependent optical lattice for component A only has been amplified more.

sufficiently localized ($s_{max,A} \gtrsim 10$). As shown in Fig. 5.13, an increase in on-site energy implies a smaller σ, hence tighter localization within the effective well. Thus Fig. 5.15 indicates, as expected, that the degree of localization is higher for deeper lattice heights. Comparing results between the two components in Fig. 5.15, the localization of component A is evidently stronger than component B for $s_{max,A} > 10$, which explains the greater phase decoherence in component A than in component B in Fig. 5.14.

As is evident from comparing Figs. 5.15 and 5.13, when the A lattice height rises, the exchange of spatial occupation between the two components that has been observed in Sec. 5.3.1 does not occur. Instead, component B's localization is strengthened as well as component A's. The atomic mean-field lattice formed by component A becomes more peaked as it enters into the Mott insulator regime so that the tunneling amplitude of component B between its neighbouring sites is reduced. The loss in first-order spatial correlation between wells can be induced by increasing the height of barriers [110], which are provided by atomic mean-field lattices in this case.

5.3.3 Non-monotonic Fragmentation (A) - Fragmentation (B)

Up to this point, component B has not been subjected directly to an optical lattice, but is localized simply by interaction with the mean field resulting from component A, and the interspecies interaction. Additional insight into the localization process can come from applying to component B an optical lattice that is out of phase with the lattice applied to component A so as to

strengthen the localization effect on B atoms in addition to the mean field produced by component A, acting on component B.

When an optical lattice is applied to only one component as in the previous sections, the decoherence as a function of lattice height has been monotonic. In this section, we examine the dependence of phase decoherence of one component on the fragmentation of the other component in the presence of two phase-mismatch optical lattices as in [111, 112].

To the BEC mixture with the asymmetric population ratio($q = 0.25$, $N_A = 1.0 \times 10^3, N_B = 4.0 \times 10^3$), we gradually apply two state-dependent optical lattices:

$$\begin{aligned} V_{o,A}(z,t) &= s_A(t) E_R \cos^2(kz), \\ V_{o,B}(z,t) &= s_B(t) E_R \sin^2(kz), \end{aligned} \tag{5.14}$$

where $s_i(t) = s_{max,i} t/\tau_{RU}$. The final lattice height for the component A is $s_{max,A} = 10$ and the final lattice height for the component B is a variable parameter in different simulations ranging from $s_{max,B} = 3$ to $s_{max,B} = 17$ and all other conditions are the same as in the previous section.

In Fig. 5.16, we show the change of phase coherence while varying the lattice height of component B. The drop in phase coherence of component B reflects the expectation that higher optical lattices induce more coherence loss between two neighboring sites, neglecting interspecies interactions for the moment. And also as expected, a higher lattice for component B leads to larger on-site interaction energies, as shown in Fig. 5.17, and this in turn implies more localization for component B, for reasons discussed above.

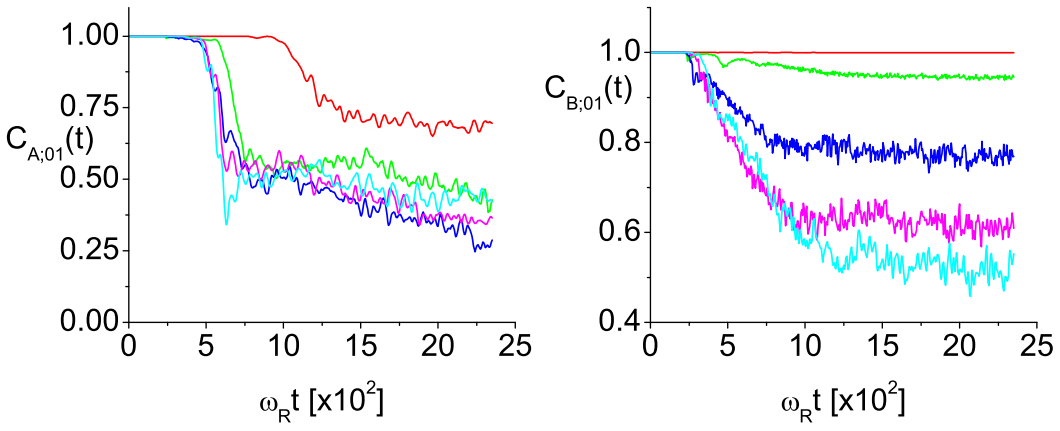

Figure 5.16: The effect of localization induced by B on phase coherence on component A (on left) and component B (on right). The final lattice height for B (s_B) is following: the red line (3), the green line (6.5), the blue line (10), the pink line (13.5), the cyan line (17).

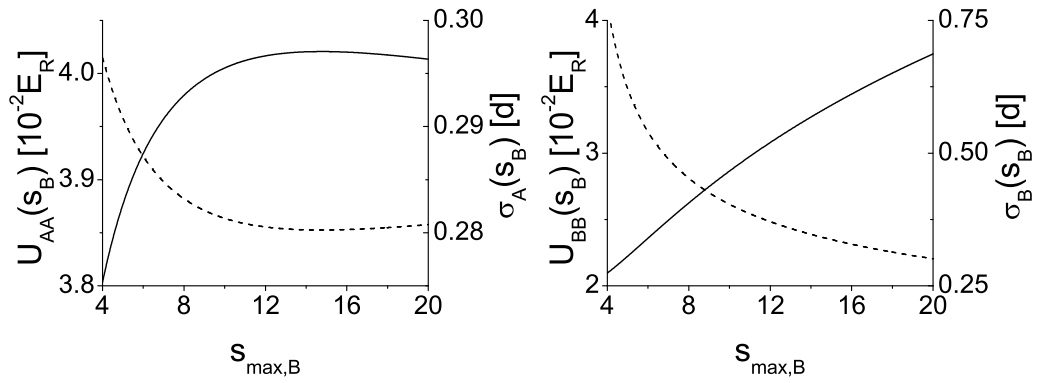

Figure 5.17: The on-site interaction energies, U_{ii} (solid line) and the widths of single-particle wavefunctions, σ_i (dashed line) for component A (U_{AA} on left) and for component B (U_{BB} on right) as a function of the lattice height for B (s_B).

The new phenomenon here is the dependence of phase coherence of component A on optical lattice heights for the component B. As can be seen from Fig. 5.16(a), the phase coherence of component A at the maximum time shown diminishes as $s_{max,B}$ increases from 3 to 10, but then rises again for $s_{max,B}$ increases beyond 10. This non-monotonic dependence on the other component's lattice height can also be seen in the on-site energy plotted in the left panel of Fig. 5.17, which shows a maximum of U_{AA} at $s_{max,B} \sim 15$, and then a small decrease. In addition to the expected fragmentation due to the optical lattice applied directly to component A, the deepening mean-field potential from component B acting on component A further reduces the tunneling of component A between adjacent sites.

Chapter 6

Concluding Remarks

In this dissertation, we have dealt with one-component and two-component Bose-Einstein condensates under the control of state-dependent optical lattices. We have focused on the equal-time nonlocal phase coherences of condensates, the impacts of nonadiabatic excitations on phase coherence, and the effects of interspecies interactions on the phase decoherence.

We have studied several phase space representations, in which stochastic time evolution of wavefunctions in the phase space is naturally introduced. We constructed the truncated Wigner representation and the hybrid model for one-component and two-component BECs with Bogoliubov quasiparticles. We have implemented the numerical method of split operators for BECs and enhanced its efficiency by reducing the sample variances of Monte Carlo methods.

For the system with 1D one-component BECs placed under an optical lattice, it is checked that the degree of phase decoherence depends on optical lattice heights. With regard to the nonequilibrium dynamics under the

superfluid-Mott insulator reversible phase transition, we have also demonstrated that the linear ramp-up of 1D optical lattices might generate nonadiabatic excitations that diffuse phase coherences of superfluid phase. For the one-component BECs, we showed the comparison between the TWA method and the hybrid method, which has revealed the similar pattern of phase coherence evolution, but the hybrid model demonstrates temporal fluctuation of coherence and sudden phase diffusion, both of which are smaller in the one by the TWA simulations. Nevertheless, both results agree with each other in overall.

For two-component BECs, we prepared an initial state as a stable mixture of overlapping two-component BECs in a harmonic trap. First, when an optical lattice is applied to the A atoms but not directly to the B atoms, both species are fragmented into localized wells differing by a half-period between the two components. The B atoms are fragmented by the effective barriers produced by interaction with the spatially varying distribution of A atoms. With a constant total atom number and constant lattice amplitude, we have observed that when the fraction of B atoms increases, then in the long-time limit, the fragmentation of A atoms increases, but the fragmentation of B atoms decreases, consistent with experimental observations in [20]. The increasing fragmentation of A atoms is associated with higher effective barriers produced by accumulation of B atoms spatially out of phase with the A atoms. Alternatively, the Gaussian variational wavefunction ansatz provides additional insight into the fragmentation mechanisms. Since intra- and interspecies interactions are all repulsive, when the wavefunction of the B species broadens within each localization site due to increasing numbers of B atoms,

the B atom fragmentation is reduced, and the increased density repels the A atoms from the high-density regions of the B atoms, thereby enhancing the localization of the A atoms and diminishing site-to-site phase coherences.

Secondly, we have seen increasing fragmentation of both A and B atoms with higher lattice heights for A. In this case, an external optical lattice drives localization and phase decoherence of A atomic fields which are directly exposed to lattice wells, whose mean-field potential in turn forms an effective lattice for B atoms, reducing the phase coherence between sites. We conclude that localization effects in deeper lattices play a key role for both components in reducing phase coherence.

Finally, when a lattice is applied also to the B atoms, then as a function of its amplitude, non-monotonic fragmentation of A atoms occurs; the A atom on-site interaction energies reach a maximum, and then decrease when the B atoms become more and more localized. This shows in a dramatic way how the effect of increased localization (or equivalently, on-site energy) of one species acting on the other, can actually saturate.

The initial states we prepared in this study have been restricted to the superfluid coherent states, which have positive-definite distributions unlike the quasiprobability distribution of Mott insulator states that might yield negative values in the representations we considered. In fact, there exists a semiclassical mean-field theory based on a discrete GPE that have studied the recovery of phase coherence when a BEC changes from the Mott-insulator to the superfluid [113]. Furthermore, we might be able to study the Mott insulator-superfluid phase transition (quantum melting) quantum mechanically, if there is a positive-definite distribution for the Mott insulator in a certain represen-

tation.

There are other possible extensions of this study. Extending this 1D model to 2D systems can add to the system rich physics, including for example, an extra scaling factor, vortices [114–121], rotating lattices [122, 123], and topological defects. Phase coherence of BECs with a 2D lattice is also another possibility for future works. In positive P representations, quantum noises naturally arose as a diffusion term of a stochastic differential equation. During time evolution, we can also consider incoherent dissipation of condensates to see its effect on phase coherence. While repulsive interaction strengths were considered in this work, the system with attractive interspecies interaction strengths might pose a new issue of instability to the dynamics.

Bibliography

[1] Matthew P. A. Fisher, Peter B. Weichman, G. Grinstein, and Daniel S. Fisher. Boson localization and the superfluid-insulator transition. *Physical Review B*, 40:546, 1989.

[2] D. Jaksch, C. Bruder, J. I. Cirac, C. W. Gardiner, and P. Zoller. Cold bosonic atoms in optical lattices. *Physical Review Letters*, 81:3108, 1998.

[3] Markus Greiner, Olaf Mandel, Tilman Esslinger, Theodor W. Hansch, and Immanuel Bloch. Quantum phase transition from a superfluid to a Mott insulator in a gas of ultracold atoms. *Nature*, 415:39–44, 2002.

[4] Thilo Stöferle, Henning Moritz, Christian Schori Michael Köhl, and Tilman Esslinger. Transition from a strongly interacting 1d superfluid to a Mott insulator. *Physical Review Letters*, 92:130403, 2004.

[5] K. B. Davis, M. O. Mewes, M. R. Andrews, N. J. van Druten, D. S. Durfee, D. M. Kurn, and W. Ketterle. Bose-Einstein condensation in a gas of sodium atoms. *Physical Review Letters*, 75:3969, 1995.

[6] M. H. Anderson, J. R. Ensher, M. R. Matthews, C. E. Wieman, and E. A. Cornell. Observation of Bose-Einstein condensation in a dilute atomic vapor. *Science*, 269:198, 1995.

[7] D. Jaksch and P. Zoller. The cold atom Hubbard toolbox. *Annals of Physics*, 315:52–79, 2005.

[8] Maciej Lewenstein, Anna Sanpera, Veronica Ahufinger, Bogdan Damski, Aditi Sen, and Ujjwal Sen. Ultracold atomic gases in optical lattices: mimicking condensed matter physics and beyond. *Advances in Physics*, 56:243, 2007.

[9] Michael Nielsen and Isaac Chuang. *Quantum Computation and Quantum Information: 10th Anniversary Edition*. Cambridge University Press, 2010.

[10] J. Preskill. Lecture notes on quantum computation. URL http://www.theory.caltech.edu/people/preskill/ph229.

[11] D. Jaksch, H. J. Briegel, J. I. Cirac, C. W. Gardiner, and P. Zoller. Entanglement of atoms via cold controlled collisions. *Physical Review Letters*, 82:1975, 1999.

[12] Jiannis K. Pachos and Peter L. Knight. Quantum computation with a one-dimensional optical lattice. *Physical Review Letters*, 91:107902, 2003.

[13] Olaf Mandel, Markus Greiner, Artur Widera, Tim Rom, Theodor W. Hansch, and Immanuel Bloch. Controlled collisions for multi-particle entanglement of optically trapped atoms. *Nature*, 425:937–940, 2003.

[14] C. Orzel, A. K. Tuchman, M. L. Fenselau, M. Yasuda, and M. A. Kasevich. Squeezed states in a Bose-Einstein condensate. *Science*, 291: 2386–2389, 2001.

[15] S. B. McKagan, D. L. Feder, and W. P. Reinhardt. Mean-field effects may mimic number squeezing in Bose-Einstein condensates in optical lattices. *Physical Review A*, 74(1):013612, 2006.

[16] L. Isella and J. Ruostekoski. Quantum dynamics in splitting a harmonically trapped Bose-Einstein condensate by an optical lattice: Truncated Wigner approximation. *Physical Review A*, 74:063625–16, 2006.

[17] Alice Sinatra, Carlos Lobo, and Yvan Castin. The truncated Wigner method for Bose-condensed gases: limits of validity and applications. *Journal of Physics B: Atomic, Molecular and Optical Physics*, 35:3599–3631, 2002.

[18] Anatoli Polkovnikov. Quantum corrections to the dynamics of interacting bosons: Beyond the truncated Wigner approximation. *Physical Review A*, 68(5):053604, November 2003.

[19] J. Catani, L. De Sarlo, G. Barontini, F. Minardi, and M. Inguscio. Degenerate Bose-Bose mixture in a three-dimensional optical lattice. *Physical Review A*, 77(1):011603, 2008.

[20] Bryce Gadway, Daniel Pertot, René Reimann, and Dominik Schneble. Superfluidity of interacting bosonic mixtures in optical lattices. *Physical Review Letters*, 105:045303, 2010.

[21] G. Thalhammer, G. Barontini, L. DenbspSarlo, J. Catani, F. Minardi, and M. Inguscio. Double species Bose-Einstein condensate with tunable interspecies interactions. *Physical Review Letters*, 100:210402, 2008.

[22] J. Catani, G. Barontini, G. Lamporesi, F. Rabatti, G. Thalhammer, F. Minardi, S. Stringari, and M. Inguscio. Entropy exchange in a mixture of ultracold atoms. *Physical Review Letters*, 103(14):140401, 2009.

[23] Daniel Pertot, Bryce Gadway, and Dominik Schneble. Collinear Four-Wave mixing of Two-Component matter waves. *Physical Review Letters*, 104:200402, 2010.

[24] C. Hamner, J. J. Chang, P. Engels, and M. A. Hoefer. Generation of Dark-Bright soliton trains in Superfluid-Superfluid counterflow. *Physical Review Letters*, 106(6):065302, February 2011.

[25] P. Soltan-Panahi, J. Struck, P. Hauke, A. Bick, W. Plenkers, G. Meineke, C. Becker, P. Windpassinger, M. Lewenstein, and K. Sengstock. Multi-component quantum gases in spin-dependent hexagonal lattices. *Nat Phys*, 7(5):434–440, May 2011.

[26] Ehud Altman, Walter Hofstetter, Eugene Demler, and Mikhail D Lukin. Phase diagram of two-component bosons on an optical lattice. *New Journal of Physics*, 5:113–113, 2003.

[27] A. Isacsson, Min-Chul Cha, K. Sengupta, and S. M. Girvin. Superfluid-insulator transitions of two-species bosons in an optical lattice. *Physical Review B*, 72(18):184507, November 2005.

[28] K. V. Krutitsky and R. Graham. Interference of atomic levels and Superfluid-Mott insulator phase transitions in a Two-Component Bose-Einstein condensate. *Physical Review Letters*, 91(24):240406, December 2003.

[29] Jonas Larson and Jani-Petri Martikainen. Coupled two-component atomic gas in an optical lattice. *Physical Review A*, 78(6):063618, December 2008.

[30] J. Ruostekoski and Zachary Dutton. Dynamical and energetic instabilities in multicomponent Bose-Einstein condensates in optical lattices. *Physical Review A*, 76(6):063607, December 2007.

[31] Julia Wernsdorfer, Michiel Snoek, and Walter Hofstetter. Lattice-ramp-induced dynamics in an interacting Bose-Bose mixture. *Physical Review A*, 81(4):043620, April 2010.

[32] Anzi Hu, L. Mathey, Ippei Danshita, Eite Tiesinga, Carl J. Williams, and Charles W. Clark. Counterflow and paired superfluidity in one-dimensional Bose mixtures in optical lattices. *Physical Review A*, 80(2): 023619, 2009.

[33] Martin Bruderer, Alexander Klein, Stephen R. Clark, and Dieter Jaksch. Polaron physics in optical lattices. *Physical Review A*, 76(1):011605, July 2007.

[34] Yvan Castin and Jean Dalibard. Relative phase of two Bose-Einstein condensates. *Physical Review A*, 55:4330, 1997.

[35] S. M. Barnett, K. Burnett, and J. A. Vaccaro. Why a condensate can be thought of as having a definite phase. *J. Res. Natl. Inst. Stand. Technol.*, 101:593, 1996.

[36] Juha Javanainen and Martin Wilkens. Phase and phase diffusion of a split Bose-Einstein condensate. *Physical Review Letters*, 78:4675, 1997.

[37] Franco Dalfovo, Stefano Giorgini, Lev P. Pitaevskii, and Sandro Stringari. Theory of Bose-Einstein condensation in trapped gases. *Reviews of Modern Physics*, 71:463, 1999.

[38] A. Smerzi, A. Trombettoni, P. G. Kevrekidis, and A. R. Bishop. Dynamical superfluid-insulator transition in a chain of weakly coupled Bose-Einstein condensates. *Physical Review Letters*, 89(17):170402, October 2002.

[39] N.A. Kostov, V. Gerdjikov, V.Z. Enol'skii, M. Salerno, and V.V. Konotop. *Nonlinear Waves: Classical and Quantum Aspects*, chapter Two-Component Bose-Einstein Condensates in Optical Lattices: Modulational Instability and Soliton Generation, page 269. Kluwer Academic Publishers, 2005.

[40] Luigi Amico and Vittorio Penna. Time-dependent mean-field theory of the superfluid-insulator phase transition. *Physical Review B*, 62:1224, 2000.

[41] Esteban Calzetta, B. L. Hu, and Ana Maria Rey. Bose-Einstein-condensate superfluid-Mott-insulator transition in an optical lattice. *Physical Review A*, 73:023610, 2006.

[42] Ana Maria Rey, B. L. Hu, Esteban Calzetta, Albert Roura, and Charles W. Clark. Nonequilibrium dynamics of optical-lattice-loaded

Bose-Einstein-condensate atoms: Beyond the Hartree-Fock-Bogoliubov approximation. *Physical Review A*, 69:033610, 2004.

[43] C. W. Gardiner, M. D. Lee, R. J. Ballagh, M. J. Davis, and P. Zoller. Quantum kinetic theory of condensate growth: Comparison of experiment and theory. *Physical Review Letters*, 81:5266, 1998.

[44] H. T. C. Stoof. Coherent versus incoherent dynamics during Bose-Einstein condensation in atomic gases. *J. Low Temp. Phys.*, 114:11, 1999.

[45] N. P. Proukakis, K. Burnett, and H. T. C. Stoof. Microscopic treatment of binary interactions in the nonequilibrium dynamics of partially Bose-condensed trapped gases. *Physical Review A*, 57:1230, 1998.

[46] E. Zaremba, T. Nikuni, and A. Griffin. Dynamics of trapped Bose gases at finite temperatures. *J. Low Temp. Phys.*, 116:277, 1999.

[47] F. Trimborn, D. Witthaut, and H. J. Korsch. Exact number-conserving phase-space dynamics of the m -site Bose-Hubbard model. *Physical Review A*, 77:043631, 2008.

[48] F. Trimborn, D. Witthaut, and H. J. Korsch. Beyond mean-field dynamics of small Bose-Hubbard systems based on the number-conserving phase-space approach. *Physical Review A*, 79:013608, 2009.

[49] B. J. Dalton. Two-mode theory of BEC interferometry. *Journal of Modern Optics*, 54:615, 2007.

[50] D. Ananikian and T. Bergeman. Gross-Pitaevskii equation for Bose particles in a double-well potential: Two-mode models and beyond. *Physical Review A*, 73:013604, 2006.

[51] Indubala I. Satija, Radha Balakrishnan, Phillip Naudus, Jeffrey Heward, Mark Edwards, and Charles W. Clark. Symmetry-breaking and symmetry-restoring dynamics of a mixture of Bose-Einstein condensates in a double well. *Physical Review A*, 79:033616, 2009.

[52] F Trimborn, D Witthaut, and S Wimberger. Mean-field dynamics of a two-mode Bose-Einstein condensate subject to noise and dissipation. *Journal of Physics B: Atomic, Molecular and Optical Physics*, 41:171001, 2008.

[53] M. Jääskeläinen and P. Meystre. Dynamics of Bose-Einstein condensates in double-well potentials. *Physical Review A*, 71:043603, 2005.

[54] G. J. Milburn, J. Corney, E. M. Wright, and D. F. Walls. Quantum dynamics of an atomic Bose-Einstein condensate in a double-well potential. *Physical Review A*, 55:4318, 1997.

[55] K. Goral, M. Gajda, and K. Rzazewski. Multi-mode description of an interacting Bose-Einstein condensate. *Optics Express*, 8:92–98, 2001.

[56] C. W. Gardiner. *Quantum Noise*. Springer-Verlag, January 1992.

[57] D.F. Walls and G.J. Milburn. *Quantum Optics*. Springer, February 1995.

[58] R. Bistritzer and E. Altman. Intrinsic dephasing in one-dimensional ultracold atom interferometers. *Proceedings of the National Academy of Sciences*, 104:9955–9959, 2007.

[59] M. Lewenstein and L. You. Quantum phase diffusion of a Bose-Einstein condensate. *Physical Review Letters*, 77:3489, 1996.

[60] J. Steinhauer R. Ozeri, N. Katz and N. Davidson. Colloquium: Bulk Bogoliubov excitations in a Bose-Einstein condensate. *Reviews of Modern Physics*, 77:187, 2005.

[61] Kai Bongs and Klaus Sengstock. Physics with coherent matter waves. *Reports on Progress in Physics*, 67:907–963, 2004.

[62] George A. Baker. Formulation of quantum mechanics based on the quasi-probability distribution induced on phase space. *Physical Review*, 109: 2198, 1958.

[63] Anatoli Polkovnikov. Phase space representation of quantum dynamics. *Annals of Physics*, 325:1790–1852, 2010.

[64] Roy J. Glauber. Coherent and incoherent states of the radiation field. *Physical Review*, 131:2766, 1963.

[65] Roy J. Glauber. The quantum theory of optical coherence. *Physical Review*, 130:2529, 1963.

[66] J. Rogel-Salazar, S. Choi, G. H. C. New, and K. Burnett. Characterisation of the dynamical quantum state of a zero temperature Bose-Einstein condensate. *Physics Letters A*, 299:476–482, 2002.

[67] M. R. Andrews, C. G. Townsend, H.-J. Miesner, D. S. Durfee, D. M. Kurn, and W. Ketterle. Observation of interference between two Bose condensates. *Science*, 275:637, 1997.

[68] Lorenzo Isella and Janne Ruostekoski. Nonadiabatic dynamics of a Bose-Einstein condensate in an optical lattice. *Physical Review A*, 72:011601–4, 2005.

[69] Frederick W. Cummings and James R. Johnston. Theory of superfluidity. *Physical Review*, 151:105, 1966.

[70] Howard J. Carmichael. *Statistical Methods in Quantum Optics 1: Master Equations and Fokker-Planck Equations (Theoretical and Mathematical Physics)*. Springer, April 2003.

[71] M. J. Steel, M. K. Olsen, L. I. Plimak, P. D. Drummond, S. M. Tan, M. J. Collett, D. F. Walls, and R. Graham. Dynamical quantum noise in trapped Bose-Einstein condensates. *Physical Review A*, 58:4824, 1998.

[72] P. B. Blakie, A. S. Bradley, M. J. Davis, R. J. Ballagh, and C. W. Gardiner. Dynamics and statistical mechanics of ultra-cold Bose gases using c-field techniques. *Advances in Physics*, 57:363, 2008.

[73] Scott E. Hoffmann, Joel F. Corney, and Peter D. Drummond. Hybrid phase-space simulation method for interacting Bose fields. *Physical Review A*, 78:013622, 2008.

[74] B J Dalton. Theory of decoherence in Bose-Einstein condensate interferometry. *Journal of Physics: Conference Series*, 67:012059, 2007.

[75] B.J. Dalton. Decoherence effects in Bose-Einstein condensate interferometry i. general theory. *Annals of Physics*, In Press, Accepted Manuscript.

[76] V. Krachmalnicoff, J. C. Jaskula, M. Bonneau, V. Leung, G. B. Partridge, D. Boiron, C. I. Westbrook, P. Deuar, P. Zinacute, M. Trippenbach, and K. V. Kheruntsyan. Spontaneous four-wave mixing of de broglie waves: Beyond optics. *Physical Review Letters*, 104:150402, 2010.

[77] D. S. Jin, J. R. Ensher, M. R. Matthews, C. E. Wieman, and E. A. Cornell. Collective excitations of a Bose-Einstein condensate in a dilute gas. *Physical Review Letters*, 77:420, 1996.

[78] J. Plata. Loading of a Bose-Einstein condensate into an optical lattice: The excitation of collective modes. *Physical Review A*, 69:033604, 2004.

[79] C. W. Gardiner. Particle-number-conserving Bogoliubov method which demonstrates the validity of the time-dependent Gross-Pitaevskii equation for a highly condensed Bose gas. *Physical Review A*, 56:1414, 1997.

[80] Y. Castin and R. Dum. Low-temperature Bose-Einstein condensates in time-dependent traps: Beyond the u(1) symmetry-breaking approach. *Physical Review A*, 57:3008, 1998.

[81] D. van Oosten, P. van der Straten, and H. T. C. Stoof. Quantum phases in an optical lattice. *Physical Review A*, 63:053601, 2001.

[82] Ana Maria Rey, Keith Burnett, Robert Roth, Mark Edwards, Carl J Williams, and Charles W Clark. Bogoliubov approach to superfluidity of atoms in an optical lattice. *Journal of Physics B: Atomic, Molecular and Optical Physics*, 36(5):825–841, 2003.

[83] William G. Cochran. *Sampling Techniques, 3rd Edition*. Wiley India Pvt. Ltd., 2007.

[84] William Edwards Deming. *Some theory of sampling*. Courier Dover Publications, 1966.

[85] Paolo Brandimarte. *Numerical methods in finance and economics: a MATLAB-based introduction*. John Wiley and Sons, 2006.

[86] J. M. Hammersley and K. W. Morton. A new monte carlo technique: antithetic variates. *Mathematical Proceedings of the Cambridge Philosophical Society*, 52:449–475, 1956.

[87] M. L. Chiofalo, S. Succi, and M. P. Tosi. Ground state of trapped interacting Bose-Einstein condensates by an explicit imaginary-time algorithm. *Physical Review E*, 62:7438, 2000.

[88] Juha Javanainen and Janne Ruostekoski. Symbolic calculation in development of algorithms: split-step methods for the GrossPitaevskii equation. *Journal of Physics A: Mathematical and General*, 39:L179–L184, 2006.

[89] J. K Freericks and H. Monien. Phase diagram of the Bose-Hubbard model. *Europhysics Letters*, 26:545–550, 1994.

[90] Tapan Mishra, Ramesh V. Pai, and B. P. Das. Phase separation in a two-species Bose mixture. *Physical Review A*, 76:013604, 2007.

[91] Robert Lynch. The quantum phase problem: a critical review. *Physics Reports*, 256:367–436, 1995.

[92] C. Brif and Y. Ben-Aryeh. Phase-state representation in quantum optics. *Physical Review A*, 50:3505, 1994.

[93] D. T. Pegg and S. M. Barnett. Unitary phase operator in quantum mechanics. *Europhysics Letters*, 6:483–487, 1988.

[94] S. M. Barnett and D. T. Pegg. On the hermitian optical phase operator. *Journal of Modern Optics*, 36:7, 1989.

[95] D. T. Pegg and S. M. Barnett. Phase properties of the quantized single-mode electromagnetic field. *Physical Review A*, 39:1665, 1989.

[96] V. W. Scarola and S. Das Sarma. Quantum phases of the extended Bose-Hubbard hamiltonian: Possibility of a supersolid state of cold atoms in optical lattices. *Physical Review Letters*, 95:033003, 2005.

[97] A. A. Burkov, M. D. Lukin, and Eugene Demler. Decoherence dynamics in low-dimensional cold atom interferometers. *Physical Review Letters*, 98:200404, 2007.

[98] Shunji Tsuchiya and Allan Griffin. Damping of Bogoliubov excitations in optical lattices. *Physical Review A*, 70:023611, 2004.

[99] J. Hecker Denschlag, J. E. Simsarian, H. Häffner, C. McKenzie, A. Browaeys, D. Cho, K. Helmerson, S. L. Rolston, and W. D. Phillips. A Bose-Einstein condensate in an optical lattice. *Journal of Physics B: Atomic, Molecular and Optical Physics*, 35:3095–3110, 2002.

[100] Guifré Vidal. Efficient classical simulation of slightly entangled quantum computations. *Physical Review Letters*, 91:147902, 2003.

[101] Jakub Zakrzewski and Dominique Delande. Breakdown of adiabaticity when loading ultracold atoms in optical lattices. *Physical Review A*, 80, 2009.

[102] S. Ramanan, Tapan Mishra, Meetu Sethi Luthra, Ramesh V. Pai, and B. P. Das. Signatures of the superfluid-to-Mott-insulator transition in cold bosonic atoms in a one-dimensional optical lattice. *Physical Review A*, 79(1):013625, January 2009.

[103] J. C. Slater. A soluble problem in energy bands. *Physical Review*, 87(5): 807, 1952.

[104] Víctor M. Pérez-García, Humberto Michinel, J. I. Cirac, M. Lewenstein, and P. Zoller. Dynamics of Bose-Einstein condensates: Variational solutions of the Gross-Pitaevskii equations. *Physical Review A*, 56(2):1424, 1997.

[105] L. Salasnich, A. Parola, and L. Reatto. Effective wave equations for the dynamics of cigar-shaped and disk-shaped Bose condensates. *Physical Review A*, 65(4):043614, April 2002.

[106] P Vignolo, Z Akdeniz, and M P Tosi. The transmittivity of a Bose–Einstein condensate on a lattice: interference from period doubling and the effect of disorder. *Journal of Physics B: Atomic, Molecular and Optical Physics*, 36(22):4535–4546, 2003.

[107] Jean-François Schaff, Zehra Akdeniz, and Patrizia Vignolo. Localization-delocalization transition in the random dimer model. *Physical Review A*, 81(4):041604, April 2010.

[108] Immanuel Bloch, Jean Dalibard, and Wilhelm Zwerger. Many-body physics with ultracold gases. *Reviews of Modern Physics*, 80(3):885, July 2008.

[109] M. Krämer, C. Menotti, L. Pitaevskii, and S. Stringari. Bose-Einstein condensates in 1D optical lattices. *The European Physical Journal D - Atomic, Molecular and Optical Physics*, 27(3):247–261, 2003.

[110] R. W. Spekkens and J. E. Sipe. Spatial fragmentation of a Bose-Einstein condensate in a double-well potential. *Physical Review A*, 59(5):3868, May 1999.

[111] Z. Shi, K.J.H. Law, P.G. Kevrekidis, and B.A. Malomed. Trapping of two-component matter-wave solitons by mismatched optical lattices. *Physics Letters A*, 372(22):4021–4027, May 2008.

[112] Arthur Gubeskys and Boris A. Malomed. Symmetric and asymmetric solitons in linearly coupled Bose-Einstein condensates trapped in optical lattices. *Physical Review A*, 75(6):063602, June 2007.

[113] Anatoli Polkovnikov, Subir Sachdev, and S. M. Girvin. Nonequilibrium Gross-Pitaevskii dynamics of boson lattice models. *Physical Review A*, 66:053607, 2002.

[114] D. A. Butts and D. S. Rokhsar. Predicted signatures of rotating Bose-Einstein condensates. *Nature*, 397:327–329, 1999.

[115] Daniel S. Goldbaum and Erich J. Mueller. Vortex lattices of bosons in deep rotating optical lattices. *Physical Review A*, 77:033629, 2008.

[116] Y. Castin and R. Dum. Bose-Einstein condensates with vortices in rotating traps. *The European Physical Journal D*, 7:14, 1999.

[117] Tin-Lun Ho. Bose-Einstein condensates with large number of vortices. *Physical Review Letters*, 87:060403, 2001.

[118] H. Pu, L. O. Baksmaty, S. Yi, and N. P. Bigelow. Structural phase transitions of vortex matter in an optical lattice. *Physical Review Letters*, 94:190401, 2005.

[119] C. Raman, J. R. Abo-Shaeer, J. M. Vogels, K. Xu, and W. Ketterle. Vortex nucleation in a stirred Bose-Einstein condensate. *Physical Review Letters*, 87(21):210402, November 2001.

[120] Congjun Wu, Han dong Chen, Jiang piang Hu, and Shou-Cheng Zhang. Vortex configurations of bosons in an optical lattice. *Physical Review A*, 69:043609, 2004.

[121] Daniel P. Arovas and Assa Auerbach. Quantum tunneling of vortices in two-dimensional superfluids. *Physical Review B*, 78:094508, 2008.

[122] Rajiv Bhat, M. J. Holland, and L. D. Carr. Bose-Einstein condensates in rotating lattices. *Physical Review Letters*, 96:060405, 2006.

[123] N. R. Cooper, N. K. Wilkin, and J. M. F. Gunn. Quantum phases of vortices in rotating Bose-Einstein condensates. *Physical Review Letters*, 87:120405, 2001.

[124] Wei-Min Zhang, Da Hsuan Feng, and Robert Gilmore. Coherent states: Theory and some applications. *Reviews of Modern Physics*, 62:867, 1990.

[125] Rodney Loudon. *The Quantum Theory of Light*. Oxford University Press, 2000.

[126] E. Schrödinger. Der stetige Übergang von der Mikro- zur Makromechanik. *Naturwissenschaften*, 14:664–666, 1926.

[127] Peter W. Milonni and Michael Martin Nieto. Coherent states. In *Compendium of Quantum Physics*. Springer, 2009.

[128] Wilhelm Zwerger. Mott-Hubbard transition of cold atoms in optical lattices. *Journal of Optics B: Quantum and Semiclassical Optics*, 5: S9–S16, 2003.

[129] N. Dupuis and K. Sengupta. Superfluid to Mott-insulator transition of cold atoms in optical lattices. *Physica B: Condensed Matter*, 404: 517–520, 2009.

[130] Fabrice Gerbier, Simon Folling, Artur Widera, Olaf Mandel, and Immanuel Bloch. Probing number squeezing of ultracold atoms across the superfluid-Mott insulator transition. *Physical Review Letters*, 96: 090401–4, 2006.

[131] J. Sebby-Strabley, B. L. Brown, M. Anderlini, P. J. Lee, W. D. Phillips, J. V. Porto, and P. R. Johnson. Preparing and probing atomic number states with an atom interferometer. *Physical Review Letters*, 98:200405–4, 2007.

[132] G.-B. Jo, Y. Shin, S. Will, T. A. Pasquini, M. Saba, W. Ketterle, D. E. Pritchard, M. Vengalattore, and M. Prentiss. Long phase coherence time and number squeezing of two Bose-Einstein condensates on an atom chip. *Physical Review Letters*, 98:030407, 2007.

[133] J. Esteve, C. Gross, A. Weller, S. Giovanazzi, and M. K. Oberthaler. Squeezing and entanglement in a Bose-Einstein condensate. *Nature*, 455: 1216–1219, 2008.

[134] Patric Navez. Macroscopic squeezing in Bose-Einstein condensate. *Mod. Phys. Lett. B*, 12:705, 1998.

[135] A. I. Solomon, Y. Feng, and V. Penna. Structure of the Bose-Einstein condensate ground state. *Physical Review B*, 60:3044, 1999.

[136] J. A. Dunningham, M. J. Collett, and D. F. Walls. Quantum state of a trapped Bose-Einstein condensate. *Physics Letters A*, 245:49–54, 1998.

[137] Masudul Haque and Andrei E. Ruckenstein. Squeezing in the weakly interacting uniform Bose-Einstein condensate. *Physical Review A*, 74: 043622–8, 2006.

[138] R. Loudon. Squeezed light. *j. mod. optics.*, 34:709, 1987.

[139] Ralf Schutzhold, Michael Uhlmann, Yan Xu, and Uwe R. Fischer. Sweeping from the superfluid to the Mott phase in the Bose-Hubbard model. *Physical Review Letters*, 97:200601–4, 2006.

[140] C. K. Hong and L. Mandel. Higher-order squeezing of a quantum field. *Physical Review Letters*, 54:323, 1985.

[141] A. Inomata, H. Kuratsuji, and C. C. Gerry. *Path Integrals and Coherent States of SU(2) and SU(1,1).* World Scientific Pub Co Inc, 1992.

[142] Luigi Amico and Vittorio Penna. Dynamical mean field theory of the Bose-Hubbard model. *Physical Review Letters*, 80:2189, 1998.

[143] C. Menotti, J. R. Anglin, J. I. Cirac, and P. Zoller. Dynamic splitting of a Bose-Einstein condensate. *Physical Review A*, 63:023601, 2001.

[144] Manuela Capello, Federico Becca, Michele Fabrizio, and Sandro Sorella. Superfluid to Mott-insulator transition in Bose-Hubbard models. *Physical Review Letters*, 99:056402, 2007.

[145] E. Gerjuoy, A. R. P. Rau, and Larry Spruch. A unified formulation of the construction of variational principles. *Reviews of Modern Physics*, 55:725, 1983.

[146] Roberto Franzosi. Nonclassical dynamics of Bose-Einstein condensates in an optical lattice in the superfluid regime. *Physical Review A*, 75: 053610, 2007.

[147] P. Buonsante, R. Franzosi, and V. Penna. From the superfluid to the Mott regime and back: triggering a non-trivial dynamics in an array of coupled condensates. *Journal of Physics B: Atomic, Molecular and Optical Physics*, 37:S195–S203, 2004.

[148] P. Buonsante, V. Penna, and A. Vezzani. Attractive ultracold bosons in a necklace optical lattice. *Physical Review A*, 72:043620, 2005.

[149] V. Chernyak, S. Choi, and S. Mukamel. Generalized coherent state representation of Bose-Einstein condensates. *Physical Review A*, 67:053604, 2003.

[150] Iacopo Carusotto and Yvan Castin. An exact reformulation of the Bose–Hubbard model in terms of a stochastic Gutzwiller ansatz. *New Journal of Physics*, 5:91, 2003.

[151] Daniel S. Rokhsar and B. G. Kotliar. Gutzwiller projection for bosons. *Physical Review B*, 44:10328, 1991.

[152] Werner Krauth, Michel Caffarel, and Jean-Philippe Bouchaud. Gutzwiller wave function for a model of strongly interacting bosons. *Physical Review B*, 45:3137, 1992.

[153] A. M. Perelomov. *Generalized coherent states and their applications*. Springer-Verlag, 1986.

[154] Daniel T. Colbert and William H. Miller. A novel discrete variable representation for quantum mechanical reactive scattering via the s-matrix kohn method. *The Journal of Chemical Physics*, 96:1982, 1992.

Appendix A

The Dynamics of Squeezed Coherent States in Shallow Lattices

A.1 Coherent States and Squeezed Coherent States

A coherent state, $|\alpha\rangle$ which is also called 'Glauber coherent state' [64], is defined to be an eigenstate of an annihilation operator in a harmonic oscillator, $\hat{a}$ with an eigenvalue of α [124, 125]:

$$\hat{a}|\alpha\rangle = \alpha|\alpha\rangle, \tag{A.1}$$

and the state that satisfies this eigenvalue equation is,

$$|\alpha\rangle = \exp\Big(-\frac{1}{2}|\alpha|^2\Big)\sum_{\mathrm{n}=0}^{\infty}\frac{\alpha^{\mathrm{n}}}{(\mathrm{n}!)^{1/2}}|\mathrm{n}\rangle. \tag{A.2}$$

The coherent state has a minimized quantum fluctuation ($\Delta x \Delta p = \hbar$), so it is a quantum state closest to a classical state. It was first discovered by Erwin Schrödinger [126, 127] in an effort to find solutions that marginally satisfy the correspondence principle between classical and quantum mechanics and thus give an approximate classical phase space interpretation of a quantum mechanical system. Later on, the coherent state was rediscovered by Glauber in his way to understand coherence properties of an electromagnetic field.

Now we show that a superfluid has the same number statistics per well as that of a coherent state. Suppose we have a homogeneous one-dimensional

system of N bosons in M lattice sites, in which its physics is well-described by the Bose-Hubbard model:

$$\begin{aligned} H &= \frac{U}{2}\sum_i \hat{a}_i^\dagger \hat{a}_i(\hat{a}_i^\dagger \hat{a}_i - 1) + \sum_i \epsilon_i \hat{a}_i^\dagger \hat{a}_i \\ &\quad -J\sum_{\langle ij\rangle}(\hat{a}_i^\dagger \hat{a}_j + \hat{a}_j^\dagger \hat{a}_i), \end{aligned} \tag{A.3}$$

where i runs over all lattice sites and $\langle ij\rangle$ is all possible combinations of nearest sites. The intrinsic parameters are defined as,

$$U = g\int dz|w(z)|^4 \tag{A.4}$$

$$\begin{aligned} J &= -\int dz w(z-R_i) \\ &\quad \Big[-\frac{\hbar^2}{2m}\bigtriangledown^2 + V_o(z,t)\Big]w(z-R_j), \end{aligned} \tag{A.5}$$

where U is an on-site interaction energy, and J is a hopping energy between neighbouring sites, $g = 4\pi\hbar^2 a/m$ is a nonlinear interaction coefficient, $w(z - R_i)$ is a single-particle Wannier function centered at R_i, and $V_o(z,t)$ is an optical lattice potential. The on-site interaction energy U and the tunneling amplitude J can be calculated as in [128, 129].

When the optical lattice is shallow, the tunneling strength is sufficiently large and the probability of a single atom to be found in a certain lattice site is equally probable in every site [3]. In that case, the many body ground state of the BEC can be written as,

$$|\psi_{SF}\rangle = \frac{1}{\sqrt{N!}}\Big(\frac{1}{\sqrt{M}}\sum_{i=1}^{M}\hat{a}_i^\dagger\Big)^N|0\rangle, \tag{A.6}$$

with $\langle\psi_{SF}|\psi_{SF}\rangle = 1$.

Since every site is equivalent to each other for a superfluid, we focus on a first site and expand the sum in A.6 as the following:

$$\begin{aligned} |\psi_{SF}\rangle &= \frac{1}{\sqrt{N!}}\Big(\frac{1}{\sqrt{M}}\hat{a}_1^\dagger + \sqrt{\frac{M-1}{M}}\frac{1}{\sqrt{M-1}}\sum_{i=2}^{M}\hat{a}_i^\dagger\Big)^N|0\rangle \\ &= \frac{1}{\sqrt{N!}}\sum_{n=0}^{N}\frac{N!}{n!(N-n)!}\frac{1}{M^{n/2}}(\hat{a}_1^\dagger)^n \end{aligned}$$

$$\left(\frac{M-1}{M}\right)^{\frac{N-n}{2}}\left(\frac{1}{\sqrt{M-1}}\sum_{i=2}^{M}\hat{a}_i^\dagger\right)^{N-n}|0\rangle$$

Before we show the number statistics of the superfluid, we check that the wavefunction is properly normalized to 1 by using induction on M. Beginning with $M=1$ and any N,

$$\begin{aligned}|\psi_{SF(N;M=1)}\rangle &= \frac{1}{\sqrt{N!}}\left(\hat{a}_i^\dagger\right)^N|0\rangle \\ &= |n\rangle, \end{aligned} \tag{A.7}$$

is a number state normalized to 1. Now suppose that the wavefunction within $M-1$ wells, $|\psi_{SF(N;M-1)}\rangle$, is normalized to 1 and then the normalization of the wavefunction within M wells in Eq. A.7 (omitting a subscript, 'SF') is

$$\begin{aligned}\langle\psi_{(N;M)}|\psi_{(N;M)}\rangle &= \frac{1}{N!}\sum_{n=0}^{N}\left(\frac{N!}{n!(N-n)!}\right)^2\frac{1}{M^n}\left(\frac{M-1}{M}\right)^{N-n}\langle 0|\hat{a}_1^n(\hat{a}_1^\dagger)^n \\ &\quad \left(\frac{1}{\sqrt{M-1}}\sum_{i=2}^{M}\hat{a}_i\right)^{N-n}\left(\frac{1}{\sqrt{M-1}}\sum_{i=2}^{M}\hat{a}_i^\dagger\right)^{N-n}|0\rangle \\ &= \frac{1}{N!}\sum_{n=0}^{N}\left(\frac{N!}{n!(N-n)!}\right)^2\frac{1}{M^n}\left(\frac{M-1}{M}\right)^{N-n}n!(N-n)! \\ &= \sum_{n=0}^{N}\frac{N!}{n!(N-n)!}\frac{1}{M^n}\left(\frac{M-1}{M}\right)^{N-n} \\ &= \left(\frac{1}{M}+\frac{M-1}{M}\right)^N \\ &= 1 \end{aligned} \tag{A.8}$$

using the normalization of $|\psi_{SF(N-n;M-1)}\rangle$ in the second line.

Next, we calculate the number distribution of the superfluid from Eq. A.7. Since each site is equally probable to host an atom, the mean number of atoms per site, α is,

$$\mu = \frac{N}{M} \tag{A.9}$$

Then, the probability that n atoms are in the first site and $N-n$ atoms are

in the rest is,

$$
\begin{aligned}
|\langle n, N-n|\psi_{SF}\rangle|^2 &= \frac{N!}{n!(N-n)!}\Big(\frac{1}{M}\Big)^n\Big(\frac{M-1}{M}\Big)^{N-n} \\
&= \frac{N!}{n!(N-n)!}\Big(\frac{\mu}{N}\Big)^n\Big(1-\frac{\mu}{N}\Big)^{N-n} \\
&= \frac{N(N-1)\cdot(N-n+1)}{N^n}\frac{\mu^n}{n!} \\
&\quad \Big(1-\frac{\mu}{N}\Big)^N\Big(1-\frac{\mu}{N}\Big)^{-n}
\end{aligned} \tag{A.10}
$$

When the number of particles N is sufficiently large($N \to \infty$), it becomes,

$$
\lim_{N\to\infty} |\langle n, N-n|\psi_{SF}\rangle|^2 = \frac{\mu^n}{n!}e^{-\mu} \tag{A.11}
$$

Therefore, if we expand the superfluid wavefunction, $|\psi_{SF}\rangle$ in the basis of number states $|n\rangle$ for the first site,

$$
\lim_{N\to\infty}\sum_{n=0}^{N}|n\rangle\langle n, N-n|\psi_{SF}\rangle = \lim_{N\to\infty}\sum_{n=0}^{N}\frac{\alpha^n}{\sqrt{n!}}e^{-|\alpha|^2/2}|n\rangle, \tag{A.12}
$$

where $|\alpha|^2 = \mu$. This is nothing but a coherent state with an amplitude of α, $|\alpha\rangle$ as defined as above in A.2.

One interesting observation is that the superfluid phase and the Mott insulator phase are different in terms of number statistics: a superfluid has an atom number of the Poisson distribution in each well, whereas a Mott insulator has a fixed number of bosons per site. During the superfluid-Mott insulator phase transition, the variance of number within each well is squeezed from the Poissonian, $\Delta n = \sqrt{n}$ of superfluid phase to the sub-Poissonian, $\Delta n < \sqrt{n}$ until it becomes zero $\Delta n = 0$ of Mott insulator phase. Experimentally, this is observed in [130–133] and theoretically the effect of number squeezing was studied using the method of TWA [16]. The squeezing effect has been recently considered for the uniform BECs too [66, 134–137].

As mentioned above, the coherent state is a minimum uncertainty state, $\Delta\hat{x}\Delta\hat{p} = \hbar/4$. For a coherent state, this relation can be translated to $\Delta\hat{n}\Delta\hat{\phi} \geq \frac{1}{2}$ for the canonically conjugate pair of operators ($[\hat{n}, \hat{\phi}] = i$). Furthermore, a coherent state preserves such a minimum uncertainty in time evolution if the Hamiltonian is time-independent. Not all physical states behave in a way with these properties. The states that satisfy these conditions include the simplest coherent state which has been discussed so far, and a squeezed coherent state

which will be discussed later.

The definition of a coherent state can be translated into an exponential operator form as the following:

$$|\alpha\rangle = \hat{D}(\alpha)|0\rangle, \tag{A.13}$$

where $|0\rangle$ is a vacuum state and $\hat{D}(\alpha)$ is a coherent state displacement operator defined as

$$\hat{D}(\alpha) \equiv \exp(\alpha\hat{\mathrm{a}}^\dagger - \alpha^*\hat{\mathrm{a}}). \tag{A.14}$$

The displacement operator is a unitary operator, and its effect on the creation and the annihilator operator is shifting the operators by the corresponding eigenvalue,α, α^*:

$$\hat{D}^\dagger(\alpha)\hat{D}(\alpha) = \hat{D}(\alpha)\hat{D}^\dagger(\alpha) = 1, \tag{A.15}$$

$$\hat{D}^\dagger(\alpha)\hat{a}\hat{D}(\alpha) = \hat{a} + \alpha, \tag{A.16}$$

$$\hat{D}^\dagger(\alpha)\hat{a^\dagger}\hat{D}(\alpha) = \hat{a^\dagger} + \alpha^*. \tag{A.17}$$

So far, we have been introduced to a coherent state. Though, we do not stop at a simple coherent state, but generalize it further. There are some experimental studies on squeezed states in BECs [3, 14]. In order to squeeze the number distribution asymptotically to a Mott insulator phase, we need another parameter. A Squeezed Coherent State(SCS) has variances of number and phase that are flexible because of this extra parameter [14, 66, 138, 139]. In this work, we construct a one-dimensional periodic lattice potential with a shallow depth and prepare as an initial state, an array of SCSs which are placed into each lattice site. The squeezed coherent state is limited to an intermediate regime between a superfluid and a Mott-insulator, where the number per well is squeezed with the sub-Poissonian distribution.

A squeezed coherent state is a generalized coherent state in the 2^{nd} order that has quadratures squeezed (Higher order squeezing is discussed in [140]). We define mixed operators in dimensionless units:

$$\begin{aligned} \hat{X} &= \frac{1}{2}(\hat{a}^\dagger + \hat{a}), \\ \hat{Y} &= \frac{i}{2}(\hat{a}^\dagger - \hat{a}), \end{aligned} \tag{A.18}$$

and $(\Delta X)^2, (\Delta Y)^2$ are quadrature variances corresponding to $\hat{X}$ and $\hat{Y}$. The Heisenberg uncertainty relation for this conjugate pair is $\Delta X \Delta Y \geq \frac{1}{4}$. If $\Delta X = \Delta Y = \frac{1}{2}$, then it is the plain coherent state which is not squeezed, and

if one variance ΔX (or ΔY) becomes smaller than the other ΔY (or ΔX), then the variance is called 'squeezed'. A squeezed coherent state, $|\alpha, \zeta\rangle$, is defined as:

$$|\alpha, \zeta\rangle \equiv \hat{D}(\alpha)\hat{S}(\zeta)|0\rangle, \tag{A.19}$$

$$\hat{S}(\zeta) \equiv \exp\big(\frac{1}{2}\zeta^*\hat{\mathrm{a}}^2 - \frac{1}{2}\zeta(\hat{\mathrm{a}}^\dagger)^2\big), \tag{A.20}$$

$$\zeta = se^{i\vartheta}, \tag{A.21}$$

where $\hat{D}(\alpha)$ is the displacement operator defined as for the coherent state, and $\hat{S}(\zeta)$ is a squeeze operator. The squeeze parameter, ζ is defined in terms of a modulus s and a phase ϑ. As we did for the displacement operator, we can check the unitarity property and effects of the squeeze operator on operators, using the Baker-Campbell-Hausdorff formula:

$$\hat{S}^\dagger(\zeta)\hat{S}(\zeta) = \hat{S}(\zeta)\hat{S}^\dagger(\zeta) = 1 \tag{A.22}$$

$$\hat{S}^\dagger(\zeta)\hat{a}\hat{S}(\zeta) = \hat{a}\cosh s - \hat{a}^\dagger e^{i\vartheta}\sinh s \tag{A.23}$$

$$\hat{S}^\dagger(\zeta)\hat{a}^\dagger\hat{S}(\zeta) = \hat{a}^\dagger\cosh s - \hat{a}e^{-i\vartheta}\sinh s \tag{A.24}$$

The effect of squeeze operators is modulating the annihilation and the creation operator by hyperbolic functions of s. A SCS is an eigenstate of mixed operators:

$$\begin{aligned}&(\hat{a}\cosh s + \hat{a}^\dagger e^{i\vartheta}\sinh s)|\alpha, \zeta\rangle \\ &= (\alpha\cosh s + \alpha^* e^{i\vartheta}\sinh s)|\alpha, \zeta\rangle.\end{aligned} \tag{A.25}$$

We can see that, for a coherent state ($s = 0$), the equation reduces to the definition of the coherent state, and for the case of $\alpha = 0$, it shrinks to a vacuum state:

$$(\hat{a}\cosh s + \hat{a}^\dagger e^{i\vartheta}\sinh s)|\alpha, \zeta\rangle = 0. \tag{A.26}$$

The properties so far we have seen enable calculation of expectation values of general operators. For example, an expected number and an expected number variance are obtained as follows:

$$\langle n\rangle = |\alpha|^2 + \sinh^2 s, \tag{A.27}$$

$$\begin{aligned}(\Delta n)^2 = {} & |\alpha|^2\big\{e^{2s}\sin^2(\theta - \frac{1}{2}\vartheta) + \mathrm{e}^{-2s}\cos^2(\theta - \frac{1}{2}\vartheta)\big\} \\ & +2\sinh^2 s(\sinh^2 s + 1).\end{aligned} \tag{A.28}$$

In the limit where the mean atom number outweighs the effect of squeezing ($|\alpha| \gg e^s$), the number variance and the phase variance asymptotically converges to the following:

$$\Delta n \simeq \langle n \rangle^{\frac{1}{2}} e^{-s} \tag{A.29}$$

$$\Delta \phi \simeq \frac{1}{2} \langle n \rangle^{-\frac{1}{2}} e^{s}, \tag{A.30}$$

and the product of the number and phase variance is still minimized as that of a coherent state, $\Delta n \Delta \phi \simeq 1/2$, but the number variance can be squeezed by a factor of e^s. For example, when s increases, number fluctuation is decreased($\Delta n \to 0$). A coherent state is a special case with $s = 0$:

$$\Delta n \simeq \langle n \rangle^{\frac{1}{2}} \tag{A.31}$$

$$\Delta \phi \simeq \frac{1}{2} \langle n \rangle^{-\frac{1}{2}}. \tag{A.32}$$

A.2 Time Dependent Variational Principle

In general, a minimum uncertainty wavepacket is the wavefunction that mimics a classical system. Note that a classical state is represented by a point in phase space. On the other hand, quantum fluctuation of a coherent state in phase space is spread around the classical expectation value, but its spread is minimized compared to other general quantum states which have broader variance. Therefore, to analyze its dynamics, we employ a semiclassical method, especially the Time Dependent Variational Principle (TDVP for a review, see [124, 141]) applied to a squeezed coherent state. The method was used with a mean field theory [40, 142] or without the mean field theory [143]. It has been also used to study superfluid-Mott insulator phase transitions in Bose-Hubbard Models with a variational wavefunction [144].

In this section, we skim a review of TDVP [124, 141, 145]. The Time Dependent Variational Principle is a variational principle that minimizes an action of a system:

$$\delta S = 0, \tag{A.33}$$

$$S = \int_{t_1}^{t_2} dt L(\psi, \bar{\psi}), \tag{A.34}$$

where S is an action of the system, and the Lagrangian $L(\psi, \bar{\psi})$ is

$$L(\psi, \bar{\psi}) = \frac{i}{2}\frac{\langle\psi|\dot{\psi}\rangle - \langle\dot{\psi}|\psi\rangle}{\langle\psi|\psi\rangle} - \frac{\langle\psi|H|\psi\rangle}{\langle\psi|\psi\rangle} \tag{A.35}$$

for an arbitrary unnormalized wavefunction, ψ. For a normalized wavefunction, it is reduced to the usual Lagrangian,

$$L(\psi, \bar{\psi}) = \langle\psi|i\frac{\partial}{\partial t} - H|\psi\rangle. \tag{A.36}$$

Using the TDVP which dictates variation of the action to be zero, we can derive the time-dependent Schrödinger equation. The variation of action is calculated as,

$$\begin{aligned}
\delta S &= \int dt \delta L \\
&= \int dt \Big[\frac{i}{2}\frac{\langle\delta\psi|\dot{\psi}\rangle + \langle\psi|\delta\dot{\psi}\rangle - \langle\delta\dot{\psi}|\psi\rangle - \langle\dot{\psi}|\delta\psi\rangle}{\langle\psi|\psi\rangle} \\
&\quad -\frac{\delta\langle\psi|H|\psi\rangle}{\langle\psi|\psi\rangle} - (\frac{i}{2}\frac{\langle\psi|\dot{\psi}\rangle - \langle\dot{\psi}|\psi\rangle}{\langle\psi|\psi\rangle} - \frac{\langle\psi|H|\psi\rangle}{\langle\psi|\psi\rangle})\frac{\delta\langle\psi|\psi\rangle}{\langle\psi|\psi\rangle}\Big],
\end{aligned} \tag{A.37}$$

and integrating by parts the variation of time derivative of wavefunction $\delta\dot{\psi}$ gives,

$$\begin{aligned}
\frac{\langle\psi|\delta\dot{\psi}\rangle}{\langle\psi|\psi\rangle} &= \frac{d}{dt}\frac{\langle\psi|\delta\psi\rangle}{\langle\psi|\psi\rangle} - \frac{\langle\dot{\psi}|\delta\psi\rangle}{\langle\psi|\psi\rangle} + \frac{\langle\psi|\delta\psi\rangle}{\langle\psi|\psi\rangle^2}\frac{d}{dt}\langle\psi|\psi\rangle \\
\frac{\langle\delta\dot{\psi}|\psi\rangle}{\langle\psi|\psi\rangle} &= \frac{d}{dt}\frac{\langle\delta\psi|\psi\rangle}{\langle\psi|\psi\rangle} - \frac{\langle\delta\psi|\dot{\psi}\rangle}{\langle\psi|\psi\rangle} + \frac{\langle\delta\psi|\psi\rangle}{\langle\psi|\psi\rangle^2}\frac{d}{dt}\langle\psi|\psi\rangle
\end{aligned} \tag{A.38}$$

Then, the variation of action is

$$\begin{aligned}
\delta S &= \int \frac{i}{2} d\Big[\frac{\langle\psi|\delta\psi\rangle}{\langle\psi|\psi\rangle} - \frac{\langle\delta\psi|\psi\rangle}{\langle\psi|\psi\rangle}\Big] \\
&\quad \int dt \Bigg[i\Big[\frac{\langle\delta\psi|\dot{\psi}\rangle - \langle\dot{\psi}|\delta\psi\rangle}{\langle\psi|\psi\rangle}\Big] - \Big[\frac{\langle\delta\psi|H|\psi\rangle + \langle\psi|H|\delta\psi\rangle}{\langle\psi|\psi\rangle}\Big] \\
&\quad + \frac{i}{2}\Big[\frac{\langle\psi|\dot{\psi}\rangle + \langle\dot{\psi}|\psi\rangle}{\langle\psi|\psi\rangle^2}\big(\langle\psi|\delta\psi\rangle - \langle\delta\psi|\psi\rangle\big)\Big] \\
&\quad - \frac{i}{2}\Big[\frac{\langle\psi|\dot{\psi}\rangle - \langle\dot{\psi}|\psi\rangle}{\langle\psi|\psi\rangle^2}\big(\langle\psi|\delta\psi\rangle + \langle\delta\psi|\psi\rangle\big)\Big]
\end{aligned}$$

$$+\frac{\langle\psi|H|\psi\rangle}{\langle\psi|\psi\rangle^2}\big(\langle\delta\psi|\psi\rangle+\langle\psi|\delta\psi\rangle\big)\Big] \tag{A.39}$$

$$= \int dt\Bigg[\frac{i\langle\delta\psi|\dot{\psi}\rangle-\langle\delta\psi|H|\psi\rangle}{\langle\psi|\psi\rangle} - \frac{\langle\psi|i\partial/\partial t-H|\psi\rangle}{\langle\psi|\psi\rangle^2}\langle\delta\psi|\psi\rangle+c.c\Bigg] \tag{A.40}$$

up to a total derivative. The first line is a total derivative term and the second line is a projection of time evolution of a wavefunction over a variation of the wavefunction, which becomes the first term in Eq. A.40. Some terms of the third line and the fourth line combine to cancel each other, and they become part of the second term in Eq. A.40. Since $\delta\psi$ is arbitrary, collecting the two terms in the last equation,

$$\begin{aligned}(i\frac{\partial}{\partial t}-H)|\psi\rangle &= \frac{\langle\psi|i\partial/\partial t-H|\psi\rangle}{\langle\psi|\psi\rangle}|\psi\rangle \\ &\equiv \phi_L(t)|\psi\rangle\end{aligned} \tag{A.41}$$

The $\phi_L(t)$ of Eq. A.41 is an eigenvalue of the operator in the left hand side. We can absorb such a global phase into the definition of a new wavefunction, $|\psi'\rangle$ as,

$$|\psi'\rangle = |\psi\rangle e^{i\int\phi_L(t)dt} \tag{A.42}$$

$$= |\psi\rangle e^{iS}, \tag{A.43}$$

then, $|\psi'\rangle$ satisfies the time dependent Schrödinger equation:

$$(i\frac{\partial}{\partial t}-H)|\psi'\rangle=0. \tag{A.44}$$

The main idea of TDVP is to approximate this time evolution equation by imposing a weaker form of a Schrödinger equation to the macroscopic wavefunction:

$$\langle\psi'|i\frac{\partial}{\partial t}-H|\psi'\rangle=0. \tag{A.45}$$

In the form of the original wavefunction, it becomes

$$\dot{S}=i\langle\psi|\frac{\partial}{\partial t}|\psi\rangle-\mathcal{H}, \tag{A.46}$$

where $\mathcal{H} = \langle\psi|H|\psi\rangle$. The semiclassical equation of motion under the TDVP is then the one obtained by setting $\delta S = 0$.

This TDVP belongs to variational methods. In order to implement it to a physical problem, therefore, we need to express a wavefunction by a few effective variables to describe its dynamics and calculate variations of action over these effective parameters. In this effective theory, an initial macroscopic wavefunction $|\psi\rangle$ should be designed to be well-defined over phase space. Accordingly, in the TDVP, all expectation values become functions of such variables for the description of ψ. In other words, the Lagrangian $\mathcal{L}[\psi]$, and the Hamiltonian $\mathcal{H}[\psi]$ are all effective functionals.

Now, we discuss how to calculate time evolution of observables under the TDVP. Suppose that $o = \langle\psi|\hat{O}|\psi\rangle$ is an expectation value of an operator $\hat{O}$, then there exists a correspondence between the Heisenberg equation in the Heisenberg picture and the time evolution equation of the expectation value in the TDVP:

$$
\begin{aligned}
i\hbar\frac{\partial}{\partial t}\hat{O} &= [H, \hat{O}] && \text{(A.47)}\\
\Longleftrightarrow \frac{\partial}{\partial t}o &= \{\mathcal{H}, o\}_{PB} && \text{(A.48)}\\
i\hbar\frac{\partial}{\partial t}\langle\psi|\hat{O}|\psi\rangle &= i\hbar\{\langle\psi|\hat{H}|\psi\rangle, \langle\psi|\hat{O}|\psi\rangle\}_{PB}, && \text{(A.49)}
\end{aligned}
$$

where Eq. A.47 is an Heisenberg equation for a quantum operator, whereas Eq. A.48 (or A.49) is an equation for a classical expectation value of the operator. Here, $\{p, q\}_{PB}$ is a Poisson bracket that satisfies the following property,

$$
\begin{aligned}
\{o_i, o_j\}_{PB} &= \frac{\delta_{ij}}{i\hbar}, && \text{(A.50)}\\
o_i &= \langle\psi|\hat{O}_i|\psi\rangle,\\
o_j &= \langle\psi|\hat{O}_j|\psi\rangle, && \text{(A.51)}
\end{aligned}
$$

if the corresponding quantum operators, O_i, O_j satisfy

$$
[O_i, O_j] = \delta_{ij}. \qquad \text{(A.52)}
$$

Therefore, a commutator of operators becomes a Poisson bracket in the TDVP. The Eq. A.49 means that every operator can be transformed to its expectation value and its commutation relation can be transformed to a Poisson bracket. In this sense, we notice that the quantum Heisenberg picture translates into classical Poisson dynamics in the TDVP.

A.3 Squeezed Coherent States in Bose-Hubbard Model

There is an application with simple coherent states in [146–148] or with generalized coherent states in [149]. As promised before, we now deal with squeezed coherent states under a shallow optical lattice in the Bose-Hubbard model. We prepare an initial state of an array of SCSs:

$$|\psi\rangle = e^{i\frac{S}{\hbar}} \prod_{i}^{L} |\alpha_i, \zeta_i\rangle, \tag{A.53}$$

where L is the number of lattice sites, and $|\alpha_i, \zeta_i\rangle$ is a SCS for each site i.

As an aside, the initial state is a special case of Gutzwiller ansatz wavefunctions [150–152] with an optical lattice,

$$|G:\phi\rangle = \prod_{r} \sum_{n=0}^{\infty} \phi(\mathbf{r}, n) \frac{\hat{\Psi}^{\dagger}(\mathbf{r})^n}{\sqrt{n!}} |0\rangle, \tag{A.54}$$

where $\mathbf{r}$ indicates a lattice site, $\phi(\mathbf{r}, n)$ is a coefficient function needed to satisfy a normalization condition. The Gutzwiller ansatz is more general than SCSs, and other discrete models based on a mean field theory can be found in [113].

The TDVP permits us to semiclassically calculate the dynamics by minimizing the variation of action, $\delta S = 0$, as we have discussed in the previous section, for the action:

$$S = i\hbar \int dt \sum_{i} \langle \alpha_i, \zeta_i | (\frac{\partial}{\partial t} - H) | \alpha_i, \zeta_i \rangle. \tag{A.55}$$

Since each α_i, ζ_i is a complex number, there are four variational parameters contained in the states. Then,

$$\begin{aligned} \langle \alpha_i, \zeta_i | \frac{\partial}{\partial t} | \alpha_i, \zeta_i \rangle &= \frac{1}{2}\alpha_i^* \dot{\alpha}_i + \frac{1}{2}\alpha_i \dot{\alpha}_i^* + (\frac{\partial \eta}{\partial \zeta}\dot{\zeta} + \frac{\partial \eta}{\partial \zeta^*}\dot{\zeta}^*) e^{-i\vartheta} \sinh s \\ &\quad + (\frac{\partial \eta^*}{\partial \zeta}\dot{\zeta} + \frac{\partial \eta^*}{\partial \zeta^*}\dot{\zeta}^*) e^{i\vartheta} \sinh s, \end{aligned} \tag{A.56}$$

where $\eta = (\tanh s) e^{i\vartheta}$, and we can find the classical Hamiltonian $\mathcal{H}$,

$$\begin{aligned} \mathcal{H} &\equiv \langle \alpha_i, \zeta_i | H | \alpha_i, \zeta_i \rangle \\ &= \frac{U}{2} \sum_{i} \left[3\sinh^4 s + \sinh^2 s + 4|\alpha_i|^2 \sinh^2 s \right. \end{aligned}$$

$$-(\alpha_i)^2 e^{-i\vartheta}\sinh s\cosh s-(\alpha_i^*)^2 e^{i\vartheta}\sinh s\cosh s+|\alpha_i|^4\big]$$
$$+\sum_i \epsilon_i\big(\sinh^2 s+|\alpha_i|^2\big)-T\sum_i\big(\alpha_i^*\alpha_{i+1}+c.c\big). \tag{A.57}$$

The Hamiltonian looks complicated, so later on we will seek another form of Hamiltonian easier to understand, but for now we consider a special case of a plain coherent state. For the coherent state, the Hamiltonian reduces to the following with no squeezing effect ($s=0$):

$$\mathcal{H} = \frac{U}{2}\sum_i|\alpha_i|^4+\sum_i\epsilon_i|\alpha_i|^2-T\sum_i(\alpha_i^*\alpha_{i+1}+c.c). \tag{A.58}$$

One can easily note that it is nothing but the classical counterpart of the Bose-Hubbard Hamiltonian for a coherent state, since $|\alpha_i|^2=\langle\hat{a}_i^\dagger\hat{a}_i\rangle$ and $\alpha_i=\langle\hat{a}_i\rangle$, $\alpha_i^*=\langle\hat{a}_i^\dagger\rangle$.

We also find the equations of motion for variational parameters. So far, the parameters, α_i,ζ_i have been treated as time-independent variables, but in fact they do not have to. We allow those variables to be time dependent, for example, $\alpha_i(t)$ is defined as,

$$\begin{aligned}\alpha_i(t) &\equiv \langle\psi(t)|\hat{a}_i|\psi(t)\rangle\\ &= \prod_j\langle\alpha_j(t),\zeta_j(t)|\hat{a}_i|\alpha_j(t),\zeta_j(t)\rangle,\end{aligned} \tag{A.59}$$

and similarly for $\alpha^*(t)$. Hereafter, we omit the dependence of parameter on time and implicitly assume that it is a function of time. Then the equation of motion for $\alpha_i(t),\alpha_i^*(t)$ are obtained as,

$$\begin{aligned}i\hbar\dot{\alpha}_i &= [\alpha_i,\mathcal{H}]_{PB}\\ &= \frac{U}{2}[8\alpha_i\sinh^2 s-2\alpha_i^* e^{i\vartheta}\sinh s\cosh s+4|\alpha_i|^2\alpha_i]\\ &\quad +2\epsilon_i\alpha_i-T(\alpha_{i+1}+\alpha_{i-1}),\end{aligned} \tag{A.60}$$

and similarly for α_i^*.

The example above is a special case for one single operator, and we can continue further to calculate such equations of motion for linear, quadratic, and higher order operators. What we calculate from now on is then the time evolution of an expectation value for operators, $\langle G_i\rangle$ of any higher orders, $i\hbar d\langle G_i\rangle/dt$. It can be obtained by the commutation relation with the classic Hamiltonian, $i\hbar\{\mathcal{H},\langle G_i\rangle\}_{PB}$ (Eq. A.47 and Eq. A.49), which follows from $[H,G_i]$ (Note that we omit the hat from operators, $\hat{G}_i$). Before we calculate

$[H, G_i]$, we need to know commutation relations of operators in the Hamiltonian with G_i.

The commutator relations are obtained as follows. We first discuss an elegant approach based on group-theoretic algebraic structures by first recognizing that the Hamiltonian is written in terms of linear or quadratic operators:

$$\begin{aligned} \mathbf{g} &= \{G_i\} = \{\hat{a}_i, \hat{a}_i^\dagger, \hat{a}_i\hat{a}_j, \hat{a}_i^\dagger\hat{a}_j^\dagger, \hat{a}_i^\dagger\hat{a}_j + \delta_{ij}I\}, \qquad \text{(A.61)} \\ H &= H(G_i) \\ &= \sum_i c_i G_i + \sum_{ij} c_{ij} G_i G_j, \qquad \text{(A.62)} \end{aligned}$$

where $\{G_i\}$ is a complete set of the operators that span a closed algebra. In other words,

$$\begin{aligned} [G_i, G_j] &= \sum_k C_{ij}^k G_k \\ &\in \mathbf{g}, \qquad \text{(A.63)} \end{aligned}$$

for any two operators in the group. Due to Eq. A.63, products of operators do not become too high-ordered. As the algebra is closed, the commutator is itself another operator in the group. Since the Bose-Hubbard Hamiltonian can be written as generators themselves or products of these generators at most, so the algebra of the Hamiltonian is closed. It turns out that this set of generators (products of operators) construct a well-known algebra, which is the extended Heisenberg-Weyl algebra [124, 153].

For the group, $\mathbf{g}$, we first define each generator as,

$$\begin{aligned} S_i &\equiv \hat{a}_i, \\ S_i^\dagger &\equiv \hat{a}_i^\dagger, \\ T_{ij}^{(-)} &\equiv \hat{a}_i\hat{a}_j, \\ T_{ij}^{(+)} &\equiv \hat{a}_i^\dagger\hat{a}_j^\dagger, \\ T_{ij}^{(0)} &\equiv \hat{a}_i^\dagger\hat{a}_j + \delta_{ij}I. \qquad \text{(A.64)} \end{aligned}$$

The commutation relations between these generators satisfy the following relations of the extended Heisenberg-Weyl group:

$$\begin{aligned} [S_i, S_j^\dagger] &= \delta_{ij}, \\ [T_{ii}^{(-)}, T_{ii}^{(+)}] &= 4T_{ii}^{(0)}, \\ [T_{ii}^{(0)}, T_{ii}^{(-)}] &= -2T_{ii}^{(-)}, \end{aligned}$$

$$
\begin{aligned}
[T_{ii}^{(0)}, T_{ii}^{(+)}] &= 2T_{ii}^{(+)}, \\
[T_{ii}^{(+)}, S_i] &= -2S_i^\dagger, \\
[T_{ii}^{(0)}, S_i] &= -S_i, \\
[T_{ii}^{(-)}, S_i^\dagger] &= 2S_i, \\
[T_{ii}^{(0)}, S_i^\dagger] &= S_i^\dagger,
\end{aligned} \tag{A.65}
$$

and all other commutators are zero.

Now, we are equipped with commutation relations. In the TDVP, we are interested in expectation values of operators:

$$
\begin{aligned}
\langle \hat{a}_i \rangle &= \alpha_i, \\
\langle \hat{a}_i^\dagger \rangle &= \alpha_i^*, \\
\langle \hat{a}_i \hat{a}_j \rangle &= [-e^{i\vartheta} \sinh s \cosh s + \alpha_i \alpha_j]\delta_{ij}, \\
\langle \hat{a}_i^\dagger \hat{a}_j^\dagger \rangle &= [-e^{-i\vartheta} \sinh s \cosh s + \alpha_i^* \alpha_j^*]\delta_{ij}, \\
\langle \hat{a}_i^\dagger \hat{a}_j \rangle &= [\sinh^2 s + \alpha_i^* \alpha_j]\delta_{ij}.
\end{aligned} \tag{A.66}
$$

Since the final goal is finding variational equations of motion for $\langle G_i \rangle$, we evaluate the time evolution of the expectation value of operator using

$$
i\frac{d\langle G_i \rangle}{dt} = \{\mathcal{H}, \langle G_i \rangle\}_{PB}, \tag{A.67}
$$

where the classical Hamiltonian $\mathcal{H}$ is now rewritten in terms of the expectation values of generators:

$$
\begin{aligned}
\mathcal{H} &= \frac{U}{2}\sum_i \Big[\langle T_{ii}^{(+)} \rangle \langle T_{ii}^{(-)} \rangle + 2\langle T_{ii}^{(0)} \rangle^2 - 2\langle S_i \rangle^2 \langle S_i^\dagger \rangle^2\Big] \\
&\quad + \sum_i \epsilon_i \langle T_{ii}^{(0)} \rangle - T\sum_i \Big[\langle S_i^\dagger \rangle \langle S_{i+1} \rangle + c.c\Big].
\end{aligned} \tag{A.68}
$$

Finally, the equations of motion for the expectation value corresponding to each generator are a set of coupled nonlinear equations:

$$
\begin{aligned}
i\frac{d\langle \hat{a}_i \rangle}{dt} &= \frac{U}{2}\Big[-2\alpha^* e^{i\theta} \sinh s \cosh s + 2|\alpha|^2 \alpha \\
&\quad + 4\alpha^* \sinh^2 s + 4|\alpha|^2 \alpha^*\Big] + \epsilon_i \alpha_i^* - T\alpha_{i+1} \\
&= \frac{U}{2}\Big[2\langle \hat{a}_i^\dagger \rangle \langle \hat{a}_i \hat{a}_i \rangle + 4\langle \hat{a}_i^\dagger \rangle \langle \hat{a}_i^\dagger \hat{a}_i \rangle\Big] + \epsilon_i \langle \hat{a}_i^\dagger \rangle - T\langle \hat{a}_{i+1} \rangle
\end{aligned} \tag{A.69}
$$

$$
\begin{aligned}
i\frac{d\langle\hat{a}_i^\dagger\rangle}{dt} &= \frac{U}{2}\Big[2\alpha e^{-i\theta}\sinh s\cosh s - 2|\alpha|^2\alpha^* \\
&\quad -4\alpha\sinh^2 s - 4|\alpha|^2\alpha\Big] + \epsilon_i\alpha_i - T\alpha_{i-1}^* \\
&= \frac{U}{2}\Big[-2\langle\hat{a}_i\rangle\langle\hat{a}_i^\dagger\hat{a}_i^\dagger\rangle - 4\langle\hat{a}_i\rangle\langle\hat{a}_i^\dagger\hat{a}_i\rangle\Big] + \epsilon_i\langle a_i\rangle - T\langle a_{i-1}^\dagger\rangle \quad \text{(A.70)}
\end{aligned}
$$

$$
\begin{aligned}
i\frac{d\langle\hat{a}_i\hat{a}_i\rangle}{dt} &= \frac{U}{2}\Big[12(|\alpha|^2+\sinh^2 s)(-e^{i\theta}\sinh s\cosh s + (\alpha)^2) \\
&\quad +8|\alpha|^2(\alpha)^2\Big] + 2\epsilon_i(-e^{i\theta}\sinh s\cosh s + (\alpha)^2) \\
&\quad -2T\alpha_i\alpha_{i+1} \\
&= \frac{U}{2}\Big[12\langle\hat{a}_i^\dagger\hat{a}_i\rangle\langle\hat{a}_i\hat{a}_i\rangle + 8\langle\hat{a}_i\rangle^3\langle\hat{a}_i^\dagger\rangle\Big] \\
&\quad -2\epsilon_i\langle\hat{a}_i\hat{a}_i\rangle - 2T\langle\hat{a}_i\hat{a}_{i+1}\rangle \quad \text{(A.71)}
\end{aligned}
$$

$$
\begin{aligned}
i\frac{d\langle\hat{a}_i^\dagger\hat{a}_i^\dagger\rangle}{dt} &= \frac{U}{2}\Big[-12(|\alpha|^2+\sinh^2 s)(-e^{-i\theta}\sinh s\cosh s + (\alpha^*)^2) \\
&\quad +8|\alpha|^2(\alpha^*)^2\Big] - 2\epsilon_i(-e^{-i\theta}\sinh s\cosh s + (\alpha*)^2) \\
&\quad -2T\alpha_i^*\alpha_{i+1}^* \\
&= \frac{U}{2}\Big[-12\langle\hat{a}_i^\dagger\hat{a}_i\rangle\langle\hat{a}_i^\dagger\hat{a}_i^\dagger\rangle + 8\langle\hat{a}_i^\dagger\rangle^3\langle\hat{a}_i\rangle\Big] \\
&\quad -2\epsilon_i\langle\hat{a}_i^\dagger\hat{a}_i^\dagger\rangle - 2T\langle\hat{a}_i^\dagger\hat{a}_{i+1}^\dagger\rangle \quad \text{(A.72)}
\end{aligned}
$$

$$
\begin{aligned}
i\frac{d\langle\hat{a}_i^\dagger\hat{a}_i\rangle}{dt} &= -T\Big[\alpha_i^\dagger\alpha_{i+1} - \alpha_{i-1}^\dagger\alpha_i\Big] \\
&= -T\Big[\langle\hat{a}_i^\dagger\hat{a}_{i+1}\rangle - \langle\hat{a}_{i-1}^\dagger\hat{a}_i\rangle\Big]. \quad \text{(A.73)}
\end{aligned}
$$

The last equation especially means the mean population at each well is reduced or increased by tunneling through adjacent wells.

Appendix B

Discrete Variable Representation

A Discrete Variable Representation (DVR) method [154] is a grid point representation as its name stands. It was developed while a quantum mechanical calculation of S-matrix Kohn variational method for quantum reactive scattering is studied. In that study, it was a square integrable discrete basis for the S-matrix. It was found to be advantageous to use this efficient method for calculation of a Hamiltonian, since it removes the requirement of difficult integral calculations which are slow.

Since it was an attempt to solve a reactive scattering problem in three dimensions, it is natural to prefer first to a spherical coordinate system for its framework. The Hamiltonian in spherical coordinates is

$$H = -\frac{\hbar^2}{2m}\frac{1}{r}\frac{\partial^2}{\partial r^2}r - \frac{\hbar^2}{2mr^2}\Big[\frac{\partial^2}{\partial\theta^2} + \frac{1}{\tan\theta}\frac{\partial}{\partial\theta}\Big] - \frac{\hbar^2}{2mr^2\sin^2\theta}\frac{\partial^2}{\partial\phi^2} + V(r,\theta,\phi). \tag{B.1}$$

The matrix element of H with respect to basis functions, $\chi_\lambda, \chi_{\lambda'}$ is

$$\begin{aligned}\langle\chi_{\lambda'}|H|\chi_\lambda\rangle \;=\; & \int_o^\infty dr \int_0^\pi d\theta \int_0^{2\pi} d\phi \chi_{\lambda'}(r,\theta,\phi) r\sqrt{\sin\theta} \\ & \Big[-\frac{\hbar^2}{2m}\frac{\partial^2}{\partial r^2} - \frac{\hbar^2}{2mr^2}\frac{\partial^2}{\partial\theta^2} - \frac{\hbar^2}{2mr^2\sin^2\theta}\frac{\partial^2}{\partial\phi^2} - \frac{\hbar^2(1+\sin^2\theta)}{8mr^2\sin^2\theta} \\ & + V(r,\theta,\phi)\Big] r\sqrt{\sin\theta}\chi_\lambda(r,\theta,\phi),\end{aligned} \tag{B.2}$$

since

$$\frac{\partial^2}{\partial\theta^2}+\frac{1}{tan\theta}\frac{\partial}{\partial\theta}=\frac{1}{\sqrt{\sin^2\theta}}\frac{\partial^2}{\partial\theta^2}\sqrt{\sin\theta}+\frac{1+\sin^2\theta}{4\sin^2\theta}, \tag{B.3}$$

and we represent this integral calculation as a summation over a discrete variable grid. Therefore, the DVR in this coordinate system is,

$$\begin{aligned} H_{ijk,i'j'k'} &= T^{(r)}_{ii'}\delta_{jj'}\delta_{kk'}+T^{(\theta)}_{jj'}\frac{\delta_{ii'}\delta_{kk'}}{r_i^2}+T^{(\phi)}_{kk'}\frac{\delta_{ii'}\delta_{jj'}}{r_i^2\sin^2\theta_j} \\ &\quad +\delta_{ii'}\delta_{jj'}\delta_{kk'}\Big[V(r_i,\theta_j,\phi_k)-\frac{\hbar^2(1+\sin^2\theta_j)}{8mr_i^2\sin^2\theta_j}\Big], \end{aligned} \tag{B.4}$$

where the $T^{(r)}_{ii'}, T^{(\theta)}_{jj'}, T^{(\phi)}_{kk'}$ are matrices for kinetic energy in one dimension, corresponding to each r, θ, ϕ partial derivative term in the Hamiltonian:

$$T^{(r,\theta,\phi)}_{mm'}=\frac{\hbar^2(-1)^{m-m'}}{2m\Delta x^2}\begin{cases}\frac{\pi^2}{3} & ,m=m'\\ \frac{2}{(m-m')^2} & ,m\neq m'.\end{cases}$$

The matrix elements for the kinetic energy term contain off-diagonal elements, but the matrix elements converge to zero as we are getting far away from diagonal entries. On the other hand, the elements for the potential energy term is diagonal, so as a whole, the complete Hilbert space can be reduced.

The above kinetic matrix is obtained by considering a one-dimensional 'particle-in-a-box' problem. Suppose that a particle is contained in a one-dimensional box which ranges over the finite interval $[a, b]$ and that a grid for DVR has N spacing between those two endpoints:

$$x_i=a+\frac{b-a}{N}i, \qquad i=1,...,N-1. \tag{B.5}$$

The common basis functions for this system is

$$\phi_n(x)=\sqrt{\frac{2}{b-a}}\sin\Big[\frac{n\pi(x-a)}{b-a}\Big], \qquad n=1,...,N-1. \tag{B.6}$$

We represent the kinetic energy term in terms of the basis functions:

$$T_{ii'} = -\frac{\hbar^2}{2m}\Delta x\sum_{n=1}^{N-1}\phi_n(x_i)\phi_n(x_{i'})$$

$$= \frac{\hbar^2}{2m}\Big(\frac{\pi}{b-a}\Big)^2 \frac{2}{N}\sum_{n=1}^{N-1} n^2 \sin\Big(\frac{n\pi i}{N}\Big)\sin\Big(\frac{n\pi i'}{N}\Big), \tag{B.7}$$

where $\Delta x = (b-a)/N$.

After simplification, it becomes:

$$T_{ii'} = \frac{\hbar^2}{2m}\frac{(-1)^{i-i'}}{(b-a)^2}\frac{\pi^2}{2}\frac{1}{\sin^2[\pi(i-i')/2N]} - \frac{1}{\sin^2[\pi(i+i')/2N]} \tag{B.8}$$

for $i \neq i'$, and

$$T_{ii} = \frac{\hbar^2}{2m}\frac{1}{(b-a)^2}\frac{\pi^2}{2}\Big[\frac{(2N^2+1)}{3} - \frac{1}{\sin^2(\pi i/N)}\Big] \tag{B.9}$$

for $i = i'$.

In the case of an open-end physical system ($a \to -\infty, b \to \infty$ with $\Delta x = (b-a)/N$ fixed),

$$T_{ii'}^{(r,\theta,\phi)} = \frac{\hbar^2(-1)^{i-i'}}{2m\Delta x^2}\begin{cases} \frac{\pi^2}{3} & , i = i' \\ \frac{2}{(i-i')^2} & , i \neq i'. \end{cases}$$